NTNU – Trondheim
Norwegian University of
Science and Technology

QUANTUM PHASE TRANSITION IN SPIN-ORBIT COUPLED BOSE-EINSTEIN CONDENSATES IN OPTICAL LATTICES OF DIFFERENT GEOMETRIES

Oladunjoye Aina Awoga

Acknowledgement

save time. Thanks to my friends Nsikak Etuk, and Ben Normann for always being there for me. I appreciate my colleagues Alex and Kyle. They both have been been wonderful.

Contents

List of Figures

List of Tables

Acronyms

1D	:	One Dimension
2D	:	Two Dimensions
3D	:	Three Dimensions
BEC	:	Bose-Einstein Condensate(s)
BHM	:	Bose-Hubbard Model
GPE	:	Gross-Pitaevski Equation
lhs	:	left hand side
MCBEC	:	Multicomponent Bose-Einstein Condensate(s)
MI	:	Mott Insulator
QCP	:	Quantum Critical Point
QPT	:	Quantum Phase Transition
rhs	:	right hand side
SF	:	Superfluid
SF-MI	:	Superfluid to Mott Insulator
SOC	:	Spin-Orbit Coupling
SOCBEC	:	Spin-Orbit Coupled Bose-Einstein Condensates

Chapter 1

Introduction

1.1 Bose-Einstein condensation

Like a particle, an atom can also be classified in terms of its spin as a fermion or a boson. Bosonic atoms have even number of neutrons while fermionic atoms have odd number of neutrons. Examples of atomic bosons include ^{23}Na, ^{58}Ni, ^{96}Ru and ^{4}He while ^{6}Li, ^{14}N and ^{40}K are fermionic atoms. Since bosons do not obey the Pauli's exclusion principle it is possible for more than one (bosonic) atom to occupy a single state. If the temperature of a bosonic system is decreased below a particular temperature, called the critical temperature (T_c), a large fraction of the atom occupies or condense into the ground state. This state is called Bose-Einstein condensate (BEC).

This low temperature below T_c is typically very close to absolute zero temperature. Since all the atoms are in the same state, they all have the same behaviour.

1

As the temperature decreases each atom forms a wavelet and as the temperature decreases further the wavelets of the atoms overlap and lose sense of identity, that is the wavelets of the atoms cannot be identified separately because of the overlaps. As the system gets yet cooler, below T_c all the wavelets form one giant wave which is the BEC state. Thus, BEC is a macroscopic quantum mechanical state. The critical temperature, T_c, depends on the particle density of the system which at the centre of a BEC of atomic cloud is typically within the range $10^{13} - 10^{15} \text{cm}^{-3}$ [89]. BEC has been achieved at temperatures below 500 picokelvin [65].

BEC was first conceived by Bose [15], between $1924 - 1925$, and later extended by Einstein [30, 31]. Bose and Einstein predicted the statistical distribution of bosons and the behaviour of BEC at low temperatures but during this period there was no technology in place to experimentally cool a system close to the needed temperature. But in 1995, the first BEC was produced in the laboratory with dilute gas of Rb [7] and soon after Na [28] using laser cooling technique [23, 24, 75, 90]. Since then BEC has been achieved in many other atoms [16, 17].

The realization of BEC has opened doors to many research areas. For instance, research has being carried out on the interference between condensates due to wave-particle duality [53], transition between superfluid and Mott insulator phases [39, 80], slowing down and stopping of light [29, 46]. The relevance of the theory of BEC is not limited to bosonic systems. Fermionic condensates consisting of Cooper pairs has been achieved in BCS–BEC crossover regime [95] and studies have been carried out on the BEC of excitons [55, 83]. In this study we are focusing only on BEC of bosonic atoms.

1.2 Optical lattices

An optical lattice is produced when laser beams propagating in opposite directions meet to produce a spatially periodic polarization pattern through their interference. The periodic potential created is used to trap neutral atoms. The trapping is made possible by the dipole-dipole interaction between the atoms and the laser. The ability of optical lattices to trap cold atoms and also allow quantum tunnelling makes it a useful tool in ultracold atomic physics. It is applied in atomic clocks [106], sub-recoil cooling [27, 90], realization of Tonks-Girardeau gas [86] and control of the degree of freedom in molecules [96].

When an optical lattice is used with BEC, some interesting features such as the superfluid-Mott insulator (SF-MI) and magnetic phase transitions are observed. Ultracold atomic system in optical lattice is a handy way of making use of Bose-Hubbard model (BHM) and it is a promising theory for investigating the advantages of quantum systems and various quantum Hamiltonians [6, 80]. We will later, in chapter 3, use the Bose-Hubbard model to diagonalize Hamiltonian of a BEC in an optical lattice. In optical lattices, many parameters can be controlled. The advantages of using optical lattices include [67, 80]:

- The system is essentially defect free.

- Different lattice geometry and dimensions can be achieved.

- The interaction is simpler than ordinary condensed matter system because it is mostly due to the s-wave (isotropic) scattering as most of the atoms in a condensate are in the ground state.

- The parameters are controllable.

- Different types of external potential can be applied.

Other advantages are listed in Ref. [67].

A wide range of phenomena can be observed by the use of ultracold atoms in optical lattices. Quantum phase transition between superfluid and Mott insulator phase [39, 67] and low dimensional systems in 1D [59, 105] and 2D [43] have already been experimentally achieved. Other applications include ferromagnetism, anti-ferromagnetism [36, 92] and quantum information [51].

1.3 Quantum phase transition

A quantum phase is a quantum state at absolute zero temperature. At $T = 0$, thermal fluctuations are frozen out but there are still quantum fluctuations in the ground state of the system. Thus, the system is capable of supporting phase transitions at $T = 0$. Hence, quantum phase transition (QPT) is a phase transition that occurs at absolute zero temperature or a phase transition between different quantum phases. QPT can be achieved by varying a physical (an external) parameter at absolute zero temperature. Such an external parameter includes magnetic field and interaction strength. QPT has been studied in details in [20, 97].

In phase transitions the order parameter, denoted here by ϑ, vanishes for some values of the external quantity and finite for others, i.e. the order parameter can be switched on or off, in the ground state of the system. So a QPT has a critical

point around which the order parameter fluctuates. An order parameter is a quantity which has a finite value in one phase (usually below the critical point) and vanishes in another phase (usually above the critical point). Examples of order parameters are magnetization for ferromagnets, Cooper-pairs for superconductors and superfluid density for superfluid.

Although, QPT occurs only at $T = 0$, QPT physical properties at $T > 0$ are used to describe the divergence at $T = 0$ (this is because experiments are done at finite temperature). At finite temperatures, the system will either exhibit a singularities at $T = 0$ or makes a phase transition at $T > 0$ near the critical value of the order parameter ϑ_c. At $T > 0$ there exist thermal energy given by $k_B T$ (where k_B is the Boltzmann constant) which competes with the characterization energy Δ of the system at absolute zero temperature. The phase diagram of a quantum system is shown in figure 1.1.
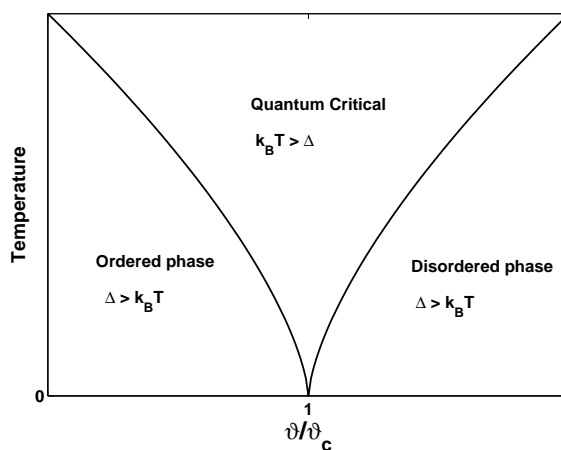
Figure 1.1: Different phases of a quantum system. The values of the order parameter ϑ and charactereistic energy Δ play major roles in determining the phase the system will be. The point $\vartheta/\vartheta_c = 1$ is the QCP.

QPT has been observed in BEC. The characterization energy, Δ, in the excitation spectrum of ^{87}Rb has been measured [39] and it has been shown, both experimentally and theoretically, that BEC loaded in optical lattices show phase transition from superfluid (SF) phase to Mott insulator (MI) phase by the varying strength of external periodic potential [5] and by varying the competing terms in the underlying Hamiltonian via commensurate and incommensurate filling of lattice sites [40] but in this research we will focus on varying the hopping matrix and spin-orbit coupling strength. A simple theory for describing the physical properties of QPT (for BEC) is the quantum rotor model. This topic will not be discussed in this thesis but details can be found in [97]. However, we will investigate phase transitions in multicomponent Bose-Einstein condensates in the presence of spin-otbit coupling in chapter 4.

1.4   Outline

We present here the outline of this thesis. In chapter 2, we present basic theory of BEC. The effect of particle interaction, like superfluidity, as well as excitation spectrum of BEC are discussed. In chapter 3, we discussed optical lattice and Bose-Hubbard model for BEC loaded into optical lattices and then generalized the theory to accommodate multicomponent BEC. We also discussed different phases of BEC, transitions between them and mean-field theories for analytical investigation of phase boundaries. In chapter 4, we studied quantum phase transition in a spin-orbit coupled BEC in the one dimensional lattice, square lattice and hexagonal lattice using perturbation and variational approaches. Finally, conclusion and outlook is presented in chapter 5.

Chapter 2

Basic theory of Bose-Einstein condensates

The basic theory of BEC has been extensively discussed in the literature. In this chapter, we present a brief discussion of the basic properties and theories of BEC. Detailed treatment can be found in textbooks [11, 58, 68, 89], review papers [27, 66] and theses [56, 80]. In depth discussion of second quantization formalism can be found in [18, 25, 32]. The chapter is based mainly on Refs. [80, 89].

2.1 Bose-Einstein condensates

As mentioned in section (1.1), bosons do not obey the Pauli exclusion principle and this makes it possible for more than one boson to occupy the same single-particle state. Theoretically, there is no limit to the number of bosons that can occupy a single state. Hence, when the temperature of a bosonic system reduces

more particles fall into the ground state of the system in accordance to Bose-Einstein statistics. Below a critical temperature, T_c, the occupation number N_o in the ground state approaches the total number of particles N in the system. Such macroscopic quantum occupation of a single particle state is called Bose-Einstein condensation. Also, as mentioned in the previous chapter the wave packets of the atoms overlap with each other and they cannot be distinguished. The behaviour of the system depends on whether there are interactions between atoms or not as we will see later. We can calculate the T_c for a uniform gas with no internal degrees of freedom.

For a system of bosons with particles of mass m the thermal de Broglie wavelength of an atom is

$$\lambda_T = \sqrt{\frac{2\pi\hbar^2}{mk_BT}} \tag{2.1}$$

At low temperatures (such as T_c), the thermal de Broglie wavelength is comparable to the distance between the atoms $n^{-\frac{1}{3}}$, where n is particle density. Thus we have

$$\lambda_T \sim n^{-\frac{1}{3}} \tag{2.2}$$

which gives

$$T_c \sim \frac{2\pi\hbar^2 n^{\frac{2}{3}}}{mk_B} \tag{2.3}$$

Therefore lower T_c is needed for massive atoms than for light atoms.

Consider a system of gas in a harmonic trap. Let the size of the gas cloud be R and N the number of particles in the system, then the density $n \sim N/R^3$, where $R \sim \sqrt{k_BT/m\omega^2}$. ω is the frequency of single-particle motion in the har-

monic trap. At $T = T_c$ we have

$$k_B T_c = C\hbar\omega N^{\frac{1}{3}} \tag{2.4}$$

$C \approx 0.94$ and this will be shown to be so in the next subsection. T_c for some systems have been measured. It is 3.13 K for helium-4 [89].

2.1.1 Non-interacting Bose gas

We consider a system of non-interacting Bose gas in a harmonic trap. The trap is anisotropic with frequencies ω_x, ω_y and ω_z in x, y and z directions respectively. The trap potential is then given by

$$V(r) = \frac{m}{2}(\omega_x{}^2 x^2 + \omega_y{}^2 y^2 + \omega_z{}^2 z^2) \tag{2.5}$$

The energy spectrum of the system is

$$E_{n_x,n_y,n_z} = (n_x + \frac{1}{2})\hbar\omega_x + (n_y + \frac{1}{2})\hbar\omega_y + (n_z + \frac{1}{2})\hbar\omega_z \tag{2.6}$$

where n_x, n_y, n_z are positive integers.

From statistical mechanics, the partition function of the system is

$$Z = \prod_{i=1}^{\infty}[1 - e^{\beta(\mu - E_{n_{x_i},n_{y_i},n_{z_i}})}]^{-1} \tag{2.7}$$

μ is the chemical potential and $\beta = \frac{1}{k_B T}$ is the Boltzmann factor. The average energy of the system is

$$E = <E> = -\frac{\partial}{\partial\beta}\ln Z = \sum_{n_x}^{\infty}\sum_{n_y}^{\infty}\sum_{n_z}^{\infty}\frac{E_{n_x,n_y,n_z}}{[e^{\beta(E_{n_x,n_y,n_z}-\mu)} - 1]} \tag{2.8}$$

And the average number of the particles is

$$N = <N> = \frac{1}{\beta}\frac{\partial}{\partial\mu}\ln Z = \sum_{n_x}^{\infty}\sum_{n_y}^{\infty}\sum_{n_z}^{\infty}\frac{1}{[e^{\beta(E_{n_x,n_y,n_z}-\mu)} - 1]} \tag{2.9}$$

9

As $T \longrightarrow 0$, $\mu \longrightarrow E_{000}$ we can write equation (2.9) as

$$N = N_o + \sum_{n_x \neq 0}^{\infty} \sum_{n_y \neq 0}^{\infty} \sum_{n_z \neq 0}^{\infty} \frac{1}{[e^{\beta(E_{n_x,n_y,n_z} - \mu)} - 1]} = N_o + N_{\text{ex}} \tag{2.10}$$

N_o is the number of particles in the ground state of the system and N_{ex} is the number of particles in the excited state. Since N is large, typically between $10^{13} - 10^{15}$, the summation in the leading equation can be replaced with an integral so that we have

$$N_{\text{ex}} = N - N_o = \zeta(3) \left(\frac{k_B T}{\hbar \omega_{ho}} \right)^3 \tag{2.11}$$

where $\omega_{ho} = (\omega_x \omega_y \omega_z)^{\frac{1}{3}}$ is oscillator frequency and $\zeta(n)$ is the Rieman zeta function with $\zeta(3) = 1.202$. Values of $\zeta(n)$ and its relations can be found in [4, 38].

The maximum value of N_{ex} occurs at $\mu = 0$ and the transition temperature T_c is calculated under the condition that the total number of particles N can be accommodated in the excited state (i.e. $N_o = 0$). Then equation (2.11) becomes

$$k_B T_c = 0.94 \hbar \omega N^{\frac{1}{3}} \tag{2.12}$$

Equation (2.12) is the same as equation (2.4) but also includes the value of the constant C as claimed earlier. Using equations (2.4) and (2.11) we obtain the condensate fraction of a three-dimensional harmonic oscillator in terms of the critical temperature as

$$\frac{N_o}{N} = 1 - \left(\frac{T}{T_c} \right)^3 \tag{2.13}$$

Figure 2.1 displays the behaviour of equation (2.13).
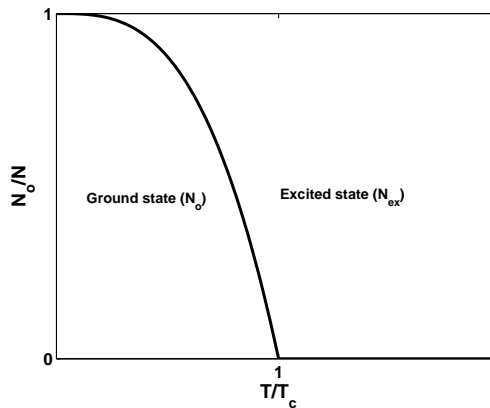
Figure 2.1: The condensate fraction (N_o/N) with normalized temperature (T/T_c) for a BEC in 3D harmonic trap

2.1.2 Interacting system

We now consider a system with interaction between the atoms in a BEC. In cold atoms particle separations, typically of order 10^2 nm, are usually larger than the length scales of atom-atom interaction. Thus, interactions in cold atoms is predominantly two-body interactions. Since the atoms in a BEC are in the ground state, the effective interaction between atoms in BEC is due to s-wave scattering process. The effective two-body interaction may then be written as a short range interaction potential

$$U\left(\mathbf{r}_i, \mathbf{r}_j\right) = U_o \delta\left(\mathbf{r}_i - \mathbf{r}_j\right) \tag{2.14}$$

where the interaction strength $U_o = 4\pi a^2/m$, a is the scattering length and m is the atomic mass. $U_o \delta\left(\mathbf{r}_i - \mathbf{r}_j\right)$ is a contact interaction with $\mathbf{r}_i$ and $\mathbf{r}_j$ the positions of particles i and j respectively. As we will see in subsequent chapters, U_o is very important, it plays a role in determining the phase of the BEC.

The many-body Hamiltonian for a system of interacting Bose gas in a trap poten-

tial can be written as

$$H = \sum_{i=1}^{N} \left[\frac{p^2}{2m} + V\left(\mathbf{r}_i\right) \right] + \frac{U_o}{2} \sum_{i \neq j} \delta\left(\mathbf{r}_i - \mathbf{r}_j\right) \qquad (2.15)$$

$V(\mathbf{r}_i)$ is the trap potential on the particle i. The Hamiltonian in equation (2.15) can be written in second quantization form as

$$\hat{H} = \int d\mathbf{r} \left[\hat{\Psi}^{\dagger}(\mathbf{r}) \left(-\frac{\hbar^2}{2m} \nabla^2 + V_{trap}(\mathbf{r}) \right) \hat{\Psi}(\mathbf{r}) + \frac{U_o}{2} \hat{\Psi}^{\dagger}(\mathbf{r}) \hat{\Psi}^{\dagger}(\mathbf{r}) \hat{\Psi}(\mathbf{r}) \hat{\Psi}(\mathbf{r}) \right] \quad (2.16)$$

$\hat{\Psi}^{\dagger}(\mathbf{r})$ and $\hat{\Psi}(\mathbf{r})$ are the boson creation and annihilation field operators.

When the temperature is close to the critical temperature, the number of atoms N_o in the condensate is large and comparable to the total number of particles N in the system. Hence, the wave function or field operator of the system can be separated into two parts: one part for the atoms in the condensate ($\Phi(\mathbf{r})$) and one part for the excited states ($\xi_o(\mathbf{r})$), due to quantum fluctuation. Taking figure 2.1 into consideration $\Phi(\mathbf{r})$ is the wave function of the atoms bound by the curve while $\xi_o(\mathbf{r})$ is the wave function of the atoms outside the curve(i.e. excited state). $\xi_o(\mathbf{r})$ is small compared to $\Phi(\mathbf{r})$ and can be treated as a perturbation. Therefore, we can apply Bogoliubov approximation [18, 25, 32] as

$$\hat{\Psi}(\mathbf{r}) = \Phi(\mathbf{r}) + \xi_o(\mathbf{r}) \qquad (2.17)$$

where the complex function $\Phi(\mathbf{r})$ is the expectation value of the operator $\hat{\Psi}(\mathbf{r})$ and the condensate density $n_o(\mathbf{r}) = |\Phi(\mathbf{r})|^2$. $\Phi(\mathbf{r})$ is a classical field which is analogous classical electric and magnetic fields.

Let us assume that $N_o \sim N$, then $\xi_o(\mathbf{r}) \ll \Phi(\mathbf{r})$ so that we can neglect $\xi_o(\mathbf{r})$. We can then replace $\hat{\Psi}(\mathbf{r})$ by $\Phi(\mathbf{r})$ in equation (2.16). The resulting Hamiltonian is

then inserted into the Heisenberg equation of motion $\left(i\hbar\frac{\partial}{\partial t}\hat{\Psi}(\mathbf{r},t) = \left[\hat{\Psi}(\mathbf{r},t),\hat{H}\right]\right)$ to obtain

$$i\hbar\frac{\partial}{\partial t}\Phi(\mathbf{r},t) = \left(-\frac{\hbar^2}{2m}\nabla^2 + V(\mathbf{r}) + U_o|\Phi(\mathbf{r})|^2\right)\Phi(\mathbf{r},t) \qquad (2.18)$$

Equation (2.18) is known as the Gross-Pitaevskii equation (GPE) and it determines the dynamics of BEC. GPE is nonlinear Schrodinger equation with a normalization condition $\int d\mathbf{r}\ n_o(\mathbf{r}) = N$. The GPE accepts solutions of the form $\Phi(\mathbf{r},t) = \phi(\mathbf{r})e^{-i\mu t/\hbar}$ which transfroms equation (2.18) into

$$\left(-\frac{\hbar^2}{2m}\nabla^2 + V(\mathbf{r}) + U_o|\phi(\mathbf{r})|^2\right)\phi(\mathbf{r}) = \mu\phi(\mathbf{r}) \qquad (2.19)$$

Equation (2.19) is the time independent form of the GPE. $\phi(\mathbf{r})$ can be taken as real and we will revisit it when we discuss order parameter in chapter 3. Equation (2.19) has been solved under different conditions. If there is no trapping potential the solutions are solitons; dark and bright soliton solutions have also been obtained for some hyperbolic potentials [57]. If there is no interaction the equation reduces to Schrodinger equation.

For a condensate with large number of atoms, the interaction between atoms becomes very strong and larger than the kinetic energy term such that the first term on the left hand side (lhs) of equation (2.19) can be neglected. The GPE then reduces to

$$\left[V(\mathbf{r}) + U_o|\phi(\mathbf{r})|^2\right]\phi(\mathbf{r}) = \mu\phi(\mathbf{r}) \qquad (2.20)$$

Then the solution of the GPE in this approximation, commonly referred to as the Thomas-Fermi approximation, is

$$n(\mathbf{r}) = |\phi(\mathbf{r})|^2 = \frac{1}{U_o}[\mu - V(\mathbf{r})] \qquad (2.21)$$

Equation (2.21) is valid for the regions with $\mu > V(\mathbf{r})$. The solution vanishes for every other points. This means that the energy that is gained by a particle at any point in the condensate is the same everywhere. Assuming a harmonic trap, the normalization condition yields the chemical potential as [89]

$$\mu = \frac{15^{2/5}}{2} \left(\frac{a}{a_{ho}} \right)^{2/5} \hbar \omega_{ho} \tag{2.22}$$

where $a_{ho} = \sqrt{\hbar / m \omega_{ho}}$ is the characteristic oscillator length.

2.2   Excitation spectrum

We take a look at a system of interacting Bose gas in a box of volume V. We start our calculations with the Hamiltonian in equation (2.16) but in lieu of the field operators $\hat{\Psi}^\dagger(\mathbf{r})$ and $\hat{\Psi}(\mathbf{r})$ we use their Fourier transforms $\hat{\Psi}(\mathbf{r}) = \frac{1}{V} \sum_{\mathbf{k}} e^{i\mathbf{k}.\mathbf{r}} \mathbf{b_k}$. The Hamiltonian then becomes

$$\hat{H} = \sum_{\mathbf{k}} \epsilon_{\mathbf{k}}^o \mathbf{b_k^\dagger b_k} + \frac{U_o}{2V} \sum_{\mathbf{q,k,k'}} \mathbf{b_{k+q}^\dagger b_{k'-q}^\dagger b_{k'} b_k} \tag{2.23}$$

where $\epsilon_{\mathbf{k}}^o = \hbar^2 \mathbf{k}^2 / 2m$ is the free particle energy. $\mathbf{b_k}$ and $\mathbf{b_k^\dagger}$ are respectively the boson annihilation and creation operators in states with wave vector $\mathbf{k}$. The operators obey the commutation relations $[\mathbf{b_k}, \mathbf{b_{k'}}] = \left[\mathbf{b_k^\dagger}, \mathbf{b_{k'}^\dagger} \right] = 0$ and $\left[\mathbf{b_k}, \mathbf{b_{k'}^\dagger} \right] = \delta_{\mathbf{kk'}}$. The transfer momentum $\mathbf{q}$ comes from the interaction potential. It is the amount of momentum exchanged by the atoms when they collide.

It is clear that the interaction part H_I, the second term on the right hand side (rhs) of equation (2.23), is not diagonalized which makes equation (2.23) difficult to solve. To solve this, we fall back on our discussion in subsection (2.1.2) where

we assumed that the number of atoms in the condensate N_o is close to the total number of atoms N in the system ($N_o \longrightarrow N$) such that the wave function of the excited state can be ignored in the Bogoliubov approximation. With this assumption, the contribution of higher order terms of the excitation wave function to the interaction term is ignorable since $\xi_o(\mathbf{r})$ is very small. Hence, it is reasonable to retain only terms that are quadratic in $\mathbf{b_k}$ and $\mathbf{b_k^\dagger}$ for $\mathbf{k} \neq 0$. The second term on the rhs of equation (2.23), becomes

$$\hat{H}_I = \frac{U_o}{2V} \left[\mathbf{b_o^\dagger b_o^\dagger b_o b_o} + \sum_{\mathbf{k}\neq 0} \left(4\mathbf{b_k^\dagger b_k b_o^\dagger b_o} + \mathbf{b_k^\dagger b_{-k}^\dagger b_o b_o} + \mathbf{b_o^\dagger b_o^\dagger b_k b_{-k}} \right) \right] \quad (2.24)$$

In arriving at equation (2.24) we have ordered the operators according to Wick's ordering [14, 63]. We can make a further approximation by replacing $\mathbf{b_o}$ and $\mathbf{b_o^\dagger}$ by $\sqrt{N_o}$. This approximation, first used by Bogoliubov [14], is obtained from the properties of the ladder operators, i.e. $(\mathbf{b_o^\dagger}|N_o\rangle = \sqrt{N_o + 1}|N_o + 1\rangle$ and $\mathbf{b_o^\dagger}|N_o\rangle = \sqrt{N_o}|N_o - 1\rangle)$ as $N_o \gg 1$. Using this approximation we have

$$\hat{H}_I \approx \frac{U_o}{2V} \left[N_o^2 + N_o \sum_{\mathbf{k}\neq 0} \left(4\mathbf{b_k^\dagger b_k} + \mathbf{b_k^\dagger b_{-k}^\dagger} + \mathbf{b_k b_{-k}} \right) \right] \quad (2.25)$$

The total number operator in the system is

$$\hat{N} = \sum_{\mathbf{k}} \mathbf{b_k^\dagger b_k} = \mathbf{b_o^\dagger b_o} + \sum_{\mathbf{k}\neq 0} \mathbf{b_k^\dagger b_k} \quad (2.26)$$

Using equation (2.26) in equation (2.25) with $n_o = N_o/V \longrightarrow n = N/V$ being the density of atoms and then substituting the result into equation (2.23) we obtain the Hamiltonian as

$$H = \frac{1}{2} U_o n^2 V + \frac{1}{2} \sum_{\mathbf{k}\neq 0} \left[2 \left(\epsilon_{\mathbf{k}}^o + nU_o \right) \mathbf{b_k^\dagger b_k} + \left(\mathbf{b_k^\dagger b_{-k}^\dagger} + \mathbf{b_k b_{-k}} \right) \right] \quad (2.27)$$

It is to be noted that equation (2.27) is an approximation of equation (2.23) up to N^2.

We can now diagonalize the Hamiltonian. This is done by using a conical transformation also referred to as Bogoliubov transformation. To do this we define new creation and annihilation operators $\alpha_{\mathbf{k}}$ and $\alpha_{\mathbf{k}}^{\dagger}$ such that

$$\begin{pmatrix} \alpha_{\mathbf{k}} \\ \alpha_{-\mathbf{k}}^{\dagger} \end{pmatrix} = \begin{bmatrix} u_{\mathbf{k}} & v_{\mathbf{k}} \\ v_{\mathbf{k}} & u_{\mathbf{k}} \end{bmatrix} \begin{pmatrix} \mathbf{b_{k}} \\ \mathbf{b_{-k}^{\dagger}} \end{pmatrix} \tag{2.28}$$

$u_{\mathbf{k}}$ and $v_{\mathbf{k}}$ are real functions of $\mathbf{k} = |\mathbf{k}|$. To make this transformation canonical we impose commutation relations on $\alpha_{\mathbf{k}}$ and $\alpha_{\mathbf{k}}^{\dagger}$ such that α-operators obey the same commutation relations as the $\mathbf{b}$-operators and also subject Wick's ordering. The condition $[\alpha_{\mathbf{k}}, \alpha_{\mathbf{k}'}] = \delta_{\mathbf{k}\mathbf{k}'}$ gives

$$u_{\mathbf{k}}^2 - v_{\mathbf{k}}^2 = 1 \tag{2.29}$$

We use equation (2.27) in equation (2.28) to get

$$\begin{aligned}
\hat{H} =& \frac{1}{2}U_o n^2 V + \frac{1}{2}\sum_{\mathbf{k}\neq \mathbf{0}}\left[\left(\epsilon_{\mathbf{k}}^o + nU_o\right)v_{\mathbf{k}}^2 - nU_o u_{\mathbf{k}}v_{\mathbf{k}}\right] \\
&+ \frac{1}{2}\sum_{\mathbf{k}\neq \mathbf{0}}\{\left[\left(\epsilon_{\mathbf{k}}^o + nU_o\right)\left(u_{\mathbf{k}}^2 + v_{\mathbf{k}}^2\right) - 2nU_o u_{\mathbf{k}}v_{\mathbf{k}}\right]\left(\alpha_{\mathbf{k}}^{\dagger}\alpha_{\mathbf{k}} + \alpha_{-\mathbf{k}}^{\dagger}\alpha_{-\mathbf{k}}\right)\} \\
&+ \frac{1}{2}\sum_{\mathbf{k}\neq \mathbf{0}}\{\left[nU_o\left(u_{\mathbf{k}}^2 + v_{\mathbf{k}}^2\right) - 2u_{\mathbf{k}}v_{\mathbf{k}}\left(\epsilon_{\mathbf{k}}^o + nU_o\right)\right]\left(\alpha_{\mathbf{k}}^{\dagger}\alpha_{-\mathbf{k}}^{\dagger} + \alpha_{\mathbf{k}}\alpha_{-\mathbf{k}}\right)\} \quad \tag{2.30}
\end{aligned}$$

The last term of equation (2.30) does not conform to diagonal matrix so we let it vanish by setting its coefficient to zero.

$$nU_o\left(u_{\mathbf{k}}^2 + v_{\mathbf{k}}^2\right) - 2u_{\mathbf{k}}v_{\mathbf{k}}\left(\epsilon_{\mathbf{k}}^o + nU_o\right) = 0 \tag{2.31}$$

We note that the condition in equation (2.29) is satisfied if $u_{\mathbf{k}} = \cosh\theta_{\mathbf{k}}$ and $v_{\mathbf{k}} = \sinh\theta_{\mathbf{k}}$ which reduce equation (2.31) to

$$\tanh 2\theta_{\mathbf{k}} = nU_o/\left(\epsilon_{\mathbf{k}}^2 + nU_o\right) \tag{2.32}$$

16

where

$$\epsilon_{\mathbf{k}} = \sqrt{(\epsilon_{\mathbf{k}}^o + nU_o)^2 - (nU_o)^2} \qquad (2.33)$$

$\epsilon_{\mathbf{k}}$ is the excitation spectrum and it is always positive. In chapter 3, we will obtain the excitation spectrum for a two component BEC and use it to discuss phase separation.

The values of $u_{\mathbf{k}}$ and $v_{\mathbf{k}}$ can be obtained from equation (2.29) by using hyperbolic identities. Using the results in equation (2.30) we obtain the diagonalized form of the Hamiltonian as

$$\hat{H} = \frac{1}{2}U_o n^2 V - \frac{1}{2}\sum_{\mathbf{k}\neq\mathbf{0}}(\epsilon_{\mathbf{k}}^o - \epsilon_{\mathbf{k}} + nU_o) + \frac{1}{2}\sum_{\mathbf{k}\neq\mathbf{0}}\epsilon_{\mathbf{k}}\left(\alpha_{\mathbf{k}}^\dagger\alpha_{\mathbf{k}} + \alpha_{-\mathbf{k}}^\dagger\alpha_{-\mathbf{k}}\right) \qquad (2.34)$$

The ground state energy is obtained using the condition that $\alpha_{\mathbf{k}}|\mathbf{0}\rangle = \mathbf{0}$, where $|\mathbf{0}\rangle$ is the ground state. It should be noted that $\mathbf{b}_{\mathbf{k}}$ and $\mathbf{b}_{\mathbf{k}}^\dagger$ are not operators of the ground state. The system behaves as a collection of non-interacting bosons and the ground state $|\mathbf{0}\rangle$ may be interpreted as a quasiparticle vacuum which is a combination of unperturbed states. If we write the number operator [equation (2.26)] in terms of $\alpha_{\mathbf{k}}$ and $\alpha_{\mathbf{k}}^\dagger$ and consider a situation where we have large momentum associated with the excitations, the interaction in the system removes particles from the zero momentum condensate. The condensate depletion is given by [89]

$$\frac{N_{\mathrm{ex}}}{N} = \frac{8}{3}\left(\frac{na^3}{\pi}\right)^{\frac{1}{2}} \qquad (2.35)$$

In weakly interacting systems the depletion is very low since $N_{\mathrm{ex}} \ll N$. From equation (2.34) it follows that the creation of an elementary excitation with wavevector $\mathbf{k}$ (obtained by $\alpha_{\mathbf{k}}^\dagger|\mathbf{0}\rangle$) is the superposition of two states $-$ one with the addition of a particle with wavevector $\mathbf{k}$ by the extraction of a particle from the condensation and the other with the extraction of a particle with wavevector $-\mathbf{k}$ and added to

the condensate.

The expectation spectrum of the condensates is given by equation (2.33). In the long wavelength limit ($\mathbf{k} \longrightarrow 0$), $u_{\mathbf{k}} \approx v_{\mathbf{k}}$, there is phonon mode excitations and the spectrum is $\epsilon_{\mathbf{k}} = \mathbf{v_s}\,(\hbar \mathbf{k})$, $\mathbf{v_s}$ is the speed of sound. In the short wavelength limit, ($\mathbf{k} \longrightarrow \infty$), $\alpha_{\mathbf{k}}^{\dagger} = \mathbf{b}_{\mathbf{k}}^{\dagger}$, the particles behave like free particles and the spectrum becomes $\epsilon_{\mathbf{k}} = \epsilon_{\mathbf{k}}^{o} + nU_o$.

2.3   Superfluidity in Bose-Einstein condensates

Superfluidity is a state of matter in which the matter behaves like a fluid without viscosity. Superfluid is one of the phases of a BEC. In a superfluid matter circulating flows are quantized which gives quantized vortices [3, 74] and like a superconductor, a superfluid can carry current without dissipation. A non-interacting BEC does not exhibit superfluidity. The ingredient that makes superfluidity possible is the interaction between the atoms in the system. The necessary condition for superfluidity is called *Landau Criterion.*

The Landau Criterion: We look at a situation a heavy object which is moving in a condensate with a constant velocity and creates excitation in the condensate as it moves [89]. The excitation created by the moving object is proportional to the velocity of the object and therfore below a certain speed of the object there will no excitation in the condensate. At this point the energy of the particle is less than the excitation energy of the condensate.

Let the potential due to the obstacle, at some reference point $\mathbf{R}(t)$ in the obstacle, be $V(\mathbf{r} - \mathbf{R}(t))$. The position of the obstacle at a given time is $\mathbf{R}(t) = \mathbf{R}(0) + \mathbf{v}(t)$, where $\mathbf{v}$ is the uniform velocity of the particle. The time-dependent potential exerted by the obstacle is capable of transferring energy to the system by creating excitations. Fourier transforming the potential gives $\tilde{V}_o(\mathbf{q})\, e^{-i\mathbf{q}\cdot\mathbf{v}}$, where $\tilde{V}_o(\mathbf{q}, \omega) = \tilde{V}_o\delta(\omega - \mathbf{q}\cdot\mathbf{v})$, which means the potential can transfer momentum $\hbar\mathbf{q}$ to the condensate if it has the ability to transfers energy $\hbar\mathbf{q}\cdot\mathbf{v}$. Therefore, the superfluid will remain stable if

$$\epsilon_{\mathbf{q}} > Max(\mathbf{q}\cdot\mathbf{v}) = \mathbf{q}\cdot\mathbf{v} \qquad \forall \mathbf{q} \tag{2.36}$$

The minimum velocity v_c required to create excitation in a superfluid is given by

$$v_c \geq Min\left(\frac{\epsilon_{\mathbf{q}}}{\mathbf{q}}\right) \tag{2.37}$$

v_c is referred to as Landau critical velocity. If $v < v_c$ creation of excitations is impossible and the liquid will exhibit superfluidity. From the excitation spectrum $v_c = c =$ velocity of sound for the long wave length limit, $\mathbf{k} \longrightarrow 0$. The critical velocity can be generalized to multicomponent BEC. For instance, v_c is calculated for a two-component BEC in [70].

Chapter 3

Bose-Einstein condensates in optical lattices

3.1 Optical lattices

Optical lattice is a very important and handy tool for studying ultra-cold atoms. As mentioned in section (1.2), it makes the physics of BEC more interesting. In this section we will discuss optical lattices, its properties and how it is used to study BEC. More discussions on BEC in optical lattices can be found in [13, 22, 41, 79].

3.1.1 Optical dipole trap

The method of trapping of atoms here is taking advantage of the interaction of the atoms with detuned light. Detuning is the difference between the laser frequency and frequency of the atomic transition. Optical dipole force arises from the dis-

persion interaction between a laser field (light) and the dipole moment of the atom.

When atoms are placed in a laser field they experience two types of forces, viz a dissipative or scattering force and a dipole force. The electric field of the light interacts with the induced dipole moment and this alters the energy levels of the atoms. This shifts in energy can be calculated using second order perturbation [41, 89] from which the scattering rate is obtained. The scattering rate for two-level system is [80]

$$\Gamma_{sc} = \Gamma . \rho_{ec} = \frac{S_o/2}{1 + S_o + (2\delta/\Gamma)^2} \tag{3.1}$$

where ρ_{ec} is the population of the excited state of the system. The subscript sc denotes scattering. Γ is a natural line width (or spontaneous decay rate of excited state) of atomic transition. S_o is a saturation parameter defined as $S_o = I/I_{sat}$. I is the intensity of the laser beam and I_{sat} is a saturation intensity of the transition. The detuning is defined as $\delta = \omega - \omega_o$. ω is the angular frequency of the laser beam and ω_o is the angular optical transition frequency between the ground state and the excited level. When $\delta < 0 \, (\omega < \omega_o)$, it is referred to as red-detuned lattice light, atoms will be drawn to high intensity and the detuning contributes a negative energy to the ground state energy. When $\delta > 0, (\omega > \omega_o)$ it is referred to as blue detuning, atoms will be repelled to lower intensity. Hence, atoms can be trapped by using a red-detuned light or repelled by using a blue–detuned light.

Light of wavevector $\mathbf{k}$ shifts the energy of an atom by giving it a momentum $\hbar \mathbf{k}$. The disspative force is then given by

$$\mathbf{F}_{sc} = \hbar \mathbf{k} \Gamma_{sc} \tag{3.2}$$

The dipole force is the AC stark shift. When $\delta \gg \Gamma$, the laser is far detuned from resonance, then the dipole force is the gradient of a potential

$$\mathbf{F}_{dip} = -\nabla V_{dip}$$

$$V_{dip} = \frac{\hbar\Gamma^2}{\delta}S_o \tag{3.3}$$

The intensity profile of a far red-detuned Gaussian light field propagating along $z-$axis focused on the atoms is [41]

$$I(r, z) = \frac{2P}{nw^2(z)}e^{-\frac{2r^2}{w^2(z)}} \tag{3.4}$$

where r denotes the radial coordinate, the radius $1/e^2$ depends on the $z-$axis by $w(z) = w_o\sqrt{1 + (z/z_R)^2}$, w_o is the minimum radius called the beam waist, z_R is the Rayleigh length and P is the total power of the laser. The trap depth V_o is given by the condition $z = R = 0$. In the limit that $z \ll z_R$ and $r \ll w$, the optical dipole trap can be approximated as a harmonic trap as

$$V_{dip}(r, z) \approx -V_o\left[1 - 2\left(\frac{r}{w_o}\right)^2 - \left(\frac{z}{z_R}\right)^2\right] \tag{3.5}$$

The oscillation frequency of the trapped atoms are given by $w_r = \sqrt{4V_o/mw_o^2}$ and $w_z = \sqrt{2V_o/mz_R^2}$ in the radial and axial directions respectively and the potential depth is $V_o = (\hbar\Gamma^2/8\delta I_{sat}).(P^2/\pi w_o^2)$

3.1.2 Producing optical lattices

From wave theory, it has been established that when two waves travel in opposite directions an interference pattern occurs depending on the frequencies of the waves. Just like waves, when two laser beams propagate in opposite directions, they interfere. This gives rise to a periodicity in the electric field intensity in space.

Thus, due to stark effect the atoms see a periodic potential. This section is based on [80, 89].

Consider two laser beams $\mathbf{E}_1(\mathbf{r}, t)$ and $\mathbf{E}_2(\mathbf{r}, t)$ propagating in opposite directions. The total electric field is

$$\mathbf{E}(\mathbf{r}, t) = \mathbf{E}_1(\mathbf{r}, t) + \mathbf{E}_2(\mathbf{r}, t) = \varepsilon_1 \mathbf{e}_1 e^{-i(\mathbf{k_1}.\mathbf{r}-\omega_1 t)} + \varepsilon_2 \mathbf{e}_2 e^{-i(\mathbf{k_2}.\mathbf{r}-\omega_2 t)} \qquad (3.6)$$

where ω_1, ω_2, $\mathbf{e}_1$, $\mathbf{e}_2$, ε_1, ε_2 and $\mathbf{k}_1$, $\mathbf{k}_2$ are respectively the frequencies, polarizations, magnitudes and wavevectors of $\mathbf{E}_1(\mathbf{r}, t)$ and $\mathbf{E}_2(\mathbf{r}, t)$. The intensity is given by

$$I(\mathbf{r}, t) \propto |\mathbf{E}(\mathbf{r}, t)|^2 = \varepsilon_1^2 + \varepsilon_2^2 + 2\varepsilon_1\varepsilon_2(\mathbf{e_1}.\mathbf{e_2})\mathrm{Re}\left[e^{-i[(\mathbf{k_1}-\mathbf{k_2}).\mathbf{r}-(\omega_1-\omega_2)t]} \right] \qquad (3.7)$$

The last term on the rhs equation (3.7) is the interference between the beams. The energy shift of an atom in the presence of an external electric field is given by

$$V = -\frac{1}{2}\alpha(\omega)\langle \varepsilon^2(\mathbf{r}, t) \rangle_t \qquad (3.8)$$

$\alpha(\omega)$ is the polarization of the atom, $\langle \ldots \rangle_t$ is the time average with time t very large compared to the period of the wave. It follows that the interference between the beams gives the periodic potential. If the beams are orthogonal ($\mathbf{e_1}.\mathbf{e_2} = 0$), there is no interference which means that $\mathbf{e_1}.\mathbf{e_2}$ determines the contrast of the potential. In practice maximum power is achieved by using beams of equal polarizations.

The relative detuning, $\Delta\omega = \omega_1 - \omega_2$, dictates the state of motion of the lattice produced. Two types of lattices can be achieved by adjusting $\Delta\omega$ and they are:

- **Static lattices:** If the frequencies are equal, then $\Delta\omega = 0$. The potential derived from the interference term is periodic and it is given by

$$V = \frac{V_o}{2}\cos(\Delta\mathbf{k}.\mathbf{r}) \tag{3.9}$$

where $V_o = -\alpha(\omega)\varepsilon_1\varepsilon_2(\mathbf{e_1}.\mathbf{e_2})$. When the two lattices propagate in opposite direction, z$-$axis say ($\Delta k = 2k$), the period of the optical lattice is given by $\lambda/2$, where λ is the wave length of the beam. If θ is the angle between the beams then, $\Delta\mathbf{k}.\mathbf{r} = (\lambda/2\sin(\theta/2))z$.

- **Moving lattices:** We can also have moving lattices. This happens when $\Delta\omega \neq 0$. The periodic potential will move with velocity $v = \lambda\Delta f/2$. We can therefore give acceleration to the optical lattice by changing the frequency as a function of time. This technique has been used to study the response of (stationary) BEC to accelerating lattices [78].

For two counter-propagating fields the optical lattices is then given from equation (3.5) as

$$V_{latt} = -\frac{V_o}{2}\cos(2kz)\left[1 - 2\left(\frac{r}{w_o}\right)^2 - \left(\frac{z}{z_R}\right)^2\right] \tag{3.10}$$

The lattice potential is easily generalized to higher dimensions. In three dimensions, the lattices cubic potential is

$$V(x, y, z) = \frac{V_o}{2}\left[\cos(2kx) + \cos(2ky) + \cos(2kz)\right] \tag{3.11}$$

3.1.3 Band structure

Optical lattices change the dynamics of atoms in a very interesting manner. Atoms in an optical lattice are like electrons in solids. Therefore, we can treat the atoms

in an optical lattice with the same formalism used for electrons in solid but we replace the electrons with atoms. We can then apply the Bloch theorem to atoms in optical lattices. The details of the Bloch theorem analysis of single atoms in periodic potential can be found in [8]. The Schrödinger equation for an atom in a periodic potential of period d i.e. $V(\mathbf{r} + d) = V(\mathbf{r})$ is

$$\left[-\frac{\hbar^2}{2m} \nabla^2 + V(\mathbf{r}) \right] \Psi = E\Psi \tag{3.12}$$

According to Bloch theorem, the wave function can be written as

$$\Psi_j = U_{\mathbf{k}}(\mathbf{r}) e^{i\mathbf{k}.\mathbf{r}} \tag{3.13}$$

where the function $U_{\mathbf{k}}(\mathbf{r})$ has the same periodicity as the potential. We can write the wavefunction and the potential using Fourier expansion as

$$\Psi_j = \sum_{\mathbf{k}} c_{\mathbf{k}} e^{i\mathbf{k}.\mathbf{r}}, \qquad V(\mathbf{r}) = \sum_{\mathbf{k}} V_{\mathbf{k}} e^{i\mathbf{k}.\mathbf{r}}$$

We can also express the lattice potential in exponential form. Substituting the Fourier expressions into equation (3.12) gives a tridiagonal matrix for the Hamiltonian. The energy eigenvalues of the Hamiltonian yields the energy band structure $E_n(\mathbf{k})$, where n is the band index . As the energy increases, the band broadens and the forbidden gap gets smaller. We do not show the derivations and results here but it can found in [60, 80].

3.2   Wannier functions

Situations arise where the atoms are localized close to lattice sites as modelled by tight binding. Then the Bloch functions given in equation (3.13) are no longer

valid as they extend over all lattice sites. An equivalent set of functions called Wannier functions [88, 111] are defined in terms of the Bloch functions as

$$W_n \left(\mathbf{r} - \mathbf{R} \right) = \frac{1}{V_{1BZ}} \int_{V_{1BZ}} d\mathbf{k} \Psi_{n\mathbf{k}} \left(\mathbf{r} \right) e^{-i\mathbf{k}.\mathbf{R}} \tag{3.14}$$

V_{1BZ} is the volume of the first Brillouine zone and $\mathbf{R}$ is the position of lattice sites. The Wannier functions are not eigenfunctions of the Hamiltonian but are very useful in theoretical calculations. Wannier functions for different lattice points form a complete set and are orthogonal

$$\int d\mathbf{r} W_n^* \left(\mathbf{r} - \mathbf{R} \right) W_{n'} \left(\mathbf{r} - \mathbf{R'} \right) = \delta_{nn'} \delta_{\mathbf{R}\mathbf{R'}} \tag{3.15}$$

The normalization condition is

$$\int d\mathbf{r} |W_n \left(\mathbf{r} \right)|^2 = 1 \tag{3.16}$$

3.3   Bose-Hubbard model

As we mentioned in section (3.1), optical lattices reshape the physics of cold atoms. The Bose-Hubbard Model (BHM) is a very good tool box in studying BEC loaded into an optical lattices. In this section, we will show that the Hamiltonian of the system reduces to the BHM, which describes the hopping of the BEC atoms between states of the optical lattice sites. Intensive discussions on BHM can be found in [33, 37, 52, 80].

We start from the many-body Hamiltonian equation (2.16) but with inclusion

of the optical lattice potential, $V_{latt}(\mathbf{r})$, so that equation (2.16) becomes

$$\hat{H} = \int d\mathbf{r}\hat{\Psi}^\dagger(\mathbf{r})\left(-\frac{\hbar^2}{2m}\nabla^2 + V_{trap}(\mathbf{r}) + V_{latt}(\mathbf{r})\right)\hat{\Psi}(\mathbf{r})$$
$$+\frac{1}{2}\int d\mathbf{r_1}d\mathbf{r_2}\hat{\Psi}^\dagger(\mathbf{r_1})\hat{\Psi}^\dagger(\mathbf{r_2})U(\mathbf{r_1},\mathbf{r_2})\hat{\Psi}(\mathbf{r_2})\hat{\Psi}(\mathbf{r_1}) \qquad (3.17)$$

The field operators $\hat{\Psi}(\mathbf{r})$ can be expanded in terms of Wannier functions $W_n(\mathbf{r})$ basis and keeping only the lowest states, $\hat{\Psi}(\mathbf{r}) = \sum_i W_n(\mathbf{r} - \mathbf{R}_i)\mathbf{b}_i$, where $\mathbf{b}_i$ is the boson annihilation operator acting on the atom at site i with lattice site position $\mathbf{R}_i$. Equation (3.17) reduces to

$$\hat{H} = -t\sum_{\langle i,j\rangle}\mathbf{b}_i^\dagger\mathbf{b}_j + \sum_i \varepsilon_i\mathbf{n}_i + \frac{1}{2}U\sum_i \mathbf{n}_i(\mathbf{n}_i - 1) \qquad (3.18)$$

where $\mathbf{n}_i = \mathbf{b}_i^\dagger\mathbf{b}_i$ is the number operator on site i (i.e. it counts the bosons on site i); the creation and annihilation operators $\mathbf{b}_i^\dagger$ and $\mathbf{b}_i$ obey the commutation relation $\left[\mathbf{b}_i, \mathbf{b}_j^\dagger\right] = \delta_{ij}$ and all other commutation relations vanish. Also the hopping term t is the combination of kinetic and lattice potential energy and it is given by

$$t = \int d\mathbf{r}W^*(\mathbf{r} - \mathbf{R}_i)\left(-\frac{\hbar^2}{2m}\nabla^2 + V_{latt}(\mathbf{r})\right)W(\mathbf{r} - \mathbf{R}_j) \qquad (3.19)$$

$\langle i,j\rangle$ implies nearest neighbor lattice sites. t is thus the hopping matrix between adjacent sites. The negative sign show that delocalizing the atoms lowers the kinetic energy. The second term on the rhs of equation (3.18) comes from the trapping potential and the off-set energy is given by

$$\varepsilon_i = \int d\mathbf{r}W^*(\mathbf{r} - \mathbf{R}_i)V_{trap}(\mathbf{r})W(\mathbf{r} - \mathbf{R}_j) \qquad (3.20)$$

We have used the normalization condition of the Wannier functions in equation (3.16) to arrive at equation (3.20). The last term is the on-site interaction strength between two atoms on lattice site i . If we consider contact interaction $U(\mathbf{r_1}, \mathbf{r_2}) =$

$U_o\delta(\mathbf{r_1} - \mathbf{r_2})$ then

$$U = U_o \int d\mathbf{r} |W_n(\mathbf{r})|^4 \tag{3.21}$$

We also used that $\mathbf{b}_i^\dagger \mathbf{b}_i^\dagger \mathbf{b}_i \mathbf{b}_i = \mathbf{b}_i^\dagger \mathbf{b}_i \mathbf{b}_i^\dagger \mathbf{b}_i - \mathbf{b}_i^\dagger \mathbf{b}_i = \mathbf{n}_i(\mathbf{n}_i - 1)$. Equation (3.18) is the BHM. Later in this chapter we will generalize it to multicomponent Bose-Einstein condensate.

Jaksch et al., in Ref. [52], showed how to calculate U and t for any given optical lattice potential from the Wannier functions. U and t play important roles in determining the transition between SF and MI phases in a BEC. We will use the parameter $\frac{t}{U}$ as a driving parameter in this study.

3.4 Phases of Bose-Einstein condensates

When a BEC is formed it will be in a particular phase. The reason is explained in section (1.3). Though a BEC can be ferromagnetic and antiferromagnetic [56], we focus our attention on only superfluid and insulating phases of BEC and also on the transition between these phases. As mentioned in section (1.2) optical lattices facilitates SF-MI transition and the matrices U and t are the determining factors of the transition. In this section, we discuss the SF and MI phases of a BEC and how it is being influence by U and t. Studies show that SF-MI transition is observable when ultra cold atoms with repulsive interactions are confined by a periodic potential (such as optical lattices) [51]. In the following we consider two extremities viz; $t \gg U$ and $t \ll U$.

3.4.1 Superfluid phase

The first case i.e $t \gg U$ is when the tunneling (hopping) term of the atoms from one site to a different one overwhelms the interaction term. Here, the atoms move effortlessly from one site to another. In other words, it costs no energy to move an atom from one site to another. The BEC is in superfluid phase in this case. If we ignore the interaction term, i.e $U \longrightarrow 0$ and assume no disorder in the system ($\varepsilon_i = 0$) the Hamiltonian for this case is obtained from equation (3.18) as $\hat{H} = -t \sum_{\langle i,j \rangle} \mathbf{b}_i^\dagger \mathbf{b}_j$. This situation fits the tight binding approach. The ground state wave function for a many-body homogeneous system is

$$|\Psi_{\text{SF}}\rangle = \left(\frac{1}{\sqrt{M}} \sum_i \mathbf{b}_i^\dagger \right)^n |0\rangle \tag{3.22}$$

Equation (3.22) is obtained from the eigenstate of the Hamiltonian for single electron case by setting $\mathbf{k} = 0$ for ground state, M is the number of lattice sites, n is the number of atoms. n and M are large number, typically $10^4 - 10^6$ and $\sim 10^4$ respectively. Hence the probability distribution for a superfluid is the Poisson distribution. Therefore, the superfluid ground state can be expressed in terms of a set of coherent states residing at lattices sites i as [80]

$$|\Psi_{\text{SF}}\rangle_{U \longrightarrow 0} = \prod_i e^{\bar{n} a_i^\dagger} |0\rangle \tag{3.23}$$

where $\bar{n} = \langle n \rangle$ is average number of atoms per site.

A superfluid state is described by a macroscopic wave function with long-range phase coherence that extend over all lattice sites. The SF ground state becomes congested as the value of U increased from zero, when $U \gg t$ the coherent state becomes a Fock states and superfluidity disappears.

3.4.2   Mott insulator phase

We now consider the second case, where there is no hopping i.e. $U \gg t$, with $t \longrightarrow 0$. It is clear that the atoms cannot move from site to site and the system is insulating in this regime. Only the last term of Hamiltonian in equation (3.18) survives. It costs energy to move from one site to another. This energy is the gap energy which prevents the particles to migrate. The eigenstate of the Hamiltonian for a commensurable filling of n atoms per lattice sites is [89]

$$|\Psi_{\mathrm{MI}}\rangle = \prod_{i=1}^{M} \frac{\left(b_i^{\dagger}\right)^n}{\sqrt{n!}} |0\rangle \tag{3.24}$$

By commensurate filling it is meant that the number of atoms per site n is an integer and all the sites have the same number of atoms.

If one atom is moved from one site to another, the states in the two sites will become $n+1$ and $n-1$. The change in interaction energy is

$$\Delta E = \frac{U}{2} \left[(n+1)^2 + (n-1)^2 - 2n^2 \right] = U \tag{3.25}$$

Then U is the energy gap between the ground state and the first excited state. Therefore, the wavefunction of the atoms at sites i and j have little or no overlapping due to lack of hopping energy. In MI phase, there is no phase coherence and phase correlation between different lattices sites and therefore there will be commensurate filling in the system. If the hopping t is increased gradually the system will eventually go into SF phase beyond a certain value of t.

However, if we have incommensurate filling, i.e the occupation number is not an integer, this happens when the number of atom at the sites are not equal, the

system goes in the SF state. In the limit $U \gg t$, we consider a system with one atom per lattice site, if we add an atom to one of the sites in the MI phase energy is not needed to transport the added atom to another site. Hence the system exhibits superfluidity. If we otherwise remove the atom from one of the lattice sites in MI phase, it does not take energy to move an atom to the empty site. Hence the system is gapless and therefore in SF phase. Figure 3.1 below shows commensurate and incommensurate fillings in one-dimensional lattice.

SF-MI transition in One component Boson with Filling factor of one

Incommensurate filling: The system is in superfluid phase

Commensurate filling: The system is in Mott insulating phase
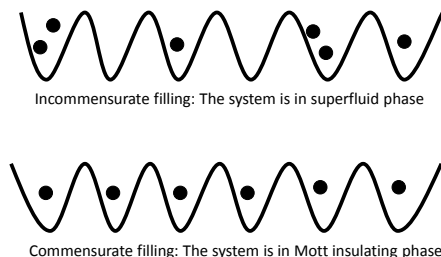
Figure 3.1: Commensurate and incommensurate fillings of a 1D lattice. In incommensurate filling of the lattice site the atoms are free to move without any energy cost whereas it cost energy U for an atom in commensurate filling to move from one site to another.

3.4.3 Superfluid – Mott insulator transition

We see that we have two extreme regimes of the ratio t/U which values determine the phase in which the system exists. For $t/U \longrightarrow \infty$ the system is in SF phase while for $t/U \longrightarrow 0$ the system is in MI phase if there is commensurable filling and SF phase if there is incommensurate filling. If t is gradually increased from

31

zero (for the $t/U \longrightarrow 0$ case) at a critical value $(\frac{t}{U})_c$ the system makes a MI–SF phase transition. The reverse is possible. Therefore, we can also effect SF–MI phase transition by increasing U of a BEC in SF phase.

These results can be generalized to multicomponent Bose-Einstein condensates (MCBEC). Research has already been carried out on this [76, 115]. One of the quests of this thesis is to investigate SF-MI phase transitions in MCBEC in the absence and presence of spin-orbit coupling. We will determine $(\frac{t}{U})_c$ for a two component BEC for these two conditions in chapter 4.

3.5 Multicomponent Bose-Einstein condensates

Hitherto, we have been discussing scalar BEC i.e BEC that contains only one type of atom or isotope and are also single spin states. It is possible to produce a BEC which contains a mixture of isotopes of atoms. This type of BEC is referred to as multicomponent Bose-Einstein condensates (MCBEC). More studies on MCBEC can be found in [89, 91]. The rest of this thesis is focused on MCBECs. We identify the following types of MCBECs.

(i) *Mixture of different atomic species*: This is a condensate of a mixture of different atomic matters with each species having one single internal state. The most interesting aspect of this type of MCBEC is the effects of cross-species interaction in the condensate. Mixture condensates have been achieved experimentally in mixture of ^{87}Rb and ^{85}Rb [26] and mixture of ^{41}K and ^{87}Rb [77]. Also, theoretical calculations have been carried out on these types of condensates [77, 107]. Mixture

condensates give interesting features that cannot observed in single condensates.

(ii) *Mixture of different hyperfine states / spinor condensates*: A spinor condensate is a condensate with more than one internal degrees of freedom. Here the same isotope of an atom is condensed into different internal spin states called hyperfine states. This is possible in atoms that have integers spins (such as alkali atoms). The hyperfine state is produced by the interaction between the nuclear spin I and the total angular momentum of the electron $\mathbf{J} = \mathbf{L} + \mathbf{S}$, where $\mathbf{L}$ and $\mathbf{S}$ are respectively orbital and spin angular momenta of the electron. The total angular momentum operator of the atoms in the system is thus

$$\mathbf{F} = \mathbf{I} + \mathbf{J} \tag{3.26}$$

$\mathbf{F}$ is the hyperfine spin operator. The hyperfine quantum number takes the values $f = |i \pm j|, (f = i + j, i + j - 1, \ldots |j + 1| - 1)$. Hence, we speak of spin-f BEC. For each value of f, there is magnetic quantum number $m_f = f, f - 1, \ldots, -f$ meaning that a spin-f BEC has $2f + 1$ possible internal degrees of freedom. Such BEC are called spinor condensates. Spin-1, 2 and 3 condensates has been realized in ^{23}Na [104], ^{87}Rb [21] and ^{52}Cr [87] respectively. Table 3.1 below show hyperfine states of some atoms and their hyperfine splitting in the ground state.

The condensate of bosonic spin-f BEC with more than one internal state is also called MCBEC. Multi-component spinor BEC of ^{87}Rb has been experimentally realized for the mixture of hyperfine states $|f = 2, m_f = 2\rangle$ and $|f = 1, m_f = 1\rangle$ [45, 81] while a two component BEC by the two different spin states ($|f = 1, m_f = 0\rangle$ and $|f = 2, m_f = 1\rangle$) of ^{23}Na has been achieved in Ref. [102].

Isotope	s	j	i	f	$\Delta E_{hf}/h(MHZ)$
^{1}H	$\frac{1}{2}$	$\frac{1}{2}$	$\frac{1}{2}$	0, 1	1420
^{7}Li	$\frac{1}{2}$	$\frac{1}{2}$	$\frac{3}{2}$	1, 2	804
^{23}Na	$\frac{1}{2}$	$\frac{1}{2}$	$\frac{3}{2}$	1, 2	1772
^{39}K	$\frac{1}{2}$	$\frac{1}{2}$	$\frac{3}{2}$	1,2	462
^{41}K	$\frac{1}{2}$	$\frac{1}{2}$	$\frac{3}{2}$	1, 2	254
^{52}Cr	3	3	0	3	–
^{85}Rb	$\frac{1}{2}$	$\frac{1}{2}$	$\frac{5}{2}$	2, 3	3036
^{87}Rb	$\frac{1}{2}$	$\frac{1}{2}$	$\frac{3}{2}$	1, 2	6835
^{133}Cs	$\frac{1}{2}$	$\frac{1}{2}$	$\frac{7}{2}$	3, 4	9193

Table 3.1: List of some bosonic spin-f atoms. ΔE_{hf} is the hyperfine splitting energy. In the table ^{6}Li and ^{40}K are omitted because they are fermionic. The table is taken from Refs. [56, 89]

Spinor BEC is more interesting than mixture of scalar BECs discussed in (i) above. For instance, there is no conservation particle number of each species during collision (though the total number of particles in the system is conserved) as the spin states can combine to form a new spin state, such is not observed in mixture of scalar condensates since the number of particles of the different species are constant. MCBEC, especially for spinor-BEC, has opened a new area of research. There have been theoretical predictions for MCBEC of spin-f BEC [22] and spinor BEC has been extensively discussed in [56]. It is also possible to load the different components of a MCBEC into different traps and allow them to interact as observed in [52].

3.5.1 Gross-Pitaevskii equation for multicomponent Bose-Einstein condensates

In subsection (2.1.2) we discussed the GPE for a single component BEC. This helps us to grasp the more complex situation of MCBEC easily. It is straight forward to generalize the Hamiltonian in equation (2.16) to that of MCBEC but to do this we reflect on our discussion in subsection (2.1.2). We note that the Hamiltonian will now include new terms such as interspecies (inter-hyperfine) state interactions, intra species interaction, spin-orbit coupling etc. The most general Hamiltonian is

$$\hat{H} = \int d\mathbf{r} \sum_{\sigma} \sum_{m_f=-f}^{f} \sum_{m'_f=-f'}^{f'} \hat{\Psi}_{m\sigma}^{\dagger} \left[-\frac{\hbar^2 \nabla^2}{2M_\sigma} + V_{trap}^i(\mathbf{r}) + V_f \right] \hat{\Psi}_{m'\sigma} + \hat{H}_I \quad (3.27)$$

The first sum is taken over different atomic species, σ, present in the system while the second and third summations are taken over all internal degrees of freedom present in the system. When we have a mixture of scalar BEC, then we consider only the first summation as the second and third summations produce just one state of f which we then sum over. Same happens when we have only one species with different hyperfine states, where we consider only the second and third summations ($\sigma = 1$ only). The superscript i of $V_{trap}(\mathbf{r})$ includes cases where the BECs are loaded into different traps as in Ref. [52]. V_f is the hyperfine splitting, it is a combination of the linear and quadratic Zeeman effects. The first term on the rhs of equation (3.27) is the non-interacting part H_o. The interacting part H_I depends on the type of MCBEC, trap and interactions under consideration. In effect equation (3.27) is valid for all types of MCBEC we can consider. It is clear from H_I that each type MCBEC presents a different nature. We now discuss them next.

(*i*). *Mixture of different atomic species*: Here there is no Zeeman effect since the system have only one degree of freedom (i.e. $V_f = 0$). For simplicity we consider two different species A and B of masses m_A, m_B, wave functions $\hat{\Psi}_A(\mathbf{r})$ and $\hat{\Psi}_B(\mathbf{r})$. The constant interaction between them is $U(\mathbf{r}_i, \mathbf{r}_j) = U_{ij} \sum \delta(\mathbf{r}_i - \mathbf{r}_j)$ $(i, j = A, B)$ with constant $U_{ij} = 2\pi\hbar^2 a_{ij}/m_{ij}$, $m_{ij} = m_i m_j/(m_i + m_j)$. The Hamiltonian in equation (3.27) becomes

$$
\begin{aligned}
\hat{H} = \int d\mathbf{r} &\left[\hat{\Psi}_A^\dagger \left(-\frac{\hbar^2 \nabla^2}{2M_A} + V_{trap}^i(\mathbf{r}) \right) \hat{\Psi}_A + \hat{\Psi}_B^\dagger \left(-\frac{\hbar^2 \nabla^2}{2M_B} + V_{trap}^i(\mathbf{r}) \right) \hat{\Psi}_B \right] \\
&+ \frac{U_{AA}}{2} \hat{\Psi}_A^\dagger \hat{\Psi}_A^\dagger \hat{\Psi}_A \hat{\Psi}_A + \frac{U_{BB}}{2} \hat{\Psi}_B^\dagger \hat{\Psi}_B^\dagger \hat{\Psi}_B \hat{\Psi}_B \\
&+ \frac{U_{AB}}{2} \hat{\Psi}_A^\dagger \hat{\Psi}_B^\dagger \hat{\Psi}_B \hat{\Psi}_A + \frac{U_{BA}}{2} \hat{\Psi}_B^\dagger \hat{\Psi}_A^\dagger \hat{\Psi}_A \hat{\Psi}_B
\end{aligned}
\tag{3.28}
$$

The last four terms on the rhs of equation (3.28) constitute the interaction term. Applying the Bogoliubov approximation and carrying out little algebra on the result we obtain the following coupled time independent GPEs.

$$
\left(-\frac{\hbar^2 \nabla^2}{2M_A} + V_{trap}^1(\mathbf{r}) + U_A|\Psi_A|^2 + U_{AB}|\Psi_B|^2 \right) \Psi_A(\mathbf{r}) = \mu_A \Psi_A(\mathbf{r})
\tag{3.29}
$$

and

$$
\left(-\frac{\hbar^2 \nabla^2}{2M_B} + V_{trap}^2(\mathbf{r}) + U_B|\Psi_B|^2 + U_{AB}|\Psi_A|^2 \right) \Psi_B(\mathbf{r}) = \mu_B \Psi_B(\mathbf{r})
\tag{3.30}
$$

where we have used the fact that $\hat{\Psi}_A$ and $\hat{\Psi}_B$ commute and that $U_{AB} = U_{BA}$ to arrive at the coupled equations above. $U_A = U_{AA}$ and $U_B = U_{BB}$ are interactions between the same species for species A and B respectively. $U_{AB} = U_{BA}$ is interaction between different species. μ_A and μ_B, the chemical potentials of species A and B respectively, subject the system to the constraint that the number of atoms N_A and N_B of each species has to be conserved. This is the major difference between the interactions between the MCBEC of different atomic species and that of spinor

BEC.

For a homogeneous gas, where the densities of the two components are constant, the energy of each component is minimized by a space independent phase such that equations (3.29) and (3.30) become [89]

$$\begin{bmatrix} U_A & U_{AB} \\ U_{AB} & U_B \end{bmatrix} \begin{pmatrix} n_A \\ n_B \end{pmatrix} = \begin{pmatrix} \mu_A \\ \mu_B \end{pmatrix} \tag{3.31}$$

The BEC is stable under the conditions that [89],

$U_A > 0$, $U_B > 0$ and $U_A U_B > U_{AB}^2$.

The first (second) conditions ensures stability when the density of A(B) is varied while last condition checks against breakdown when the changes in both components densities will lead to lower energy. The stability can be written as

$$U_A - \frac{U_{AB}^2}{U_B} > 0 \tag{3.32}$$

U_A is the direct interaction between atoms of species A, the second term is referred to as the induced interaction, it gives interaction mediated by the atoms of B. If $U_A U_B < U_{AB}^2$ and U_{AB} is negative the gas will quickly reach instability as the number of species A and B increases but if U_{AB} is positive, the two components will move apart leading to phase separation as shown in figure 3.2. We will discuss more on phase separation in subsection (3.5.4).

Applying the Thomas-Fermi approximation to equations (3.29) and (3.30) we obtain the density of species as

$$n_A = \frac{U_B (\mu_A - U_A) - U_{AB} (\mu_B - U_B)}{U_A U_B - U_{AB}^2} \tag{3.33}$$

and

$$n_B = \frac{U_A \left(\mu_B - U_B\right) - U_{AB} \left(\mu_A - U_A\right)}{U_A U_B - U_{AB}^2} \tag{3.34}$$

It is clear from the stability condition in equation (3.32) that both n_A and n_B are positive.

(ii). *Spinor condensates*: Here, the number of particles in the different hyperfine states is not conserved. This is due to interconversion between the states. For instance, two particles with $F = 1$ in an s-state can couple to give $F = 0$ or $F = 2$. In this case the first summation in equation (3.27) is unity. The interaction has rotational symmetry, thus the total angular momentum of the two atoms is diagonal. Due to constraints, the interaction term for spin-1 BEC is [56, 85]

$$U \left(\mathbf{r}_1 - \mathbf{r}_2\right) = \left(c_o + c_1 \mathbf{F}_1.\mathbf{F}_2\right) \delta \left(\mathbf{r}_1 - \mathbf{r}_2\right) \tag{3.35}$$

where

$$c_o = \frac{4\pi\hbar^2}{M} \left(\frac{2U_2 + U_o}{3}\right), \qquad c_1 = \frac{4\pi\hbar^2}{M} \left(\frac{U_2 - U_o}{3}\right) \tag{3.36}$$

Thus for a spin-1 spinor condensate the Hamiltonian is

$$\hat{H} = \int d\mathbf{r} \sum_{m=-1}^{1} \hat{\Psi}_m^\dagger \left(-\frac{\hbar^2 \nabla^2}{M} + U_{trap}\left(\mathbf{r}\right) + V_f\right) \hat{\Psi}_m$$

$$+ \int d\mathbf{r} \sum_{m=-1}^{1} \sum_{m'=-1}^{1} \left[\frac{c_o}{2} \hat{\Psi}_m^\dagger \hat{\Psi}_{m'}^\dagger \hat{\Psi}_{m'} \hat{\Psi}_m + \frac{c_1}{2} \hat{\Psi}_m^\dagger \hat{\Psi}_{m'}^\dagger \mathbf{F}_1.\mathbf{F}_2 \hat{\Psi}_{m'} \hat{\Psi}_m\right] \tag{3.37}$$

The Hamiltonian for high $\mathbf{F}$ can be obtained by using the appropriate interaction term [56]. The stability conditions for spinor-condensate can be explored when it is loaded in an optical lattice. For a two-component spinor condensate the stability condition is analogous to that of a two-component ordinary BEC and we will show this to be so in chapter 4.

3.5.2 Bose-Hubbard model for multicomponent Bose-Einstein condensates

We discussed the BHM for a single BEC in section (3.3) but here we wish to generalize the BHM to MCBEC. The Hamiltonians in equations (3.27) and (3.28) are written in terms of field operators and thus cannot be used to investigate SF-MI transitions in the system. Hence the need to transform the Hamiltonian to BHM form. To do this we follow the same procedure as in section (3.3) but we now write the field operators in terms of Wanniers functions as $\Psi_i(\mathbf{r}) = \sum_n \mathbf{b}_{ni} W_n(\mathbf{r} - \mathbf{r}_i)$ with n being the species/component of the atom and i the site. The general Hamiltonian in equation (3.27) then becomes

$$H = -\sum_{<i,j>} t_{ij}^{mn}\left(\mathbf{b}_{mj}^\dagger \mathbf{b}_{ni} + \text{h.c.}\right) + \sum_i \varepsilon_{mi} \mathbf{b}_{mi}^\dagger \mathbf{b}_{mi} + \frac{U_{mn,pq}}{2}\sum_i \mathbf{b}_{mi}^\dagger \mathbf{b}_{ni}^\dagger \mathbf{b}_{pi}\mathbf{b}_{qi} \quad (3.38)$$

Here m, n, p, and q represents the species in the MCBEC. Each term in the leading is a generalization of the ones described in section (3.3) with

$$t_{ij}^{mn} = -\int \mathrm{d}\mathbf{r} W_n^*(\mathbf{r} - \mathbf{r}_i)\left[-\frac{\hbar^2}{2m}\nabla^2\delta_{mn} + V_n(\mathbf{r})\,\delta_{mn} + U_{mn} - \frac{1}{2}\left(U_{nn} + U_{mm}\right)\right]$$
$$\times\, W_m(\mathbf{r} - \mathbf{r}_j) \quad (3.39)$$

The generalized off-set energy is given by

$$\varepsilon_{ni} = \int \mathrm{d}\mathbf{r} U_{nn} |W_n(\mathbf{r} - \mathbf{r}_i)|^2 \quad (3.40)$$

where only the lowest band in the optical lattice is considered.

The on-site interaction strength between the atoms is

$$U_{nm,pq} = U_o \int \mathrm{d}\mathbf{r} W_n^*(\mathbf{r} - \mathbf{r}_{i1}) W_m^*(\mathbf{r} - \mathbf{r}_{i2}) W_p(\mathbf{r} - \mathbf{r}_{i3}) W_q(\mathbf{r} - \mathbf{r}_{i4}) \quad (3.41)$$

$$U_{nm,pq} \approx U_o \int \mathrm{d}\mathbf{r} W_n^*(\mathbf{r}) W_m^*(\mathbf{r}) W_p(\mathbf{r}) W_q(\mathbf{r}) \quad (3.42)$$

The Hubbard approximation or model allows the hopping integral to be site independent such that $t_{ij}^{mn} \approx t^{mn}$. Equation (3.38) will be studied in chapter 4 for spin-orbit coupled MCBEC.

3.5.3 Superfluid-Mott insulator transition in multicomponent Bose-Einstein condensates

In section (3.4) we discussed SF-MI transition in BECs loaded into optical lattices and we noted that the number of atoms per lattice site plays an important role in SF-MI transitions. MCBECs also undergo SF-MI transition depending on whether the filling of the lattice sites is commensurable or incommensurable. Figure 3.2 displays the commensurate and incommensurate filling of lattice sites and phase separation of the MCBEC for a two-component MCBEC. Figure 3.2 is simply an extension of figure 3.1
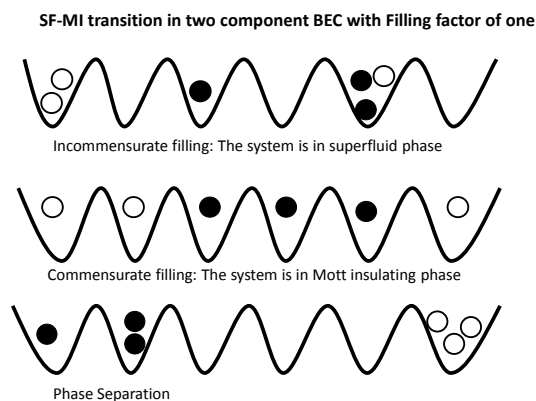
Figure 3.2: Commensurate filling, incommensurate filling and phase separation in Two-component BEC in 1D optical lattice.

3.5.4 Phase separation in multicomponent Bose-Einstein condensates

We wish to address the issue of phase separation mentioned in subsection (3.5.1). Our focus is to determine the condition under which the components of a MCBEC will move apart as illustrated in figure 3.2.

We consider the Hamiltonian in equation (3.28) and we use same steps used in section (2.2). For the binary system under consideration we follow Refs. [71, 108]. After some calculations, the expectation spectrum obtained for a symmetric system ($t_A = t_B = t$) is

$$\epsilon_{\mathbf{k}}^{\pm} = \left[\left(\epsilon_{\mathbf{k}}^0 \right)^2 + \left[U_A n_A + U_B n_B \pm \sqrt{(U_A n_A - U_B n_B)^2 + 4U_{AB}^2 n_A n_B} \right] \epsilon_{\mathbf{k}}^0 \right]^{\frac{1}{2}} \quad (3.43)$$

where $\epsilon_{\mathbf{k}}^0 = -2zt \sum_{\mathbf{k}} \cos\left(\mathbf{k} \cdot \mathbf{a} \right)$ for a homogenous system.

When $n_A = n_B$, $U_A = U_B$, and $U_{AB} = 0$ equation (3.43) reduces to equation (2.33) for the special case of single component BEC.
The spectrum is real except when

$$U_A n_A + U_B n_B \pm \sqrt{(U_A n_A - U_B n_B)^2 + 4U_{AB}^2 n_A n_B} < 0 \quad (3.44)$$

This implies that when $U_A U_B < U_{AB}^2$ the system will be unstable since the excitation spectrum will be imaginary. Under this condition the instability in the system force the components apart and therefore there will be phase separation in the system. This is the same condition arrived at in equation (3.32). It is straightforward to extend the investigation of phase separation to asymmetric systems, $t_A \neq t_B$.

3.6 Spin-orbit coupling in Bose-Einstein condensates

Spin-orbit coupling, a purely quantum mechanical effect, is the interaction between a particle's spin and its momentum. Spin-orbit coupling (SOC) appears almost everywhere in physics. In condensed matter, topological materials [48, 93] and spin-Hall effect [61] heavily rely on SOC. It also play an important role in spintronic devices [62] and leads to exotic phenomena in cold atoms [35].

In solids, which can be treated with nonrelativistic quantum mechanics, SOC occurs as a relativistic correction to Schrodinger equation. This additional term is proportional to $\mathbf{L} \cdot \mathbf{S}$ coupling in atomic physics while in relativistic theory it is inherent in the solution of the Dirac equation. SOC can also be viewed in terms of Zeeman effect, $-\mu \cdot \mathbf{B}$, which results from the interaction between the magnetic moment of the particle and the magnetic field it experiences. SOC is a symmetry breaking interaction and it is notoriously uncontrollable due to the fact that it is an intrinsic property.

Due to the importance of SOC there has been copious theoretical proposals for creating tunable SOC especially in cold atoms [54, 103]. In Ref. [69] Lin and coworkers, in a pioneering work, experimentally achieved a tunable SOC in a BEC of ^{87}Rb using two of its $F = 1$ hyperfine spin state. The coupling between the pseudospin states $| \uparrow \rangle = |F = 1, m_F = 0\rangle$ and $| \uparrow \rangle = |F = 1, m_F = -1\rangle$ were generated using a pair of Raman lasers. The state $| \uparrow \rangle = |F = 1, m_F = +1\rangle$ was adiabatically eliminated from the system.

The effective Hamiltonian generated in this scheme is of the form [69, 73]

$$H_{eff} = \frac{\hbar^2 k^2}{2m} \mathbf{I} + H_{soc} + H_d + H_c \qquad (3.45)$$

where $\mathbf{I}$ is an identity matrix, $H_{soc} = \frac{E_l}{k_l} k_x \sigma_y$ is the SOC term originating from the non-Abelian nature of position dependence of rotation about the pseudo-spin z-axis and kinetic energy, $H_d = \frac{\delta}{2} \sigma_y$ comes from the detuning of the Raman lasers and $H_c = \frac{\Omega}{2} \sigma_z$, with Ω the coupling strength of lasers to the atoms in the BEC, σ represents the Pauli matrices.

This development has been a source of motivation for a now vibrant research area in condensed matter physics as spin-orbit coupled systems promise novel and exotic phenomena. Recently, there have been more experimental successes in creating SOC and there have been several theoretical works on spin-orbit coupled Bose-Einstein condensates (SOCBEC) [64, 94, 110, 113, 114].

On our part, in chapter 4, we will investigate SF-MI transition in SOCBEC in optical lattices of different geometries and also study the exotic SF phase(s) that can be initiated in the system by SOC.

3.7 Mean-field approximations

To investigate SF-MI transition in MCBEC we will adopt two approaches. Either method will give us access to the mean field boundary of the transition but each method has its own advantages as well as limitations. The methods are decoupling approximation and variational method.

3.7.1 Decoupling approximation

It is clear that there is need to decompose the hopping term of equation (3.38). The most efficient mean field approach to investigate the MI phase is carried out by writing

$$\mathbf{b}_i^\dagger \mathbf{b}_j \approx \langle \mathbf{b}_i^\dagger \rangle \mathbf{b}_j + \mathbf{b}_i^\dagger \langle \mathbf{b}_j \rangle - \langle \mathbf{b}_i^\dagger \rangle \langle \mathbf{b}_j \rangle \tag{3.46}$$

In section (2.2) we discussed Bogoliubov approximation and showed that when the number of atoms in the system is large, $N \gg 1$, we can replace the ladder operators by $\sqrt{N_o}$. This leads the mean-field approach of subsection (2.1.2) which is another form of Bogoliubov approximation in equation (2.17). We noted that the condensate density is $n_o(\mathbf{r}) = |\Phi(\mathbf{r})|^2$. The parameter Δ which is the magnitude of $\Phi(\mathbf{r})$ is the superfluid order parameter. From equation (2.19) it is clear that the order parameter is the solution of the time independent GPE just as $\phi(\mathbf{r})$. We can then write

$$\langle \mathbf{b}_i \rangle = \langle \mathbf{b}_i^\dagger \rangle = \frac{1}{N} \sum_i \mathbf{b_i} = \Delta = \sqrt{N_o} = \sqrt{n_i} \tag{3.47}$$

Hence

$$\mathbf{b}_i^\dagger \mathbf{b}_j \approx \Delta \left(\mathbf{b}_i^\dagger + \mathbf{b}_j \right) - \Delta^2 \tag{3.48}$$

We shall apply this method in conjunction with perturbation theory in chapter 4 to investigate QPT of MCBEC.

3.7.2 Variational method

Another method we will use to carry out mean field calculations is by using the variational Gutzwiller wave function. We make use of an ansatz that is a product of the ground states of the system at each lattice site such that the approximate

wave function of the many particle system for a single occupation is $|\psi\rangle = \prod_i |\psi_i\rangle$. Details of the Gutzwiller wave function can be found in [42].

Since there are various occupation combinations, there should be a sum over all possible states of the system. This gives the complete wave function as

$$|\Psi\rangle = \prod_i \sum_{\sigma,\sigma'} |\psi_i\rangle \qquad (3.49)$$

where $|\psi_i\rangle = |\sigma \ \sigma'\rangle_i = |\sigma_i \ \sigma_i'\rangle$ are Fock states and σ_i, σ_i' represent the number of each type of atom in a state.

Although this approximation neglects off-site correlations, it has been shown to be efficient. Since the wave function gives the ground state of the system in extremely strong interaction regime (deep in the MI phase) and extremely weak interaction (deep in the SF phase) it is useful in describing SF-MI phase transition boundary [9]. It has been shown that the approximation level in the Gutzwiller wave function, i.e. ignoring the off-site correlation, is equivalent to decoupling approximation in the analysis of MI-SF boundary [33, 99].

Chapter 4

Quantum phase transition in multicomponent Bose-Einstein condensates

In this chapter the aim is to investigate a two-component BEC from different angles. The two methods discussed in section (3.7), viz decoupling approximation and variational method via Gutzwiller wave functions, will be used to analyse the system. We start by using the decoupling approximation in conjuction with perturbation theory to investigate the SF-MI transition in the system in the absence of SOC and then with SOC present in 1D lattice and later the variational method will be used to investigate the SF-MI transition as well as the type of the SF phase realised in the system when SOC is present in a binary BEC loaded into a square and a hexagonal optical lattices. The reason for investigating the system under different scenarios is to determine the effects of SOC and the geometry of the lattice on the system and also the robustness of the theories used in relation

to exotic SF phases.

The two component BEC, the components are labelled species A and B in this research, under consideration is loaded into an optical lattice in the presence of SOC. We consider the case where A and B are different hyperfine states of the same atom and it is also applicable to spin-1 condensate as discussed earlier. The Hamiltonian of the system is given by

$$H = H_1 + H_2 \tag{4.1}$$

where

$$H_1 = -\sum_{<i,j>} \sum_{\alpha,\alpha'} t_{\alpha,\alpha'} b_{i\alpha}^\dagger b_{j\alpha'} + \text{h.c} + \sum_{i,\alpha} (\varepsilon_{i\alpha} - \mu_\alpha) n_{i,\alpha}$$
$$+ \frac{1}{2} \sum_{i,\alpha} U_\alpha n_{i\alpha} (n_{i\alpha} - 1) + U_{AB} \sum_i n_{iA} n_{iB} \tag{4.2}$$

$$H_2 = i\gamma \sum_{<i,j>} \hat{\Psi}_i^\dagger \hat{\mathbf{z}} \cdot (\sigma \times \mathbf{d}) \hat{\Psi}_j + \sum_i \left[\delta \hat{\Psi}_i^\dagger \sigma_y \hat{\Psi}_i - \Omega \hat{\Psi}_i^\dagger \sigma_z \hat{\Psi}_i \right] \tag{4.3}$$

where $\alpha(\alpha') = \{A, B\}$, γ is the SOC coupling strength, $\hat{\Psi}_i = (b_{iA} \quad b_{iB})^T$, $\sigma = (\sigma_x, \sigma_y, \sigma_z)$ are the Pauli matrices and $\mathbf{d}$ is a unit vector in the lattice plane between neighbouring sites i, j and it is geometry dependent. The whole of the first term of H_2 represents the BHM form of the SOC generated by Raman lasers [44]. Ω is the shift in the chemical potential of each boson species which splits the energy bands of the system and δ is the detuning parameter. Other symbols in equation (4.1) remain as previously defined in earlier chapters.

The phase diagram of H_1 with $t_{AB} = 0$ and $t_A = t_B$ has been investigate in Ref. [22] while [73] used H to predict the phase transition of a two component BEC in a square lattice. It should be noted that $t_{AA} (t_{BB})$ has been replaced by

47

$t_A (t_B)$ and that $t_{AB} = t_{BA}$. In the sections to follow the system will be studied under different conditions.

4.1 Free energy expansion approach

In this section perturbation theory will be applied to investigate the MI-SF transition in the system. From perturbation theory the ground state energy can be written as

$$E_g = \lambda^{(0)} E_g^{(0)} + \lambda^{(1)} E_g^{(1)} + \lambda^{(2)} E_g^{(2)} + ... \tag{4.4}$$

where λ is the perturbation parameter.

In this section, we will use equation (4.4) to explore the MI-SF transition as well as the coupling between the components of the system. Throughout this section we will consider the case where there is no detuning.

4.1.1 Mott insulating phase

To obtain the insulating phase of the system strong coupling expansion is deployed. Strong coupling expansion has been shown to be a good analysis theory for BHM [22, 34, 98]. It allows one to treat the hopping term as a perturbation and the Hamiltonian is decoupled from the site. The system will be insulating when $t_A = t_B = t_{AB} = \gamma = 0$. The wave function of the system is a product of the occupation number of each species and can be written as [22, 50]

$$|\Psi_{MI}\rangle = \frac{1}{\sqrt{n_{iA}! n_{iB}!}} \prod_i \left(b_{iA}^\dagger\right)^{n_A} \left(b_{iB}^\dagger\right)^{n_B} |0\rangle \tag{4.5}$$

which has the same form as equation (3.24). Using equation (4.5) the unperturbed energy of the system is obtained from equation (4.1) as a function of the number of bosons as

$$E(n_A, n_B) = (\varepsilon_A - \mu_A - \Omega) n_A + (\varepsilon_B - \mu_B + \Omega) n_B$$
$$+ \frac{1}{2} [U_A n_A (n_A - 1) + U_B n_B (n_B - 1) + 2U_{AB} n_A n_B] \qquad (4.6)$$

The site index has been dropped. Equation (4.6) represents the energy that is needed to be minimized in order to obtain the ground state energy of the system. We need to find the occupation numbers that minimize the unperturbed energy. Minimizing $E(n_A, n_B)$ and solving the the resulting two coupled linear equations we obtained

$$n_A = \frac{U_B (U_A - U_{AB}) + 2 [\Omega (U_B + U_{AB}) + U_{AB} (\varepsilon_B - \mu_B) - U_B (\varepsilon_A - \mu_A)]}{2 (U_A U_B - U_{AB}^2)} \qquad (4.7)$$

$$n_B = \frac{U_A (U_B - U_{AB}) + 2 [\Omega (U_A + U_{AB}) - U_{AB} (\varepsilon_A - \mu_A) + U_A (\varepsilon_B - \mu_B)]}{2 (U_A U_B - U_{AB}^2)} \qquad (4.8)$$

In the last equations we have ignored the fact that the occupation numbers are integral numbers. If $\Omega = \varepsilon_{A/B} = 0$ equations (4.7) and (4.8) will have the same form as equations (3.33) and (3.34). Therefore, a spinor BEC loaded into an optical lattice is subject to the same stability condition as a MCBEC of scalar condensates in the absence of optical lattice. Also the densities are similar.

Following [22], we write $n_A = g_A + \nu$ and $n_B = g_B + \varrho$ where the numbers ν and ϱ satisfy

$$-\frac{1}{2} < \nu = n_A - g_A < \frac{1}{2}, \quad -\frac{1}{2} < \varrho = n_B - g_B < \frac{1}{2}$$

We therefore, have that

$$g_A - 1 < \frac{U_{AB} [U_{AB} - U_B + 2 (\varepsilon_B - \mu_B + \Omega)] - 2U_A (\varepsilon_A - \mu_A - \Omega)}{2 (U_A U_B - U_{AB}^2)} < g_A \qquad (4.9)$$

49

$$g_B - 1 < \frac{U_{AB}\left[U_{AB} - U_A + 2\left(\varepsilon_A - \mu_A - \Omega\right)\right] - 2U_A\left(\varepsilon_B - \mu_B + \Omega\right)}{2\left(U_A U_B - U_{AB}^2\right)} < g_B \quad (4.10)$$

g_A and g_B are the occupation numbers that minimize $E\left(n_A, n_B\right)$.

To determine the stability condition we consider a homogenous system i.e. $\varepsilon_{A/B} = 0$. Since the occupation numbers cannot be negative or null then we have from equations (4.9) and (4.10) that system will be unstable if $U_A U_B \leq U_{AB}^2$. Hence, the species will be forced to move apart and there will be phase separation in the system. This is rather a crude way of determining phase separation condition but it gives the same result as discussed in section (3.5.4). This result is the same as that of a mixture of scalar BECs in the absence of optical lattice derived in equation (3.32).

4.1.2 Mott insulator-superfluid transition in the absence of spin-orbit coupling

We apply mean field theory to the system to study the Hamiltonian and the boundary between MI and SF phases of the system. In this subsection we will look at the case where $\gamma = 0$. We apply the decoupling approximation discussed in subsection (3.7.1) and effective Hamiltonian is obtained from equation (4.1) as

$$H_{\text{eff}} = \sum_i H_{\text{eff}}^i \quad (4.11)$$

where

$$\begin{aligned}
H_{\text{eff}}^i = {}&\left(\varepsilon_{iA} - \mu_A - \Omega\right) n_{iA} + \left(\varepsilon_{iB} - \mu_B + \Omega\right) n_{iB} \\
&+ \frac{1}{2}\left[U_A n_{iA}\left(n_{iA} - 1\right) + U_B n_{iB}\left(n_{iB} - 1\right) + 2U_{AB} n_{iA} n_{iB}\right] \\
&- z\left[t_A \Delta_A\left(b_{iA}^\dagger + b_{iA}\right) + t_B \Delta_B\left(b_{iB}^\dagger + b_{iB}\right)\right] - z\left(t_A \Delta_A^2 + t_B \Delta_B^2\right) \quad (4.12)
\end{aligned}$$

The site index can now be dropped since the sum is over a single lattice site. The phase diagram of the system has been investigated by Ref. [22] for a symmetric homogenous system with no detuning i.e. $\varepsilon_\alpha = \delta = \Omega = 0$ and $t_A = t_B = t$.

4.1.2.1 Second order perturbation

We are going to use the second order correction to the ground state energy, using perturbation theory, to chart out the phase diagram of the system in the absence of SOC. A brief review of perturbation theory is presented in appendix A. We rewrite equation (4.12) as

$$H_{\text{eff}} = H^{(o)} + \Delta V \tag{4.13}$$

with

$$H^{(o)} = (\varepsilon_A - \mu_A - \Omega) \, n_A + (\varepsilon_B - \mu_B + \Omega) \, n_B - z \left(t_A \Delta_A^2 + t_B \Delta_B^2 \right)$$
$$+ \frac{1}{2} \left[U_A n_A \left(n_A - 1 \right) + U_B n_B \left(n_B - 1 \right) + 2 U_{AB} n_A n_B \right] \tag{4.14}$$

$$\Delta V = -z \left[t_A \Delta_A \left(b_{iA}^\dagger + b_{iA} \right) + t_B \Delta_B \left(b_{iB}^\dagger + b_{iB} \right) \right] \tag{4.15}$$

The unperturbed ground state energy of the system is therefore obtained as

$$E_g(g_A, g_B) = (\varepsilon_A - \mu_A - \Omega) \, g_A + (\varepsilon_B - \mu_B + \Omega) \, g_B - \left(\Delta_A^2 + \Delta_B^2 \right)$$
$$+ \frac{1}{2} \left[U_A g_A \left(g_A - 1 \right) + U_B g_B \left(g_B - 1 \right) + 2 U_{AB} g_A g_B \right] \tag{4.16}$$

where $g_A(g_B)$ is the number of atoms of boson species A(B) in the ground state.

We see that the first order correction does not contribute to the ground state energy because the ladder operators have vanishing averages. The second order correction is given by (see appendix A),

$$E_g^{(2)} = \psi^2 \sum_{n \neq g} \frac{|< g \mid V \mid n >|^2}{E_g^{(0)} - E_n^{(0)}} \tag{4.17}$$

51

with

$$E_g^{(0)}(g_A, g_B) = (\varepsilon_A - \mu_A - \Omega)\, g_A + (\varepsilon_B - \mu_B + \Omega)\, g_B$$
$$+ \frac{1}{2}\left[U_A g_A\,(g_A - 1) + U_B g_B\,(g_B - 1) + 2U_{AB} g_A g_B\right] \tag{4.18}$$

where $|n\rangle = |n_A, n_B\rangle$ represents the unperturbed wave function with n_A (n_B) atoms of species A(B) and $|g\rangle = |g_A, g_B\rangle$ represents the ground state with g_A (g_B) atoms of species A(B).

We have for a homogenous system

$$E_g^{(2)} = z^2 t_A^2 \Delta_A^2 \frac{g_A}{\left[-(\mu_A + \Omega) + U_A\,(g_A - 1) + U_{AB} g_B\right]}$$
$$+ z^2 t_A^2 \Delta_A^2 \frac{g_A + 1}{\left[(\mu_A + \Omega) - U_A g_A - U_{AB} g_B\right]}$$
$$+ z^2 t_B^2 \Delta_B^2 \frac{g_B}{\left[-(\mu_B - \Omega) + U_B\,(g_B - 1) + U_{AB} g_A\right]}$$
$$+ z^2 t_B^2 \Delta_B^2 \frac{g_B + 1}{\left[(\mu_B - \Omega) - U_B g_B - U_{AB} g_A\right]} \tag{4.19}$$

From Landau theory for two order parameters (see Appendix B), the coefficients of Δ_A^2 and Δ_B^2 are obtained from equations (4.16) and (4.19) as

$$\alpha_2 = (zt)^2 \left\{ \frac{g_A}{\left[-(\mu_A + \Omega) + U_A\,(g_A - 1) + U_{AB} g_B\right]} \right.$$
$$+ \frac{g_A + 1}{\left[(\mu_A + \Omega) - U_A g_A - U_{AB} g_B\right]} + \frac{1}{zt} \tag{4.20}$$

$$\beta_2 = (\eta z t)^2 \left\{ \frac{g_B}{\left[-(\mu_B - \Omega) + U_B\,(g_B - 1) + U_{AB} g_A\right]} \right.$$
$$+ \frac{g_B + 1}{\left[(\mu_B - \Omega) - U_B g_B - U_{AB} g_A\right]} + \frac{1}{\eta z t} \right\} \tag{4.21}$$

α_2 and β_2 will vanish at the boundary between two different phases and using this fact the chemical potentials are obtained as

$$\mu_A^{\pm} = -\Omega + \frac{1}{2}\{2U_{AB}g_B + U_A(2g_A - 1)$$
$$- zt \pm \left[U_A^2 - 2ztU_A\left(2g_A + 1\right) + (zt)^2\right]^{\frac{1}{2}}\} \tag{4.22}$$

$$\mu_B^{\pm} = \Omega + \frac{1}{2}\{2U_{AB}g_A + U_B(2g_B - 1)$$
$$- \eta zt \pm \left[U_B^2 - 2\eta ztU_B\left(2g_B + 1\right) + (\eta zt)^2\right]^{\frac{1}{2}}\} \tag{4.23}$$

where $t_A = t$ and $t_B = \eta t$.

The critical condition for the MI-SF transition for each species is when the terms under the square root in equations (4.22) and (4.23) vanish or when $\mu_{A/B}^{-}$ and $\mu_{A/B}^{+}$ coincide. This condition yields the maximum critical values as

$$\left(\frac{zt}{U_A}\right)_c = \left[1 + 2g_A\left(1 + \sqrt{1 + \frac{1}{g_A}}\right)\right]^{-1} \tag{4.24}$$

$$\left(\frac{zt}{U_B}\right)_c = \frac{1}{\eta}\left[1 + 2g_B\left(1 + \sqrt{1 + \frac{1}{g_B}}\right)\right]^{-1} \tag{4.25}$$

Thus, the critical values are independent of interspecies interaction U_{AB} but depend mainly on the number of atoms of each species in the ground state. For $g_A = g_B = \eta = 1$ we have that $\left(\frac{zt}{U_A}\right)_c = \left(\frac{zt}{U_B}\right)_c \approx 0.172$ which is the same result obtained by [99] whereas $g_A = g_B = 1$, $\eta = 0.5$ gives $\left(\frac{zt}{U_A}\right)_c \approx 0.172$, $\left(\frac{zt}{U_B}\right)_c \approx 0.343$ showing that η influences MI-SF in species B.

Phase Diagrams

We obtain the phase diagram under three conditions:

(i) $\eta = 1$, $\Omega = 0.0$ (ii) $\eta = 1$, $\Omega = 0.02U_{A/B}$ (iii) $\eta = 0.5$, $\Omega = 0.02U_{A/B}$ for three

different cases. The

CASE 1: $g_A = g_B = 1$ - Figure 4.1(a) show that the phase diagrams of both species coincide, as found in [22], for $\Omega = 0$, $U_{AB} = 0.4U_{A/B}$ and $\eta = 1$. This is in concordance with Landau theory that coupled order parameters order together. The MI phase is bounded by the lobe while the SF region is outside the lobe. The superfluid phase realised here is a 2-SF. However, from figure 4.1(b), for $\Omega = 0.02U_{A/B}$ the boundaries split. The black lobe represents species A and the blue lobe represents species B. The red lobe represents species B for $\eta \neq 0$. As one might guess from equations (4.22)-(4.24) η does not affect the lobe of species A but affects the lobe of species B. For the nonsymmetric case, η dictates how costly it is for boson species B to move from MI to SF. In this case, $\eta = 0.5$ the lobe of B increases suggesting that the MI phase has increased and therefore more difficult for species B to go into SF.

CASE 2: $g_A = 1, g_B = 2$ - The diagrams are obtained with $U_{AB} = 0.4U_{A/B}$ for the three conditions above. Here, the lobes do not coincide but intercepts as depicted in figure 4.2(a). Thus, the two species can be in MI phase together but not always. The region where both species are in MI is reduced. There are also regions of 1-SF where one of the species is in MI and the other in SF. This is not observed in CASE 1. The effects of finite Ω and $\eta \neq 1$ is the same as CASE 1 above as can be seen from figure 4.2(b). We also note that increasing the occupation number increases the chemical potential and decreases the size of the lobe. In this case $g_B = 2$ increases the magnitude of the potential but reduces the critical value of $\frac{zt}{U_B}$ from 0.172 to 0.101.
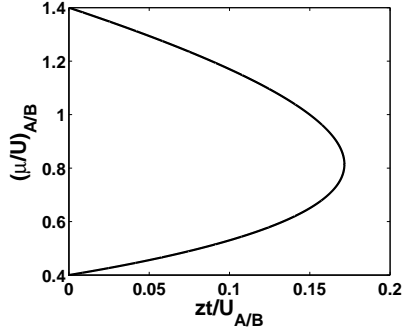
(a) Symmetric case with $g_A = g_B = 1$ and $\Omega = 0$. The chemical potential of both species coincide.
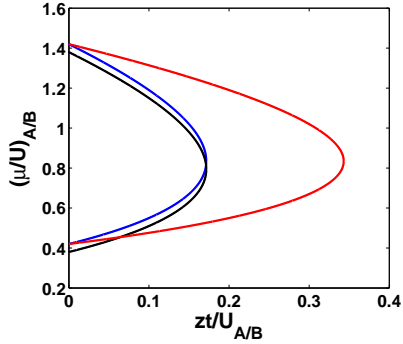
(b) Symmetric case with $g_A = g_B = 1$, $\Omega = 0.02U_{A/B}$. Ω splits the energy of the species. The black lobe represents species A and blue lobe represents species B and asymmetric case with $\eta = 0.5$ gives the red lobe which represents species B.

Figure 4.1: Phase diagrams of a two component BEC with $g_A = g_B = 1$, $U_{AB} = 0.4U_{A/B}$ in the absence of SOC for different values of η and Ω.

CASE 3: $g_A = 1, g_B = 2$ - The phase diagram for an attractive interspecies potential with $U_{AB} = -0.4U_{A/B}$ is displayed in figure 4.3. The lobes neither coincides nor intercepts like the earlier cases. This depicts phase separation in the system which is in agreement with our discussion in subsection (4.1.1). Ω increases the separation between the lobes and η has the same effect as in the earlier cases.
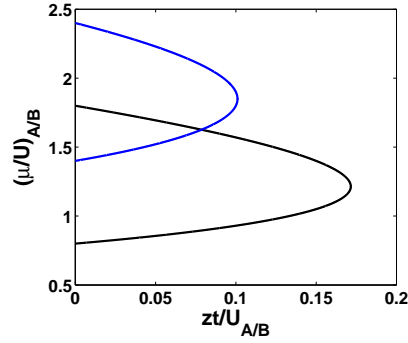
(a) Symmetric case with $g_A = 1, g_B = 2$ and $\Omega = 0$. The lobes intercept and both species can be MI together and the system can also exhibit 1-SF.
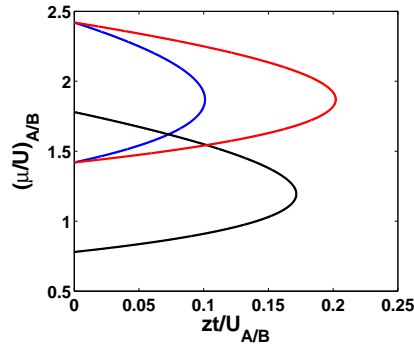
(b) Symmetric case with $g_A = 1, g_B = 2$, $\Omega = 0.02U_{A/B}$. The black lobe is species A and blue lobe represents species B and asymmetric case with $\eta = 0.5$ gives the red lobe which represents species B.

Figure 4.2: Phase diagrams of binary BEC with $g_A = 1, g_B = 2$, with repulsive interparticle interaction $U_{AB} = 0.4U_{A/B}$ in the absence of SOC for different values of η and Ω.

It is noted that for $\eta > 1$, in all cases, the lobe of species B decreases making MI-SF transition more favourable. Also increase in the number of boson type-B reduces the size of lobe B making MI-SF transition of species B less costly.
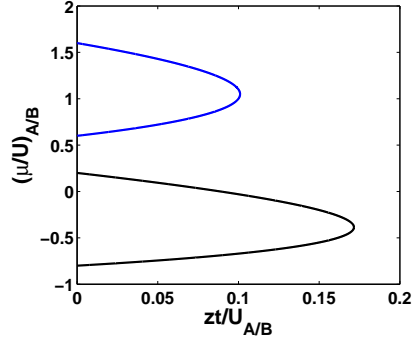
(a) Symmetric case with $g_A = 1, g_B = 2$ and $\Omega = 0$.
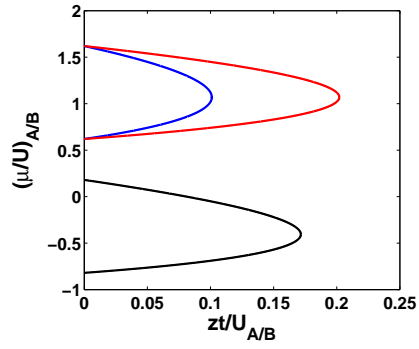
(b) Symmetric case with $g_A = 1, g_B = 2$, $\Omega = 0.02U_{A/B}$. The black lobe is species A and blue lobe represents species B and asymmetric case with $\eta = 0.5$ gives the red lobe which represents species B.

Figure 4.3: Phase diagrams of binary BEC with $g_A = 1, g_B = 2$, with attractive interparticle interaction $U_{AB} = -0.4U_{A/B}$ in the absence of SOC for different values of η and Ω. There is phase separation in the system due to the attractive interparticle interaction.

4.1.2.2 Fourth Order Perturbation

To have a deeper understanding of phase transition in MCBEC we take a look at
the fourth order expansion of the energy and thus, go beyond previous works. This
gives us an insight of the coupling between the components in the system, which
is not predicted by the second order perturbation, and also sheds more light on
the energy and its behaviour as a function of the order parameters in the different
phases of the system. A straightforward method of obtaining higher order terms
in the perturbation is presented in appendix A. Full details of perturbation theory
can be found in quantum mechanics textbooks [12, 47, 63]. The fourth order
correction to the ground state energy is obtained as

$$E_g^{(4)} = \left(\alpha_4 \Delta_A^4 + \gamma_4 \eta^2 \Delta_A^2 \Delta_B^2 + \beta_4 \eta^4 \Delta_B^4 \right) (zt)^4 \tag{4.26}$$

where

$$\alpha_4 =$$

$$\frac{g_A \left(g_A - 1 \right)}{\left[-\left(\mu_A + \Omega \right) + U_A \left(g_A - 1 \right) + U_{AB} g_B \right]^2 \left[-2 \left(\mu_A + \Omega \right) + U_A \left(2g_A - 3 \right) + 2U_{AB} g_B \right]}$$
$$+ \frac{\left(g_A + 1 \right) \left(g_A + 2 \right)}{\left[\left(\mu_A + \Omega \right) - U_A g_A - U_{AB} g_B \right]^2 \left[2 \left(\mu_A + \Omega \right) - U_A \left(2g_A + 1 \right) - 2U_{AB} g_B \right]}$$
$$- \left[\frac{g_A}{\left[-\left(\mu_A + \Omega \right) + U_A \left(g_A - 1 \right) + U_{AB} g_B \right]} + \frac{g_A + 1}{\left[\left(\mu_A + \Omega \right) - U_A g_A - U_{AB} g_B \right]} \right]$$
$$\times \left[\frac{g_A}{\left[-\left(\mu_A + \Omega \right) + U_A \left(g_A - 1 \right) + U_{AB} g_B \right]^2} + \frac{g_A + 1}{\left[\left(\mu_A + \Omega \right) - U_A g_A - U_{AB} g_B \right]^2} \right]$$

$$\tag{4.27}$$

$$\beta_4 =$$

$$\frac{g_B\,(g_B - 1)}{[-(\mu_B - \Omega) + U_B\,(g_B - 1) + U_{AB}g_A]^2\,[-2\,(\mu_B - \Omega) + U_B\,(2g_B - 3) + 2U_{AB}g_A]}$$

$$+ \frac{(g_B + 1)\,(g_B + 2)}{[(\mu_B - \Omega) - U_B g_B - U_{AB}g_A]^2\,[2\,(\mu_B - \Omega) - U_B\,(2g_B + 1) - 2U_{AB}g_A]}$$

$$- \left[\frac{g_B}{[-(\mu_B - \Omega) + U_B\,(g_B - 1) + U_{AB}g_A]} + \frac{g_B + 1}{[(\mu_B - \Omega) - U_B g_B - U_{AB}g_A]}\right]$$

$$\times \left[\frac{g_B}{[-(\mu_B + \Omega) + U_B\,(g_B - 1) + U_{AB}g_A]^2} + \frac{g_B + 1}{[(\mu_B - \Omega) - U_B g_B - U_{AB}g_A]^2}\right]$$

$$(4.28)$$

$$\gamma_4 =$$

$$- \left[\frac{g_A}{[-(\mu_A + \Omega) + U_A\,(g_A - 1) + U_{AB}g_B]} + \frac{g_A + 1}{[(\mu_A + \Omega) - U_A g_A - U_{AB}g_B]}\right]$$

$$\times \left[\frac{g_B}{[-(\mu_B + \Omega) + U_B\,(g_B - 1) + U_{AB}g_A]^2} + \frac{g_B + 1}{[(\mu_B - \Omega) - U_B g_B - U_{AB}g_A]^2}\right]$$

$$- \left[\frac{g_B}{[-(\mu_B - \Omega) + U_B\,(g_B - 1) + U_{AB}g_A]} + \frac{g_B + 1}{[(\mu_B - \Omega) - U_B g_B - U_{AB}g_A]}\right]$$

$$\times \left[\frac{g_A}{[-(\mu_A + \Omega) + U_A\,(g_A - 1) + U_{AB}g_B]^2} + \frac{g_A + 1}{[(\mu_A + \Omega) - U_A g_A - U_{AB}g_B]^2}\right]$$

$$(4.29)$$

The fourth order expansion shows that the order parameters, and therefore the two components of the system, are coupled. This is not obvious in the second order expansion. The coupling appears as γ_4. If either $\Delta_A = 0$ or $\Delta_B = 0$ equation (4.26) reduces to equation (32) of Ref. [109] which is for a single a single component BEC.

The ground state energy as a function of the order parameters

$$E_g\,(\Delta_A, \Delta_B) = E_g^{(0)} + E_g^{(2)} + E_g^{(4)} \tag{4.30}$$

shows the form of Landau theory for coupled order parameter (see appendix B).

If there is no coupling between the components the competition between the components will disappear and the system will behave like two single BECs. Under this condition $\gamma_4 = 0$. Figure 4.4 shows the behaviour of the chemical potential with interaction strength in this regime for $g_A = g_B = 1$, $U_{AB} = 0.4U_{A/B}$ and $\Omega = 0.02U_{A/B}$. The values of the chemical potential obtained here are not within the mean-field phase boundaries. This behaviour is similar to that in figure 5 in Ref. [109] for its behaviour with density outside $\mu^{\pm}_{A/B}$.

Figure 4.5 shows plots of equation (4.30) as a function of the order parameters for $g_A = g_B = 1$, $U_{AB} = 0.4U_{A/B}$, $zt/U_{A/B} = 0.1$, $(\mu/U)_{A/B} = 0.8$. For these values figure 4.1 dictates that both species are in MI phase and this is clearly seen in figure 4.5(b) as the case. Also figure 4.6 depicts the behavior of the energy for $g_A = g_B = 1$, $U_{AB} = 0.4U_{A/B}$, $zt/U_{A/B} = 0.1$, $(\mu/U)_{A/B} = 1.3$. Here figure 4.1 indicates that both species are in SF, that is the system is in a 2-SF while figure 4.7 shows the same plots for $g_A = 1$, $g_B = 2$, $U_{AB} = 0.4U_{A/B}$, $zt/U_{A/B} = 0.18/0.02$, $(\mu/U)_{A/B} = 1.4/1.8$. Taking these values into consideration we see from figure 4.2(a) that species A is in SF phase while species B is MI phase i.e. the system is in one of its 1-SF phases, A-SF in this case and this is confirmed by figure 4.7.
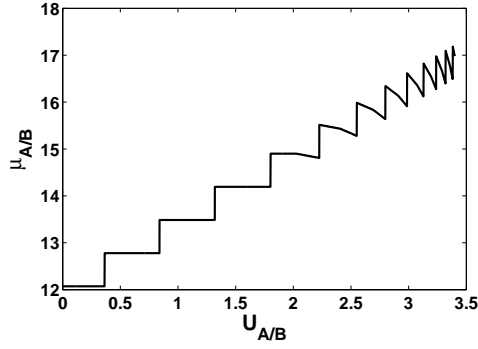
(a) Symmetric case for $\Omega = 0$. The values of the chemical potential for which the coupling vanishes
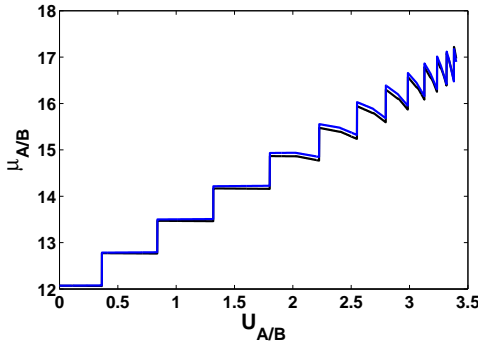
(b) Symmetric case for $\Omega = 0.02 U_{A/B}$. The black line represents species A and blue line represents species B

Figure 4.4: The chemical potential for $\gamma_4 = 0$ for $U_{AB} = 0.4 U_{A/B}$. The values of the chemical potential along the curves uncouple the systems.
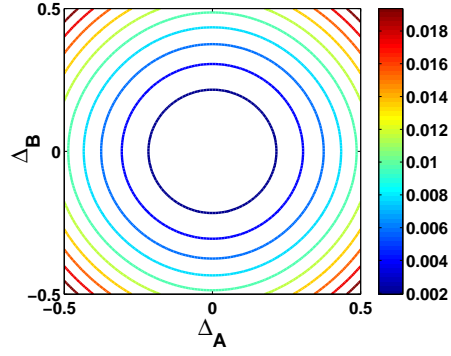
(a) Contour plot of the energy in a region when both species are in MI phase
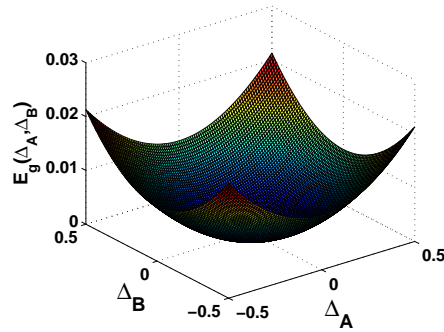
(b) Surface plot of the energy in a region when both species are in MI phase

Figure 4.5: Plots of energy as function of the order parameters with $U_{AB} = 0.4U_{A/B}$, $zt/U_{A/B} = 0.1$, $(\mu/U)_{A/B} = 0.8$ for $g_A = g_B = 1$. Both plots show that the minimum energy is at $(\Delta_A, \Delta_B) = (0,0)$ suggesting that the entire system is in MI phase.
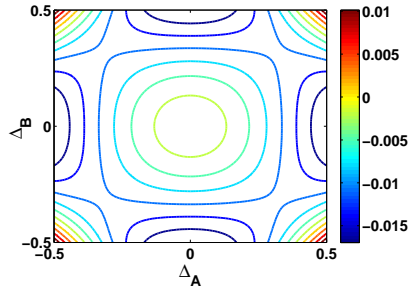
(a) Contour plot of the energy in a region when both species are in SF phase
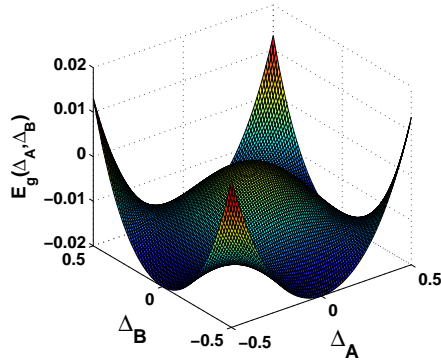
(b) Surface plot of the energy in a region when both species are in SF phase

Figure 4.6: Plots of energy as function of the order parameters with $U_{AB} = 0.4U_{A/B}$, $zt/U_{A/B} = 0.1$, $(\mu/U)_{A/B} = 1.3$ for $g_A = g_B = 1$. The plots show that the minima of the energy are away from $(\Delta_A, \Delta_B) = (0, 0)$ which implies that the system is in 2-SF.
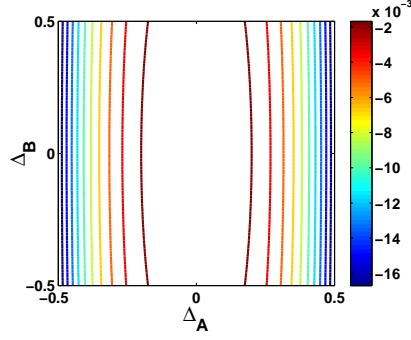
(a) Contour plot of the energy for $g_A = 1$, $g_B = 2$ in a 1-SF region. Species A is in SF while species B is in MI.
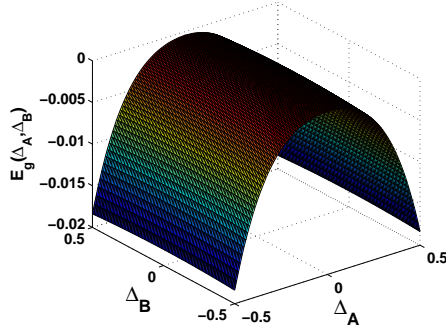
(b) Surface plot of the energy for $g_A = 1$, $g_B = 2$ in a 1-SF region. Species A is in SF while species B is in MI

Figure 4.7: Plots of energy as function of the order parameters with $U_{AB} = 0.4U_{A/B}$, $zt/U_{A/B} = 0.18/0.02$, $(\mu/U)_{A/B} = 1.4/1.8$. for $g_A = 1$, $g_B = 2$. The minimum value of the energy occurs at $\Delta_A \neq 0$, $\Delta_B = 0$. This means that the system is in a 1-SF phase with species A in SF phase and species B in MI phase.

64

4.1.3 Mott insulator to superfluid transition in the presence of spin-orbit coupling

Our goal here is to determine the MI-SF transition in our binary BEC in the presence of SOC in a 1D optical lattice. Like the last two subsections we will use perturbation theory but limit ourselves to second order.

In 1D optical lattice first term of equation (4.3) can be reduced to

$$-\gamma \sum_{\langle i,j \rangle} \left(b_{iA}^{\dagger} b_{jB} - b_{iB}^{\dagger} b_{jA} \right) \tag{4.31}$$

This is the same as SOC Hamiltonian used by [19, 82] for one dimensional optical lattices.

We have already established the effects of η and increase in occupation number so here we will consider only symmetric case. Using the decoupling approximation and following the same steps earlier used for second order perturbation we obtained two coupled equations

$$(zt)^2 \frac{g_A}{[-(\mu_A + \Omega) + U_A(g_A - 1) + U_{AB}g_B]} + (zt)^2 \frac{g_A + 1}{[(\mu_A + \Omega) - U_A g_A - U_{AB}g_B]}$$
$$+ \gamma^2 \frac{g_B}{[-(\mu_B - \Omega) + U_B(g_B - 1) + U_{AB}g_A]} + \gamma^2 \frac{g_B + 1}{[(\mu_B - \Omega) - U_B g_B - U_{AB}g_A]}$$
$$+ zt = 0 \tag{4.32}$$

$$(zt)^2 \frac{g_B}{[-(\mu_B - \Omega) + U_B(g_B - 1) + U_{AB}g_A]} + (zt)^2 \frac{g_B + 1}{[(\mu_B - \Omega) - U_B g_B - U_{AB}g_A]}$$
$$+ \gamma^2 \frac{g_A}{[-(\mu_A + \Omega) + U_A(g_A - 1) + U_{AB}g_B]} + \gamma^2 \frac{g_A + 1}{[(\mu_A + \Omega) - U_A g_A - U_{AB}g_B]}$$
$$+ zt = 0 \tag{4.33}$$

The coupled equations are obtained for a homogenous system with $t_{AB} = \delta = 0$. If there is no SOC, then $\gamma = 0$, equations (4.32) and (4.33) reduce to equations (4.20) and (4.21) for the case without SOC. It is seen that, contrary to the case without SOC, the chemical potentials are not independent in the presence of SOC. The equations can be solved analytically and the solutions are

$$\mu_A^{\pm} = -\Omega + \frac{1}{2}\{2U_{AB}g_B + U_A(2g_A - 1) - D$$
$$\pm \left[U_A^2 - 2DU_A(2g_A + 1) + D^2\right]^{\frac{1}{2}}\} \tag{4.34}$$

$$\mu_B^{\pm} = \Omega + \frac{1}{2}\{2U_{AB}g_A + U_B(2g_B - 1) - D$$
$$\pm \left[U_B^2 - 2DU_B(2g_B + 1) + D^2\right]^{\frac{1}{2}}\} \tag{4.35}$$

where

$$D = D(zt, \gamma) = \frac{(zt)^2 + \gamma^2}{zt} \tag{4.36}$$

Again when $\gamma = 0$, $D = zt$ equations (4.34) and (4.35) reduce to the case without SOC presented in equations (4.22) and (4.23). The position of the tip of phase diagram is modified in the presence of SOC. The new critical value of the hopping strength is

$$\left(\frac{zt}{U}\right)_c = \frac{1}{2}\left[C + \sqrt{C^2 - 4\left(\frac{\gamma}{U}\right)^2}\right] \tag{4.37}$$

where C is the critical value in the absence of SOC and it is given by equation (4.24). When $\gamma = 0$ the critical value reduce to its value in the absence of SOC. For $g_A = g_B = 1$, $\left(\frac{zt}{U}\right)_c \approx 0.172, 0.169$ and 0.162 for $\frac{\gamma}{U} = 0, 0.02$ and 0.04 respectively. Thus, SOC reduces the phase boundary or the insulating region of the system.

Figure (4.8) below shows the phase diagram of the system. The diagram is generated for $U_A = U_B = U$, $U_{AB} = 0.4U_{A/B} = 0.4U$, $g_A = g_B = 1$ and various fixed

66

values of $\frac{\gamma}{U} = 0, 0.02, 0.04$. The figure gives the indication that SOC aids MI-SF transition since the size of the lobe and the critical value of $\frac{zt}{U}$ decrease as the value of coupling strength γ increases. The black lobe, which represents $\frac{\gamma}{U} = 0$, is the same as figure 4.1(a) as expected.
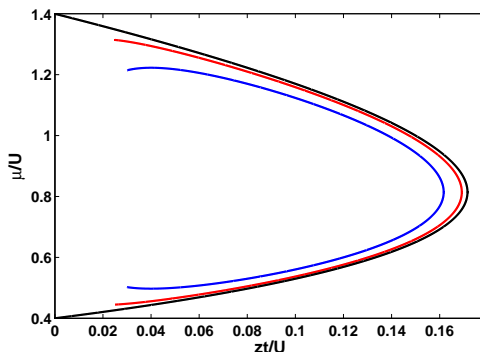
Figure 4.8: Phase diagram of the system for various values of $\frac{\gamma}{U}$ with $U_{AB} = 0.4U$, $g_A = g_B = 1$. Black, red and blue lobes represent $\frac{\gamma}{U} = 0, 0.02, 0.04$ respectively.

Although, we have been able to study the phase diagrams of a two-component BEC under different conditions and also investigated the effect of SOC on the BEC the method does not tell us the type of SF phase realised in the system. We have so far taken the SF phase to be a normal superfluid phase. Strong coupling approach does not give us access to unconventional SF phases that may be present in the system. These exotic SF phases are not only lattice dependent but are also shaped by the geometry of the lattice the BEC is loaded into. Since lattice indices are dropped in the strong coupling approach, used in this section via equation (4.5), it cannot predict the effect of the geometry of the lattice on the system. To investigate the type of exotic SF phase realised during MI-SF transition we will use the variational approach of mean field theory and use Gutzwiller wave function

as our ansatz. We now focus on this aspect for the rest of this research.

4.2 Variational Approach

As mentioned earlier we are using Gutzwiller wave function discussed in subsection
(3.7.2) in order to investigate the MI-SF transition and also for a deeper look into
the SF phases. We use the generalized wave function of the form [9]

$$|\Psi_G\rangle = \prod_i \left(\sum_{n_A, n_B} C^i_{n_A, n_B} |\psi_i\rangle \right) \tag{4.38}$$

$$|\psi_i\rangle = |n_{iA}\ n_{iB}\rangle = |n_A\ n_B\rangle_i \tag{4.39}$$

The coefficients $C^i_{n_A, n_B}$ are, in general, complex and depend on the number of
atoms at each lattice site.

It is clear that the wave function is lattice dependent and we can be certain that
the geometry of the system will contribute to the characteristics of the system. For
simplicity we split the Hamiltonian into three parts and the corresponding energy
of each part will be calculated as

$$E_M = \langle |\Psi_G| H_M |\Psi_G\rangle$$

$$E_h = \langle |\Psi_G| H_h |\Psi_G\rangle$$

$$E_{\text{soc}} = \langle |\Psi_G| H_{\text{soc}} |\Psi_G\rangle \tag{4.40}$$

with

$$H_M = \sum_{i,\alpha} (\varepsilon_{i\alpha} - \mu_\alpha) n_{i,\alpha} + \frac{1}{2} \sum_{i,\alpha} U_\alpha n_{i\alpha} (n_{i\alpha} - 1)$$

$$+ \sum_i U_{AB} n_{iA} n_{iB} + \sum_i \left[\delta \hat{\Psi}_i^\dagger \sigma_y \hat{\Psi}_i - \Omega \hat{\Psi}_i^\dagger \sigma_z \hat{\Psi}_i \right] \tag{4.41}$$

$$H_h = -\sum_{<i,j>} \sum_{\alpha,\alpha'} t_{\alpha,\alpha'} b_{i\alpha}^\dagger b_{j\alpha'} + \text{h.c} \qquad (4.42)$$

$$H_{soc} = i\gamma \sum_{<i,j>} \hat{\Psi}_i^\dagger \hat{\mathbf{z}} \cdot (\sigma \times \mathbf{d}) \hat{\Psi}_j \qquad (4.43)$$

where the subscripts M, h and soc represent the Mott, hopping and SOC terms of the Hamiltonian respectively. The phase diagram and atomic limit of E_M has been discussed in [9, 73].

We are now ready to investigate different geometries of optical lattice and lattice dependence of the energy. In this thesis, we consider square and hexagonal lattices.

4.2.1   Quantum Phase transition in binary Bose-Einstein condensate in a square lattice

The SF-MI transition in square lattice has been investigated by [73] but it requires a review due to some errors in the analytical solutions in that work. For a square lattice, shown in Figure 4.9 below, the unit vector is $\mathbf{d} = \delta_{j,i\pm\hat{x}} + \delta_{j,i\pm\hat{y}}$, where $\delta_{j,i\pm\hat{x}} (\delta_{j,i\pm\hat{y}})$ is for hopping along the positive and negative $x(y)$-axis.
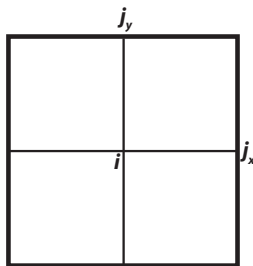
Figure 4.9: A square lattice with reference site i and neighbouring j sites.

We will adopt the method used by Ref. [73]. From equations (4.1) and (4.40) the

energy is obtained as

$$E^{sq} = E_M^{sq} + E_h^{sq} + E_{soc}^{sq} \tag{4.44}$$

where the superscript sq denotes square lattice and

$$
\begin{aligned}
E_M^{sq} = \sum_i \sum_{n_A,n_B} &\left\{ \left[(\varepsilon_{iA} - \mu_A - \Omega) \, n_{iA} + (\varepsilon_{iB} - \mu_B + \Omega) \, n_{iB} \right] |C_{n_A,n_B}^i|^2 \right. \\
&+ \frac{1}{2} \left[U_A n_{iA} \left(n_{iA} - 1 \right) + U_B n_{iB} \left(n_{iB} - 1 \right) + 2U_{AB} n_{iA} n_{iB} \right] |C_{n_A,n_B}^i|^2 \\
&\left. + i\delta \left[\sqrt{n_{iA} \left(n_{iB} + 1 \right)} C_{n_A,n_B}^{i*} C_{n_A-1,n_B+1}^i - \sqrt{\left(n_{iA} + 1 \right) n_{iB}} C_{n_A,n_B}^{i*} C_{n_A+1,n_B-1}^i \right] \right\}
\end{aligned}
\tag{4.45}
$$

$$E_h^{sq} = -t \sum_{\langle i,j \rangle} \left(\Delta_{iA}^* \Delta_{jA} + \eta \Delta_{iB}^* \Delta_{jB} \right) + \text{h.c} \tag{4.46}$$

$$E_{soc}^{sq} = -\gamma \left[\sum_{\langle i,j_x \rangle} \left(\Delta_{iA}^* \Delta_{j_x B} - \Delta_{iB}^* \Delta_{j_x A} \right) - i \sum_{\langle i,j_y \rangle} \left(\Delta_{iA}^* \Delta_{j_y B} + \Delta_{iB}^* \Delta_{j_y A} \right) \right] + \text{h.c} \tag{4.47}$$

where

$$\Delta_{iA} = \sum_{n_A,n_B} \sqrt{n_A + 1} C_{n_A,n_B}^{i*} C_{n_A+1,n_B}^i \tag{4.48}$$

$$\Delta_{iB} = \sum_{n_A,n_B} \sqrt{n_B + 1} C_{n_A,n_B}^{i*} C_{n_A,n_B+1}^i \tag{4.49}$$

are the SF order parameters of species A and B. $\sum_{\langle i,j \rangle}$ represents sum over neighbouring lattice sites in both x and y directions, $\sum_{\langle i,j_x \rangle} (\sum_{\langle i,j_y \rangle})$ represents sum over $x(y)$ neighbour sites.

We can now discuss the phase diagram of the system we obtained from the total energy. But it is necessary to discuss the numerical minimization of the energy, E^{sq}, since the phase diagram is obtained numerically from the energy.

4.2.1.1 Numerical Analysis

Since higher order states in the wave function, equation (4.38), have small overlap with the ground state it is sufficient to include only the lowest order states in the calculation. In this research we take the maximum number of bosons at a lattice site $N = n_{iA} + n_{iB} = 2$ and also the maximum of each species per lattice site $n_{iA}(\text{max}) = n_{iB}(\text{max}) = 2$. This approach is valid as N is a good quantum number, in the MI phase, for both type MCBECs discussed earlier in chapter 3. From equation (4.38) we then have six C-coefficients at each lattice site. Our quest here is to minimize the energy and we considered several approaches in finding the minimum energy.

We write the energy as $E = \sum_i E_i$, where $E_i = \sum_\tau E_{i,\tau}$ is the energy at site i and $\tau = i \pm \hat{x}, i \pm \hat{y}$ represent the neighbouring sites. The approaches discussed below are used to calculate E_i. This is based on the assumption if we find the minimum energy at a particular site then we have in effect found the overall minimum energy since we just have to sum over all sites. We now discuss the methods attempted in this research.

a. First we consider using method of iterative relaxation by inputting initial values of Δ_{iA} and Δ_{iB} and then iterate till the minimum energy is found. But E_M does not depend on the order parameters which makes this approach unacceptable. Although it is possible to fix the value of E_M but we will not be able to calculate the coefficients. We, therefore, cannot use this approach.

b. Another option is to let the coefficients be real and the same at all sites. Then there are six unknowns to calculate. This greatly simplifies the problem but

the price to pay is that E_{soc} vanishes which means that the effect of SOC is suppressed. This is not acceptable.

c. Next we consider the coefficients to be complex and the same at all site. Now there are twelve coefficients to calculate. However, this approach also have the same problem as (b) above, namely $E_{soc} = 0$.

d. Another way of solving the problem is to let the coefficients be real and different for adjacent sites i and j but equal for all neighbouring sites j. Here we have twelve coefficients but we encountered the same problem as earlier options, $E_{soc} = 0$.

e. We consider again the last approach but allow the coefficients to be complex. We then have twenty four variables in the energy equation. Here E_{soc} is finite but there is problem with the method. In the lattice there is point reflection with respect to the reference site i i.e. moving from a site i to an adjacent site, say j_x, is negative of the movement in the opposite direction $(-j_x)$. This approach does not conserve this property of the lattice as it gives bosonic movement in opposite directions to be the same. Hence, this approach is also discarded.

f. We now consider the coefficient to be complex and different at all sites. There are four neighbouring sites to each site i in the square lattice which leads to sixty coefficients. Calculating this large number of unknowns is almost not feasible. However, we can take advantage of the definitions of $\Delta_{i\alpha}$. Since the order parameters are complex they can be written in terms of magnitude and phase i.e $\Delta_{i\alpha} = |\Delta_{i\alpha}|e^{i\phi_{i\alpha}}$. Also the coefficients can be treated in the

same way as the order parameter such that

$$C^i_{n_A,n_B} = |C^i_{n_A,n_B}|e^{i\phi^i_{n_A,n_B}} \tag{4.50}$$

Assuming that the magnitudes of the coefficients are constant but phases vary throughout the lattice reduces the number of magnitudes to just six and number of phases to thirty, where we have used the fact that the magnitude of the phases are equal for the coefficients and their complex conjugates. Now considering the definition of the $\Delta_{i\alpha}$ we see that the phases of $\Delta_{i\alpha}$ at a particular site are the relative phases of the coefficients at that site, that is

$$\phi_{iA} = \phi^i_{n_A+1,n_B} - \phi^i_{n_A,n_B}$$
$$\phi_{iB} = \phi^i_{n_A,n_B+1} - \phi^i_{n_A,n_B} \tag{4.51}$$

Using equation (4.51) we end up with six phases and we now have a total of twelve unknowns to calculate in order to minimize the energy.

This is the approach adopted in this research. It should be noted that E_M does not depend on the phases. E_M^{sq} has been used to determine the atomic limit and momentum distribution in the MI in [73]. Also it is noted that the normalization of the wave function acts as a constraint on the magnitudes and the fact that the magnitudes of the coefficients are always positive implies that $|C^i_{n_A,n_B}|$ are in the interval $[0,1]$. Also the phases are 2π periodic. This makes the problem a bounded constrained nonlinear optimization.

4.2.1.2 Phase diagram

The accuracy of the numerical minimization of the energy depends on the number of initial points used. In this study we used four initial values for each of the

relative phases and two initial values for each of the magnitudes which is about 2.6×10^5 initial values for each value of $\frac{\gamma}{U}$*. For each value of $\frac{\gamma}{U}$ we obtain 2.6×10^5 solutions and then choose the solution that gives the lowest value of the energy. The values of the twelve variables are then used to calculate $\Delta_{i\alpha}$ from which the phase diagram is obtained. We have taken $U_A = U_B = U$. A MATLAB code for the numerical minimization of the energy is presented in appendix C.1.

The phase diagram of the system for $\frac{\mu}{U}$ vs $\frac{\gamma}{U}$ is shown in figure 4.10. We find
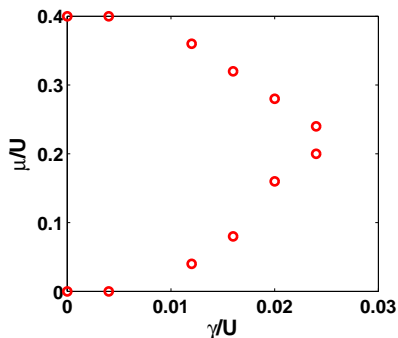
Figure 4.10: Ground state phase diagram of SOCBEC in a square lattice. The MI-SF phase boundary is shown for $\frac{\mu}{U}$ as a function of $\frac{\gamma}{U}$ for $\Omega = 0.01U$, $\eta = 0.5$, $U_{AB} = 0.4U$ and $\frac{t}{U} = 0$.

that both components are always in the MI or SF phase together. The numerical minimization show that the system is in MI phase when $(n_{iA}, n_{iB}) = (1, 0)$ and there is transition to SF phase when $n_{iA}, n_{iB} \neq 0$. Thus, the SF phase realized is

---

*The phase diagram would be more accurate if we used more initial guesses but the time constraint on the submission of this thesis did not allow this . Currently numerical minization with more initial guesses and number of points is being carried out in order to improve the phase diagram.

a 2-SF phase. We also find $\Delta_{0A} > \Delta_{0B}$ for all values of $\frac{\mu}{U}$ and $\frac{\gamma}{U}$. The result also show that the phases are not uniform in the lattice. This means that the SF phase is a twisted SF phase. We next study this exotic superfluid phase.

4.2.1.3 Unconventional superfluid phase in a binary Bose-Einstein condensate in a square lattice

Numerical minimization of equation (4.44) shows that the magnitude of the order parameters are uniform in the ground state while the phases are not uniform. Taking advantage of this outcome the order parameters can be written in terms of magnitude and phase i.e $\Delta_{i\alpha} = \Delta_{0\alpha} e^{i\phi_{i\alpha}}$. The phases of the order parameters are defined as follows

$\phi_{iA} = 0$: phase of the order parameter of species A at the ith site.

$\phi_{iB} = \beta_o$: phase of the order parameter of species B at the ith site.

$\phi_{j_{x(y)}A} = \theta_{x(y)}$: phase of the order parameter of species A at a neighbouring site along $x(y)$-axis.

$\phi_{j_{x(y)}B} = \beta_{x(y)}$: phase of the order parameter of species B at a neighbouring site along $x(y)$-axis.

Using this definitions E_h^{sq} and E_{soc}^{sq} can be written as

$$E_h^{sq} = -2t\Delta_{0A}^2 \sum_{\langle i,j \rangle} \{[\cos(\theta_x) + \cos(\theta_y)] + \eta\kappa^2 [\cos(\beta_x - \beta_o) + \cos(\beta_y - \beta_o)]\}$$

$$(4.52)$$

$$E_{soc}^{sq} = -2\gamma\Delta_{0A}^2\kappa \left[\sum_{\langle i,j_x \rangle} \cos(\beta_x) - \cos(\theta_x - \beta_o) + \sum_{\langle i,j_y \rangle} \sin(\beta_y) + \sin(\theta_y - \beta_o) \right]$$

$$(4.53)$$

where $\kappa = \Delta_{0B}/\Delta_{0A}$.

It has been shown that because of the mean-field definition of the SF order parameter β_o may not be gauge-independent [9]. However, the relative phases are always gauge invariant and we therefore define the relative phases as follows

$$\Phi_{l_{x(y)}A} = \theta_{x(y)}, \quad \Phi_{l_{x(y)}B} = \beta_{x(y)} - \beta_o, \quad \Phi_{l_x AB} = \theta_x - \beta_o \qquad (4.54)$$

Then equations (4.52) and (4.53) become

$$E_h^{sq} = -2t\Delta_{OA}^2 \sum_{l_x,l_y}\{\cos\left(\Phi_{l_x A}\right) + \cos\left(\Phi_{l_y A}\right) + \eta\kappa^2\left[\cos\left(\Phi_{l_x B}\right) + \cos\left(\Phi_{l_y B}\right)\right]\} \quad (4.55)$$

$$E_{soc}^{sq} = -2\gamma\kappa\Delta_{OA}^2 \sum_{l_x,l_y}\{\cos\left(\Phi_{l_x B} - \Phi_{l_x AB} + \Phi_{l_x A}\right) - \cos\left(\Phi_{l_x AB}\right)$$
$$+ \sin\left(\Phi_{l_y A} + \Phi_{l_x AB} - \Phi_{l_x A}\right) + \sin\left(\Phi_{l_y B} - \Phi_{l_x AB} + \Phi_{l_x A}\right)\} \qquad (4.56)$$

Since the energy in terms of the relative phases depends on κ it also depends on equation (4.44). The equation that minimizes the energy in terms of the phases is

$$\frac{\partial}{\partial\Phi_\varphi}[E_h^{sq} + E_{soc}^{sq}] = 0 \qquad (4.57)$$

where φ represents the phases. We have neglected E_M^{sq} since it is independent of the relative phases.

Equation (4.57) gives five coupled self-consistent equations as follows

$$\sin\left(\Phi_{l_x A}\right) + \frac{\gamma\kappa}{t}\{\sin\left(\Phi_{l_x B} - \Phi_{l_x AB} + \Phi_{l_x A}\right)$$
$$+ \cos\left(\Phi_{l_y A} + \Phi_{l_x AB} - \Phi_{l_x A}\right) - \cos\left(\Phi_{l_y B} - \Phi_{l_x AB} + \Phi_{l_x A}\right)\} = 0$$

$$\sin\left(\Phi_{l_y A}\right) - \frac{\gamma\kappa}{t}\cos\left(\Phi_{l_y A} + \Phi_{l_x AB} - \Phi_{l_x A}\right) = 0$$

$$\eta\kappa\sin\left(\Phi_{l_x B}\right) + \frac{\gamma}{t}\sin\left(\Phi_{l_x B} - \Phi_{l_x AB} + \Phi_{l_x A}\right) = 0$$

$$\eta\kappa\sin\left(\Phi_{l_y B}\right) - \frac{\gamma}{t}\cos\left(\Phi_{l_y B} - \Phi_{l_x AB} + \Phi_{l_x A}\right) = 0$$

$$\sin \left(\Phi_{l_x B} - \Phi_{l_x AB} + \Phi_{l_x A} \right) + \sin \left(\Phi_{l_x AB} \right)$$

$$- \cos \left(\Phi_{l_y A} + \Phi_{l_x AB} - \Phi_{l_x A} \right) - \cos \left(\Phi_{l_y B} - \Phi_{l_x AB} + \Phi_{l_x A} \right) \} = 0 \qquad (4.58)$$

Simultaneous solution of equation (4.58) will yield the phases. The coupled equations contain sinusoidal functions and therefore, we are likely to have multiple minima (as well as maxima). Hence, it is imperative for one to be certain that the solutions obtained actually yield the ground state of the system. First, we calculated κ from the energy by numerically minimizing equation (4.44) and then substitute the values of κ that minimizes equation (4.44) into the self consistent equations using seven initial guesses for each of the relative phases, about 1.7×10^4 initial guesses in total for each value of $\frac{\gamma}{t}$. Each of the 1.7×10^4 solutions are then substituted into the representing the energy as a function of the phases and the solutions that yield the minimum value of the energy is kept. MATLAB code for these steps is presented in appendix C.2.

Although our self consistent equations are different from that of Ref. [73], we find that the numerical results are the same. For arbitrary values of $\frac{\gamma}{t}$ equation (4.58) has to be solved numerically. It is important to mention that for all values of $\frac{\gamma}{t}$ that we find $\Phi_{l_x A(B)} = -\Phi_{l_y A(B)}$. Figure 4.11 below shows the variation of the relative phases as a function of $\frac{\gamma}{t}$. $\Phi_{l_x AB}$ and $\Phi_{l_x B}$ have discontinuous jumps around $\frac{\gamma}{t}$ equals zero.

When $\frac{\gamma}{t} \gg 1$ the equations can be solved analytically and the value of the phases in this limit are

$$\Phi_{l_{x(y)} A} = \frac{\pi}{4} \left(-\frac{\pi}{4} \right), \quad \Phi_{l_{x(y)} B} = \frac{3\pi}{4} \left(-\frac{3\pi}{4} \right), \quad \Phi_{l_x AB} = \pi \qquad (4.59)$$
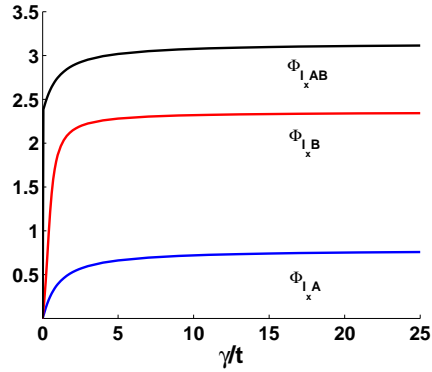
Figure 4.11: Plot of the relative phases of the order parameters vs $\frac{\gamma}{t}$ in optical square lattice. The plot is obtained for $\frac{\mu}{U} = 0.25$, $U_{AB} = 0.4U$, $\eta = 0.5$ and $\Omega = 0.01U$.

This values agree with our numerical results as can be seen from figure 4.11 above. The distribution of the phases of the order parameters in this limit is shown in figures 4.12(a) and 4.12(b) below respectively for species A and B. The variation in the contrast of the colors indicates that the phases are twisted and the repeating pattern show 2π periodicity of the SF order parameter phases.

This unconventional superfluid phase is caused by the complex nature of the order parameters. In normal superfluid phase the order parameter is taken to be real which is the reason we could not observe this twisted superfluid phase when we used the decoupling approximation. In normal superfluid rotational symmetry is conserved but twisted superfluid leads to symmetry breaking and this symmetry breaking is caused by SOC. This symmetry breaking suggests that the phases of the SF order parameters are localized and vary from site to site, which is confirmed by the numerical minimization, unlike in normal SF where it is global and site independent.
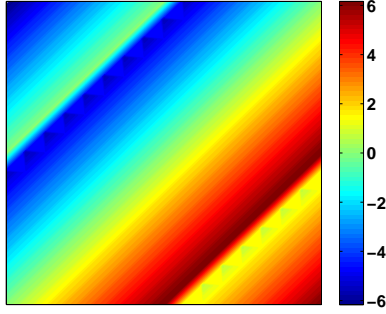
(a) Distribution of the phases of the order parameter of species A, θ_x and θ_y.
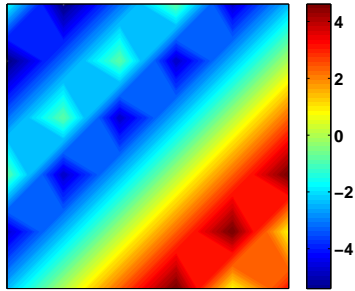
(b) Distribution of the phases of the order parameter of species B, β_x and β_y

Figure 4.12: Distribution of the phases of the order parameters in a square lattice in the limit $\frac{\gamma}{t} \gg 1$. The phases of species B are shifted by $\beta_o = \frac{-3\pi}{4}$. The SF phase realised in the system is twisted. The contrast of the colors represent the magnitude of the phases and the color represents the sign of the phases.

4.2.2 Quantum phase transition in a two-component Bose-Einstein condensate in hexagonal lattice

Following recent experimental studies of ultracold atomic systems in noncubic optical lattices and confirmation of SF-MI transitions in such lattices [10, 72, 101, 100] we are motivated to study MCBEC in hexagonal lattice. In hexagonal lattice there are six neighbouring sites to each ith site and there are three directions in which the atoms can move to a neighbouring site j. Figure 4.13 shows a hexagonal lattice with equilateral triangular lattice as its building block.
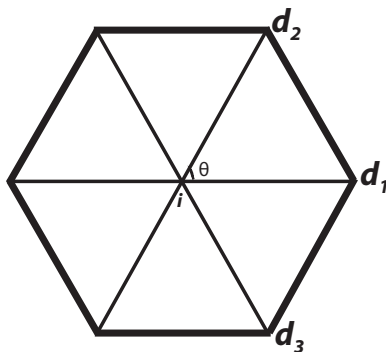
Figure 4.13: Hexagonal lattice showing reference site i and its six neighbouring site at positions **d**.

Using the site i as a reference site, there are three neighbouring sites are at directions d_1, d_2 and d_3 and the remaining three are in the opposite direction. The neighbouring sites make different angles at the reference site i. We have represented the angles by a general angle ϕ such that $\phi = (0, \theta, 2\pi - \theta)$.

As mentioned earlier **d** is geometry dependent. To accommodate the shape of the

lattice we write the unit vector in a generalized form as

$$\mathbf{d} = \sum_{\phi} \left[\cos\left(\phi\right) \delta_{i\pm\hat{x}} + \sin\left(\phi\right) \delta_{i\pm\hat{y}} \right] \tag{4.60}$$

If $\phi = 0$ the situation reduces to that of 1D lattice. For the square lattice, where $\phi = \left(0, \frac{\pi}{2}\right)$, $\mathbf{d}$ reduces to $\delta_{i\pm\hat{x}} + \delta_{i\pm\hat{y}}$ as defined previously.

Next we calculate each part of the energy from equation (4.40) as

$$
\begin{aligned}
E_M^{tr} = \sum_{i} \sum_{n_A,n_B} & \Big\{ \left[\left(\varepsilon_{iA} - \mu_A - \Omega\right) n_{iA} + \left(\varepsilon_{iB} - \mu_B + \Omega\right) n_{iB} \right] |C_{n_A,n_B}^i|^2 \\
& + \frac{1}{2} \left[U_A n_{iA} \left(n_{iA} - 1\right) + U_B n_{iB} \left(n_{iB} - 1\right) + 2U_{AB} n_{iA} n_{iB} \right] |C_{n_A,n_B}^i|^2 \\
& + i\delta \left[\sqrt{n_{iA} \left(n_{iB} + 1\right)} C_{n_A,n_B}^{i*} C_{n_A-1,n_B+1}^i - \sqrt{\left(n_{iA} + 1\right) n_{iB}} C_{n_A,n_B}^{i*} C_{n_A+1,n_B-1}^i \right] \Big\}
\end{aligned}
\tag{4.61}
$$

$$E_h^{tr} = -t \sum_{\langle i,d \rangle} \left(\Delta_{iA}^* \Delta_{dA} + \eta \Delta_{iB}^* \Delta_{dB} + \zeta \Delta_{iA}^* \Delta_{dB} \right) + \text{h.c} \tag{4.62}$$

$$
\begin{aligned}
E_{soc}^{tr} = -\gamma \Big\{ & \sum_{\langle i,d_1 \rangle} \left(\Delta_{iA}^* \Delta_{d_1 B} - \Delta_{iB}^* \Delta_{d_1 A} \right) \\
& + \sum_{\langle i,d_2 \rangle} \left[\cos\left(\theta\right) \left(\Delta_{iA}^* \Delta_{d_2 B} - \Delta_{iB}^* \Delta_{d_2 A} \right) - i \sin\left(\theta\right) \left(\Delta_{iA}^* \Delta_{d_2 B} + \Delta_{iB}^* \Delta_{d_2 A} \right) \right] \\
& + \sum_{\langle i,d_3 \rangle} \left[\cos\left(\theta\right) \left(\Delta_{iA}^* \Delta_{d_3 B} - \Delta_{iB}^* \Delta_{d_3 A} \right) + i \sin\left(\theta\right) \left(\Delta_{iA}^* \Delta_{d_3 B} + \Delta_{iB}^* \Delta_{d_3 A} \right) \right] \Big\} + \text{h.c}
\end{aligned}
\tag{4.63}
$$

where $\zeta = t_{AB}/t$ and superscript tr denotes triangular lattice.

We see that the energy depends on the geometry of the lattice as indicated by the appearance of θ in the SOC part of the energy in equation (4.63). For the special case of square lattice $\theta = \frac{\pi}{2}$ and the third component vanishes. When these

substitutions are made equation (4.63) reduces to its square lattice counterpart, equation (4.47). The order parameters are as defined earlier in equations (4.48) and (4.49).

4.2.2.1 Phase diagram

The minimization of the energy, $E^{tr} = E^{tr}_M + E^{tr}_h + E^{tr}_{soc}$, is carried out with the same approach used for the square lattice. The method gives six magnitudes and eight phases but by taking the symmetry in hexagonal lattice into consideration the phases reduce to six. The MATLAB code to carry out the minimization is the same with that used for the square lattice (see appendix C.1) but with modification to include θ and the appropriate energy equation.

The phase diagram is presented in figure 4.14 below. The numerical solution shows
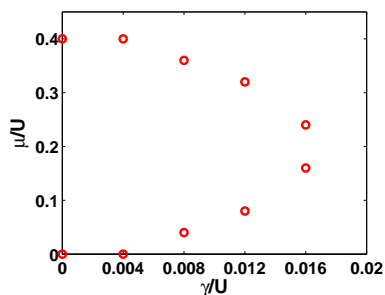
Figure 4.14: Phase diagram showing SF-MI boundary in hexagonal lattice for $\frac{\mu}{U}$ vs $\frac{\gamma}{U}$ for $t = 0.0$. The diagram is obtained for $\eta = 0.5$, $U_{AB} = 0.4U$, $\Omega = 0.01U$ and $\delta = 0$.

that, like the square lattice case, the system is in 2-SF. Qualitatively, the results of the numercal solution is the same as that of the square lattice. Also, we find that

82

the energy of the system in the MI phase is equal for both lattices whereas there is disparity in the energies in the SF phase. The phase diagram show that the transition boundary is smaller in hexagonal lattice than in the square lattice i.e. the critical value of $\frac{\gamma}{U}$ in hexagonal lattice is smaller than that of square lattice. Hence, MI-SF transition is achieved at a lower value of SOC coupling strength when the BEC loaded into a hexagonal lattice than when a square lattice is used. The numerical result also show that the superfluid state phase is twisted just like square lattice case.

4.2.2.2 Twisted superfluid phase in a binary Bose-Einstein condensate in hexagonal lattice

We will now study the SF phase of our system in hexagonal lattice. Following our numerical approach we write $\Delta_{i\alpha} = \Delta_{0\alpha} e^{i\phi_{i\alpha}}$ with $\phi_{0A} = 0$, $\phi_{0B} = \beta_o$ and we define the phase at neighbouring sides

$$\phi_{\mathbf{d}\alpha} = \phi_{i\alpha} + \sum_{\mathbf{d}} \mathbf{d}\phi_{\mathbf{d}\alpha} \tag{4.64}$$

Using equation (4.64) and letting $t_{AB} = 0$ equations (4.62) and (4.63) become

$$E_h^{tr} = -2t\Delta_{OA}^2 \sum_{\langle i,\mathbf{d}\rangle} \left[\cos\left(\phi_{\mathbf{d}A}\right) + \eta\kappa^2 \cos\left(\phi_{\mathbf{d}B} - \beta_o\right)\right] \tag{4.65}$$

$$E_{soc}^{tr} = -2\gamma\kappa\Delta_{OA}^2 \sum_{\langle i,\mathbf{d}\rangle} \sum_{\rho_{\mathbf{d}}} \{\cos\left(\rho_{\mathbf{d}}\theta\right)\left[\cos\left(\phi_{\mathbf{d}B}\right) - \cos\left(\phi_{\mathbf{d}A} - \beta_o\right)\right]$$
$$+ \sin\left(\rho_{\mathbf{d}}\theta\right)\left[\sin\left(\phi_{\mathbf{d}B}\right) + \sin\left(\phi_{\mathbf{d}A} - \beta_o\right)\right]\} \tag{4.66}$$

where $\rho_{\mathbf{d}} = \{\rho_{d_1}, \rho_{d_2}, \rho_{d_3}\} = \{0, 1, -1\}$.

Aside from the appearance of θ in the energy, another effect of geometry is the

83

number of terms in the energy as we see here. E_h^{tr} six terms whereas E_h^{sq} has four terms and E_{soc}^{tr} has ten terms but E_{soc}^{sq} has six terms. Following the definitions in equation (4.54) the relative phases are

$$\Phi_{l_1 A} = \phi_{d_1 A} \qquad \Phi_{l_1 B} = \phi_{d_1 B} - \beta_o \qquad \Phi_{l_1 AB} = \phi_{d_1 A} - \beta_o$$

$$\Phi_{l_2 A} = \phi_{d_2 A} \qquad \Phi_{l_2 B} = \phi_{d_2 B} - \beta_o$$

$$\Phi_{l_3 A} = \phi_{d_3 A} \qquad \Phi_{l_3 B} = \phi_{d_3 B} - \beta_o \qquad \qquad (4.67)$$

Using the relative phases we obtain

$$E_h^{tr} = -2t\Delta_{OA}^2 \sum_{l_1,l_2,l_3} \{[\cos(\Phi_{l_1 A}) + \cos(\Phi_{l_2 A}) + \cos(\Phi_{l_3 A})]$$

$$+ \eta\kappa^2 \left[\cos(\Phi_{l_1 B}) + \cos(\Phi_{l_2 B}) + \cos(\Phi_{l_3 B})\right]\} \qquad (4.68)$$

$$E_h^{tr} = -2\gamma\kappa\Delta_{OA}^2 \sum_{l_1,l_2,l_3} \{[\cos(\Phi_{l_1 B} - \Phi_{l_1 AB} + \Phi_{l_1 A}) - \cos(\Phi_{l_1 AB})]$$

$$+ \cos(\theta)\left[\cos(\Phi_{l_2 B} - \Phi_{l_1 AB} + \Phi_{l_1 A}) - \cos(\Phi_{l_2 A} + \Phi_{l_1 AB} - \Phi_{l_1 A})\right]$$

$$+ \sin(\theta)\left[\sin(\Phi_{l_2 B} - \Phi_{l_1 AB} + \Phi_{l_1 A}) + \sin(\Phi_{l_2 A} + \Phi_{l_1 AB} - \Phi_{l_1 A})\right]$$

$$+ \cos(\theta)\left[\cos(\Phi_{l_3 B} - \Phi_{l_1 AB} + \Phi_{l_1 A}) - \cos(\Phi_{l_3 A} + \Phi_{l_1 AB} - \Phi_{l_1 A})\right]$$

$$+ \sin(\theta)\left[\sin(\Phi_{l_3 B} - \Phi_{l_1 AB} + \Phi_{l_1 A}) + \sin(\Phi_{l_3 A} + \Phi_{l_1 AB} - \Phi_{l_1 A})\right]\} \qquad (4.69)$$

It seems there are seven relative phases but we will see later that there are five different phases just like the square lattice case. Minimizing the total energy, $E^{tr} = E_M^{tr} + E_h^{tr} + E_{soc}^{tr}$ with respect to the phases leads to the following set of

self-consistent equations

$$\sin\left(\Phi_{l_1A}\right) + \kappa\frac{\gamma}{t}\{\sin\left(\Phi_{l_1B} - \Phi_{l_1AB} + \Phi_{l_1A}\right)$$

$$+ \cos\left(\theta\right)\left[\sin\left(\Phi_{l_2B} - \Phi_{l_1AB} + \Phi_{l_1A}\right) + \sin\left(\Phi_{l_2A} + \Phi_{l_1AB} - \Phi_{l_1A}\right)\right]$$

$$- \sin\left(\theta\right)\left[\cos\left(\Phi_{l_2B} - \Phi_{l_1AB} + \Phi_{l_1A}\right) - \cos\left(\Phi_{l_2A} + \Phi_{l_1AB} - \Phi_{l_1A}\right)\right]$$

$$+ \cos\left(\theta\right)\left[\sin\left(\Phi_{l_3B} - \Phi_{l_1AB} + \Phi_{l_1A}\right) + \sin\left(\Phi_{l_3A} + \Phi_{l_1AB} - \Phi_{l_1A}\right)\right]$$

$$- \sin\left(\theta\right)\left[\sin\left(\Phi_{l_3B} - \Phi_{l_1AB} + \Phi_{l_1A}\right) - \cos\left(\Phi_{l_3A} + \Phi_{l_1AB} - \Phi_{l_1A}\right)\right]\} = 0$$

$$\sin\left(\Phi_{l_1B}\right) + \kappa\frac{\gamma}{t}\sin\left(\Phi_{l_1B} - \Phi_{l_1AB} + \Phi_{l_1A}\right) = 0$$

$$\sin\left(\Phi_{l_2A}\right) - \kappa\frac{\gamma}{t}\{\cos\left(\theta\right)\sin\left(\Phi_{l_2A} + \Phi_{l_1AB} - \Phi_{l_1A}\right)$$

$$+ \sin\left(\theta\right)\cos\left(\Phi_{l_2A} + \Phi_{l_1AB} - \Phi_{l_1A}\right)\} = 0$$

$$\sin\left(\Phi_{l_2B}\right) + \kappa\frac{\gamma}{t}\{\cos\left(\theta\right)\sin\left(\Phi_{l_2B} - \Phi_{l_1AB} + \Phi_{l_1A}\right)$$

$$- \sin\left(\theta\right)\cos\left(\Phi_{l_2B} - \Phi_{l_1AB} + \Phi_{l_1A}\right)\} = 0$$

$$\sin\left(\Phi_{l_3A}\right) - \kappa\frac{\gamma}{t}\{\cos\left(\theta\right)\sin\left(\Phi_{l_3A} + \Phi_{l_1AB} - \Phi_{l_1A}\right)$$

$$+ \sin\left(\theta\right)\cos\left(\Phi_{l_3A} + \Phi_{l_1AB} - \Phi_{l_1A}\right)\} = 0$$

$$\sin\left(\Phi_{l_3B}\right) + \kappa\frac{\gamma}{t}\{\cos\left(\theta\right)\sin\left(\Phi_{l_3B} - \Phi_{l_1AB} + \Phi_{l_1A}\right)$$

$$- \sin\left(\theta\right)\cos\left(\Phi_{l_3B} - \Phi_{l_1AB} + \Phi_{l_1A}\right)\} = 0$$

$$\sin\left(\Phi_{l_1B} - \Phi_{l_1AB} + \Phi_{l_1A}\right) + \sin\left(\Phi_{l_1AB}\right)$$

$$+ \cos\left(\theta\right)\left[\sin\left(\Phi_{l_2B} - \Phi_{l_1AB} + \Phi_{l_1A}\right) + \sin\left(\Phi_{l_2A} + \Phi_{l_1AB} - \Phi_{l_1A}\right)\right]$$

$$- \sin\left(\theta\right)\left[\cos\left(\Phi_{l_2B} - \Phi_{l_1AB} + \Phi_{l_1A}\right) - \cos\left(\Phi_{l_2A} + \Phi_{l_1AB} - \Phi_{l_1A}\right)\right]$$

$$+ \cos\left(\theta\right)\left[\sin\left(\Phi_{l_3B} - \Phi_{l_1AB} + \Phi_{l_1A}\right) + \sin\left(\Phi_{l_3A} + \Phi_{l_1AB} - \Phi_{l_1A}\right)\right]$$

$$- \sin\left(\theta\right)\left[\cos\left(\Phi_{l_3B} - \Phi_{l_1AB} + \Phi_{l_1A}\right) - \cos\left(\Phi_{l_3A} + \Phi_{l_1AB} - \Phi_{l_1A}\right)\right] = 0 \qquad (4.70)$$

The seven equations has to be solved self-consistently. The solution of the coupled equations yields the relative phases. The equations are solved numerically with the same approach used for that of the square lattice only that this time we are solving for seven variables. The MATLAB code for the numerical solution is the same as that presented in appendix C.2 but with slight adjustment. We used five initial guesses for each of the relative phases given a total of about 7.8×10^4 initial guesses. From the numerical solution we find that $\Phi_{l_2\alpha} = \Phi_{l_3\alpha}$ for all values of $\frac{\gamma}{t}$. Hence there is inversion symmetry in the optical hexagonal lattice. Therefore, there are five different phases just like the optical square lattice. Figure 4.15 shows the variation of the relative phases. Apart from the discontinuous jump around $\frac{\gamma}{t} = 0$, there is also a fluctuation around $\frac{\gamma}{t} = 1.0$ which is not present in the square lattice case.
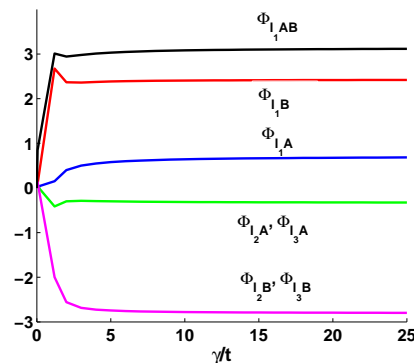
Figure 4.15: Plot of the relative phases of the order parameters vs $\frac{\gamma}{t}$ in a hexagonal optical lattice. The plot is obtained for $\frac{\mu}{U} = 0.25$, $U_{AB} = 0.4U$, $\eta = 0.5$ and $\Omega = 0.01U$.

Equation (4.70) can be solved analytically in the limit $\gamma/t \gg 1$. Using the fact that the building block of the hexagonal lattice is an equilateral triangle such that

$\theta = \frac{\pi}{3}$ and that the last equation in the self consistent equations in equation (4.70) gives $\Phi_{l_1 AB} = \pi$ in this limit, the relative phases are obtained as

$$\Phi_{l_1 A} = \frac{5\pi}{18} \qquad \Phi_{l_1 B} = \frac{13\pi}{18} \qquad \Phi_{l_1 AB} = \pi$$

$$\Phi_{l_2 A} = \Phi_{l_3 A} = \frac{-\pi}{18} \qquad \Phi_{l_2 B} = \Phi_{l_3 B} = \frac{-17\pi}{18} \tag{4.71}$$

This values are quite different from that of the square lattice.

The distribution of the phases of each species are shown in figure 4.16. The variation of the colors of the plots suggests that the phases are twisted and thus making the SF phase realised a twisted-superfluid phase. The distribution of phases is different from that of the square lattice. The result for species B shown in figure 4.16(b) is very unique. The underlying physics of the twisted superfluid phase is the coupling between s and p orbitals at zero quasimomentum [100]. Twisted SF cannot be observed in single component systems because it depends on the admixture of different p orbitals.
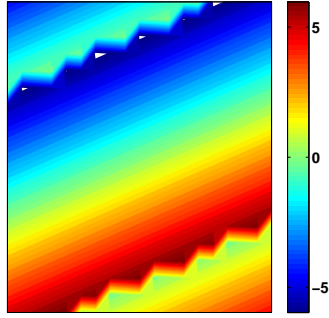
(a) Distribution of the phases $\phi_{d_1 A}$, $\phi_{d_2 A}$ and $\phi d_3 A$.
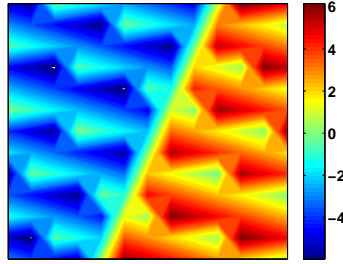
(b) Distribution of the phases $\phi_{d_1 A}$, $\phi_{d_2 A}$ and $\phi_{d_3 A}$. The phases are shifted by $\beta_o = \frac{-13\pi}{18}$ in comparison to that of species A

Figure 4.16: Distribution of the phases of the order parameters in hexagonal lattice in the limit $\frac{\gamma}{t} \gg 1$. The contrast of the colors represent the magnitude of the phases and the color represents the sign of the phases.

Chapter 5

Conclusion and outlook

We have analytically investigated quantum phase transition in a two component Bose-Einstein condensate in the presence of spin-orbit coupling loaded in optical lattices using the Bose-Hubbard model. We have demonstrated the importance of the geometry of optical lattice by showing that the phase transition is influenced by the lattice shape. Our results show that the superfluid to Mott insulator transition is affected by the approach considered.

By using the decoupling approximation and perturbation theory we charted the phase boundary of a two component Bose-Einstein condensate for two instances. (1) In the absence of spin orbit coupling investigation shows that the system can exhibit different superfluid phases namely 2-SF, 1-SF and phase separation depending on the occupation number of the species and the interspecies interaction. (2) When the system is in a one dimensional lattice and spin-orbit coupling is present we find that finite values of the coupling strength, γ, decreases the lobe of the phase diagram compared to the case without spin-orbit coupling. The critical

value of the point at which superfluidity disappears is found to reduce as the γ increases.

We also used variational approach to find the mean-field phase boundary of MI-SF transition in square and hexagonal lattices. Results from numerical minimization of the energy shows that the geometry of the system contributes to the transition. The critical value of $\frac{\gamma}{U}$ in the square lattice is higher than that of the hexagonal lattice. By treating the order parameters as being complex we find that the superfluid realised is twisted. We also find the values of the relative phases of the relative phases of the order parameters for both square and hexagonal lattice and results show that the geometry of the lattice also affect the twisted superfluid phase.

In a race against to beat the submission deadline we used few points to illustrate the SF-MI phase boundary for the square and hexagonal lattice in order to reduce the programming time. As at the submission of this thesis MATLAB codes with more points and increased initial guesses are being run for the generation of the phase diagrams of the system for $\frac{\mu}{U}$ versus $\frac{\gamma}{U}$ for various values of $\frac{t}{U}$ and $\frac{\mu}{U}$ versus $\frac{t}{U}$ for various values of $\frac{\gamma}{U}$ for both square and hexagonal lattice.

We are motivated by the experimental realization of other geometries of optical lattices to investigate SF-MI transition in honeycomb and Kagomé lattices in the near future using the same analytical methods. We believe the study will aid us to determine the lattice geometry with the smallest phase boundary for MI-SF transition and also to compare the twisted superfluid phases.

90

Appendix A

Time independent perturbation theory

Perturbation theory can be found in quantum mechanics books. Here we have followed closely the method used in [12]. Consider the Schrodinger equation in the eigenvalue form

$$H|N\rangle = E|N\rangle \tag{A.1}$$

The total Hamiltonian $\hat{H}$ can be written as

$$H = H_o + \lambda V \tag{A.2}$$

where H_o is known and has the solution $H_o|n\rangle = \epsilon_n|n\rangle$, $|n\rangle$ is the known wave function. λ is a small perturbation parameter ($\lambda = 0, 1, 2, ...$) and V is a small perturbation.

We expand the eigenvalue and eigenfunction in the powers of λ as

$$E = \lambda^0 E^{(0)} + \lambda E^{(1)} + \lambda^2 E^{(2)} + \ldots \tag{A.3}$$

$$|N\rangle = \lambda^0 |N^{(0)}\rangle + \lambda |N^{(1)}\rangle + \lambda^2 |N^{(2)}\rangle + \dots \tag{A.4}$$

It should be noted that $E^{(0)} = \epsilon_n$, $|N^{(0)}\rangle = |n\rangle$ and $\lambda^0 = 1$. Substituting equations (A.2) - (A.4) into equation(A.1) and using the conditions that $(i)\langle n|N\rangle = \langle n|N^{(1)}\rangle = \dots = \langle n|N^{(k)}\rangle = 0$, $(ii)\langle n|m\rangle = \delta_{mn}$ and $(iii)\langle n|N^{(k)}\rangle \neq 0$ we obtain the k-th order correction to the energy as

$$E^{(k)} = \langle n|V|N^{(k-1)}\rangle \tag{A.5}$$

Similarly, using closure relation we can write k-th order correction to the wave function as

$$|N^{(k)}\rangle = \sum_{n \neq m}^{\infty} |m\rangle \langle m|N^{(k)}\rangle \tag{A.6}$$

The factor $\langle m|N^{(k)}\rangle$ can be obtained by using the combined expansions of equations (A.2) and (A.4). Using the result, the k-th order correction to the wave function is obtained as

$$|N^{(k)}\rangle = \sum_{n \neq m}^{\infty} \frac{|m\rangle}{(\epsilon_n - \epsilon_m)} \left(\langle m|V|N^{(k-1)}\rangle - E^{(1)}\langle m|N^{(k-1)}\rangle - E^{(2)}\langle m|N^{(k-2)}\rangle - \dots \right) \tag{A.7}$$

Now from equation (A.5) the first order corrections to the energy and wave function are

$$E^{(1)} = \langle n|V|n\rangle \tag{A.8}$$

and

$$|N^{(1)}\rangle = \sum_{n \neq m}^{\infty} \frac{\langle m|V|n\rangle}{(\epsilon_n - \epsilon_m)} |m\rangle \tag{A.9}$$

Using the same same set of equations the second order corrections are

$$E^{(2)} = \langle n|V|N^{(1)}\rangle = \sum_{n \neq m}^{\infty} \frac{|\langle m|V|n\rangle|^2}{(\epsilon_n - \epsilon_m)} \tag{A.10}$$

and

$$N^{(2)}\rangle = \sum_{\substack{p,m\neq n}}^{\infty} \frac{|m\rangle}{(\epsilon_n - \epsilon_m)} \left(\frac{\langle m|V|p\rangle\langle p|V|n\rangle}{(\epsilon_n - \epsilon_p)} - \frac{\langle n|V|n\rangle\langle m|V|n\rangle}{(\epsilon_n - \epsilon_m)} \right) \qquad (A.11)$$

The same manner of substitution is used to obtain the higher order corrections for the energy as follows (higher order corrections to the wave functions are not written down since we are only interested in the energy but they can be obtained in a similar way)

$$E^{(3)} = \langle n|V|N^{(2)}\rangle$$
$$= \sum_{\substack{p,m\neq n}}^{\infty} \langle n|V|m\rangle \left(\frac{\langle m|V|p\rangle\langle p|V|n\rangle}{(\epsilon_n - \epsilon_m)(\epsilon_n - \epsilon_p)} - \frac{\langle n|V|n\rangle\langle m|V|n\rangle}{(\epsilon_n - \epsilon_m)^2} \right) \qquad (A.12)$$

$$E^{(4)} = \langle n|V|N^{(3)}\rangle$$
$$= \sum_{\substack{p,q,m\neq n}}^{\infty} \langle n|V|m\rangle \left(\frac{\langle m|V|p\rangle\langle p|V|q\rangle\langle q|V|n\rangle}{(\epsilon_n - \epsilon_m)(\epsilon_n - \epsilon_p)(\epsilon_n - \epsilon_q)} - E^{(2)}\frac{\langle m|V|n\rangle}{(\epsilon_n - \epsilon_m)^2} \right) \qquad (A.13)$$

Higher order terms can be obtained in the same manner.

In our study our focus is on the ground state energy. Thus, E is replaced with E_g , ϵ with $E^{(0)}$ and all the orders i.e superscripts remain the same. Also in our study the odd order terms vanish due to the nature of the problem as we discussed in the thesis.

Appendix B

Landau theory for two order parameters

We briefly discuss Landau free energy expansion for a system with two order parameters. More discussions on this theory can be found in [49, 84, 112]. Although the theory is developed for classical systems with phase transition at finite temperature, it is applicable to our system. Here the hopping term or more accurately $\frac{t}{U}$ replaces temperature. Following [49, 112], the free energy of a system with two other parameters can be written as

$$F = F_o + \alpha_2 \Delta_A^2 + \beta_2 \Delta_B^2 + \frac{1}{2}\alpha_4 \Delta_A^4 + \gamma_4 \Delta_A^2 \Delta_B^2 + \frac{1}{2}\beta_4 \Delta_B^4 \qquad \text{(B.1)}$$

where F_o is a constant energy which is $E_g^{(0)}$ in our case, γ_4 is the coupling constant which introduces a competition between the two components A and B. Odd order terms do not appear in the energy due to symmetry.

Since the phase the system is ordered into is determined by the minimum of the

free energy we have that the system can be in any of the following four phases

- Insulating when $[\Delta_A, \Delta_B] = [0, 0]$

- A-SF when $[\Delta_A, \Delta_B] = \left[\pm\sqrt{\frac{-\alpha_2}{\alpha_4}}, 0\right]$

- B-SF when $[\Delta_A, \Delta_B] = \left[0, \pm\sqrt{\frac{-\beta_2}{\beta_4}}\right]$

- Both SF when $[\Delta_A, \Delta_B] = \left[\pm\sqrt{\frac{\alpha_2\beta_4 - \beta_2\gamma_4}{\gamma_4^2 - \alpha_4\beta_4}}, \pm\sqrt{\frac{\alpha_4\beta_2 - \alpha_2\gamma_4}{\gamma_4^2 - \alpha_4\beta_4}}\right]$

The stability of the SF phase is determined by conditions

$$\frac{\partial^2 F}{\partial \Delta_A^2} > 0 \tag{B.2}$$

$$\frac{\partial^2 F}{\partial \Delta_B^2} > 0 \tag{B.3}$$

$$\left(\frac{\partial^2 F}{\partial \Delta_A^2}\right)\left(\frac{\partial^2 F}{\partial \Delta_B^2}\right) - \left(\frac{\partial^2 F}{\partial \Delta_A \partial \Delta_B}\right)^2 > 0 \tag{B.4}$$

The analysis of the phases can be carried out just as in [49, 112].

Appendix C

MATLAB codes

We present here some of the MATLAB codes used to carry out the numerical calculations in the study. We used two MATLAB functions to carry out the numericals. They are:

- fmincon - finds the minimum of a nonlinear function of several variables with constraints. It can take any type of constraint. Details of the properties of the fmincon and how to use it can be found in [1]

- fsolve - finds the roots of system of nonlinear equations i.e. it solves the problem $F(\mathbf{x}) = 0$ where $\mathbf{x}$ is a vector. Details can be found in [2]

In the following all variables, except eta (η), are in the unit of the intra-species interaction, $U_{A/B} = U$. The codes are written for the square lattice but they can also be used for the hexagonal lattice by replacing the energy equations with that of its hexagonal lattice counterpart and also declaring the value of θ.

The called functions energy(x, mu, gamma, t), selfconsistent(y, gamma, kappa/t),

energyphases(z, gamma, kappa/t) and constgutz(x) are user defined functions which defines the energy in terms of the magnitudes and phases of the coefficients, the self consistent equations, the energy equation in terms of the relative phases and the constraint on the magnitudes of the coefficients respectively, where x, y and z are vectors containing the solutions.

C.1   Code for obtaining the phase diagrams

The following code is used to obtain the order parameters in the square lattice. The phase diagram is obtained by analyzing the values of the order parameters. $x(1)$, $x(2)$,...,$x(6)$ represent the magnitudes of the coefficients $|C_{1,0}^i|$, $|C_{0,1}^i|$, $|C_{1,1}^i|$, $|C_{2,0}^i|$, $|C_{0,2}^i|$, $|C_{0,0}^i|$ respectively and $x(7)$, $x(8)$, ..,$x(12)$ represent the relative phase of the coefficients i.e. the phase of the order parameters, where $x(7)$, $x(8)$ and $x(9)$ represent the values of the phases of the order parameter of species A at sites i, $i \pm x$, $i \pm y$ respectively and $x(10)$, $x(11)$ and $x(12)$ represent the values of the phases of the order parameter of species B at sites i, $i \pm x$, $i \pm y$ respectively. All other symbols remain as defined earlier.

```
1  clear
2  global omega U_AB delta eta;
3  omega = 0.01;
4  U_AB = 0.4;
5  delta = 0;
6  eta = 0.5;
7  t = 0.0;
8  format long                    % increase accuracy
```

```matlab
 9  muvec = 0:0.04:0.4;              % The values of the chemical potential
10  nummu = length(muvec);          % The values of the SOC parameter
11  gammavec=0.0:0.004:0.04;
12  numgamma=length(gammavec);
13  lowerbound = zeros(12,1);
14  upperbound = [ones(6,1); 2*pi*ones(6,1)];
15  x = zeros(numgamma,nummu); % Preallocate the vector
16  fvals = 0;
17  %Preallocate a matrix to save the global minimum of x and fvals
18  P = cell(numgamma,2*nummu);
19  % iterate over the chemical potential
20  for g = 1:nummu;
21      mu = muvec(g);
22  % iterate over gamma
23  for j = 1:1:numgamma
24      gamma=gammavec(j);
25      M = cell(262144,2*nummu);    % store all solution
26      position = 1;
27      % use many initial values
28          for k1 = 0.1:0.5:0.6
29              for k2 = 0.1:0.5:0.6
30                  for k3 = 0.1:0.5:0.6
31                      for k4 = 0.1:0.5:0.6
32                          for k5 = 0.1:0.5:0.6
33                              for k6 = 0.1:0.5:0.6
34          for k7 = 0:pi/2:3*pi/2
35              for k8 = 0:pi/2:3*pi/2
36                  for k9 = 0:pi/2:3*pi/2
37                      for k10 =  0:pi/2:3*pi/2
38                          for k11 = 0:pi/2:3*pi/2
39                              for k12 = 0:pi/2:3*pi/2
```

```matlab
40                          x0=[k1;k2;k3;k4;k5;k6;k7;k8;k9;k10;k11;k12];
41  % Choose algorithm, ensure solutions obey constraint and supply the
42  % gradients of the energy and constraint
43   options=optimset('Algorithm','interior-point','AlwaysHonorConstraints',...
44                  'bounds','GradObj','On','GradConstr','On');
45          % call the function (i.e. energy) and the  constraint
46                  [x,fvals]=fmincon(@(x) energy(x,mu,gamma,t),x0, [],...
47                  [], [], [], lowerbound, upperbound,@(x) constgutz(x));
48                      % store the results in a matrix
49                      M(position, 2*g-1)= {x};
50                      M(position, 2*g) = {fvals};
51                      position = position+1;
52                          end
53                      end
54                  end
55              end
56          end
57      end
58                          end
59                      end
60                  end
61              end
62          end
63      end
64  % Take the solutions that give the global minimum for each value of gamma
65      [~, ind] = min([M{:,2*g}]);
66      P(j,2*g-1:2*g) = M(ind,2*g-1:2*g);
67  end
68  end
69  % Preallocate
70   x1 = zeros(numgamma,nummu);
```

```matlab
71    x2 = zeros(numgamma,nummu);

72    x3 = zeros(numgamma,nummu);

73    x4 = zeros(numgamma,nummu);

74    x5 = zeros(numgamma,nummu);

75    x6 = zeros(numgamma,nummu);

76    x7 = zeros(numgamma,nummu);

77    x8 = zeros(numgamma,nummu);

78    x9 = zeros(numgamma,nummu);

79    x10 = zeros(numgamma,nummu);

80    x11 = zeros(numgamma,nummu);

81    x12 = zeros(numgamma,nummu);

82  for r = 1:nummu

83    for i = 1:numgamma

84        x = P{i,2*r-1}; % takes x vector from P

85        x1(i,r) = x(1);

86        x2(i,r) = x(2);

87        x3(i,r) = x(3);

88        x4(i,r) = x(4);

89        x5(i,r) = x(5);

90        x6(i,r) = x(6);

91        x7(i,r) = x(7);

92        x8(i,r) = x(8);

93        x9(i,r) = x(9);

94        x10(i,r) = x(10);

95        x11(i,r) = x(11);

96        x12(i,r) = x(12);

97    end

98  end

99  % Prealloacte the magnitude of the order parameters

100    O1 = zeros(numgamma,nummu);

101    O2 = zeros(numgamma,nummu);
```

```matlab
102   % Calculate the magnitude of the order parameters
103   for r = 1:nummu
104     for i = 1:numgamma
105         O1(i,r) = (x6(i,r)).*x1(i,r) + (x2(i,r)).*x3(i,r) + ...
106                     sqrt(2)*(x1(i,r)).*x4(i,r);
107         O2(i,r) = (x6(i,r)).*x2(i,r) + (x1(i,r)).*x3(i,r) + ...
108                     sqrt(2)*(x2(i,r)).*x5(i,r);
109     end
110   end
111   % Preallocate the order parameters
112   Delta1 = zeros(numgamma,nummu);
113   Delta2 = zeros(numgamma,nummu);
114   % Calculate the order parameters
115   for r = 1:nummu
116   for i = 1:numgamma
117       Delta1(i,r) = O1(i,r).*exp(1i.*x7(i,r));
118       Delta2(i,r) = O2(i,r).*exp(1i.*x10(i,r));
119   end
120   end
121   % Make contour plots
122   contour(gammavec,muvec,Delta1);figure(gcf)
123   contour(gammavec,muvec,Delta2);figure(gcf)
```

where constgutz is the constraint on the magnitudes of the coefficients, it is obtained from the normalization of the Gutzwiller wave function, and the MATLAB code for it is

```matlab
1   function [c, constraint, gc, gconstraint] = constgutz(x)
2   c = []; %nonlinear inequality constraint: not available
3   constraint = x(1).*x(1) + x(2).*x(2) + x(3).*x(3)+ x(4).*x(4) + ...
```

101

```
4        x(5).*x(5) +x(6).*x(6) - 1; %nonlinear equality constraint
5    % supply the gradients
6    gc = [];
7    gconstraint = [2.*x(1); 2.*x(2); 2.*x(3); 2.*x(4); 2.*x(5); 2.*x(6)];
8    end
```

C.2   Code to calculate κ and the relative phases

This code has three parts. In the first part κ is calculated and the values of κ are substituted into the self consistent equation in the second part. Lastly, to be sure that the solution obtained actually minimizes the energy, the relative phases calculated from the second part are substituted into the equation representing the energy as a function of the relative phases and the solutions that yield the minimum energy are retained. The x's are as defined in section C.1 above while the y's and z's represent the relative phases of the order parameters with $y(1)$, $y(2)$, $y(3)$, $y(4)$ and $y(5)$ representing $\Phi_{l_x A}, \Phi_{l_y A}$, $\Phi_{l_x B}$, $\Phi_{l_y B}$ and $\Phi_{l_x AB}$ respectively.

```
1    global omega delta eta U_AB
2    omega = 0.01;
3    U_AB = 0.4;
4    delta = 0;
5    eta = 0.5;
6    mu = 0.25;
7    lowerbound = zeros(12,1);
8    upperbound = [ones(6,1);2*pi*ones(6,1)];
9    format long
10   gammavec =[0:0.05:0.1,0.2:0.1:1,2:1:5,7:2:25];%Values of the SOC strength
```

```matlab
11  % divided by t
12  numgamma=length(gammavec);
13  %PART 1:Calculate kappa
14  x = zeros(numgamma,1); % Preallocate the vector
15  fvals = 0;
16  %Preallocate the matrices to save the final solutions
17  P = cell(numgamma,2);
18  H = cell(numgamma,2);
19  % iterate over gamma
20  for j = 1:1:numgamma
21      position = 1;
22      gamma=gammavec(j);
23  %Preallocate the matrix to save all x and fvals for each value of gamma
24      M = cell(262144,2);
25   % Use several initial values
26      for k1 = 0.1:0.5:0.6
27          for k2 = 0.1:0.5:0.6
28              for k3 = 0.1:0.5:0.6
29                  for k4 = 0.1:0.5:0.6
30                      for k5 = 0.1:0.5:0.6
31                          for k6 = 0.1:0.5:0.6
32          for k7 = 0:pi/2:3*pi/2
33            for k8 = 0:pi/2:3*pi/2
34              for k9 = 0:pi/2:3*pi/2
35                for k10 =  0:pi/2:3*pi/2
36                  for k11 = 0:pi/2:3*pi/2
37                    for k12 = 0:pi/2:3*pi/2
38                      x0=[k1;k2;k3;k4;k5;k6;k7;k8;k9;k10;k11;k12];
39  % Choose algorithm, ensure solutions obey constraint and supply the
40  % gradients of the energy and constraint
41   options=optimset('Algorithm','interior-point','AlwaysHonorConstraints',...
```

```matlab
42                    'bounds','GradObj','On','GradConstr','On');
43              % calling the function (i.e. enery) and the constraint
44                    [x,fvals]=fmincon(@(x) energy(x,mu,gamma),x0, [],...
45                    [], [], [], lowerbound, upperbound,@(x) constgutz(x));
46                        % storing the results as a matrix
47                        M(position, 1)= {x};
48                        M(position, 2) = {fvals};
49                        position = position+1;
50                            end
51                        end
52                    end
53                end
54            end
55        end
56                        end
57                    end
58                end
59            end
60        end
61        end
62 % Take the solutions that give the global minimum for each value of gamma
63        [~, ind] = min([M{:,2}]);
64        P(j,:) = M(ind,:);
65 end
66 % Preallacote the solutions
67  x1 = zeros(numgamma,1);
68  x2 = zeros(numgamma,1);
69  x3 = zeros(numgamma,1);
70  x4 = zeros(numgamma,1);
71  x5 = zeros(numgamma,1);
72  x6 = zeros(numgamma,1);
```

104

```matlab
73   x7 = zeros(numgamma,1);

74   x8 = zeros(numgamma,1);

75   x9 = zeros(numgamma,1);

76   x10 = zeros(numgamma,1);

77   x11 = zeros(numgamma,1);

78   x12 = zeros(numgamma,1);

79   % Extract the solutions from P

80   for i = 1:numgamma

81       x = P{i,1}; % takes x vector from P

82       x1(i) = x(1);

83       x2(i) = x(2);

84       x3(i) = x(3);

85       x4(i) = x(4);

86       x5(i) = x(5);

87       x6(i) = x(6);

88       x7(i) = x(7);

89       x8(i) = x(8);

90       x9(i) = x(9);

91       x10(i) = x(10);

92       x11(i) = x(11);

93       x12(i) = x(12);

94   end

95   % Initialize the magnitudes of the order parameters

96   Delta_O1 = zeros(numgamma,1);

97   Delta_O2 = zeros(numgamma,1);

98   % Calculate the magnitude of the order parameters

99   for i = 1:numgamma

100      Delta_O1(i) = x6(i).*x1(i) +  x2(i).*x3(i) + sqrt(2).*x1(i).*x4(i);

101      Delta_O2(i) = x6(i).*x2(i) +  x1(i).*x3(i) + sqrt(2).*x2(i).*x5(i);

102  end

103 %calculate kappa
```

```matlab
104  kappa1 = zeros(numgamma,1);
105  for n = 1:numgamma
106  % substitute kappa into the self consistent equations and iterate over
107  %gamma
108      kappa1(n) = Delta_O2(n)./Delta_O1(n);
109      kappa = kappa1(n);
110  %PART 2: Calculate the phases from the self consistent equations
111      gamma = gammavec(n);
112      iter = 1;
113      G = cell(78125,2);
114   % using many initial values
115     for l1 = 0:1:6
116         for l2 = 0:1:6
117             for l3 = 0:1:6
118                 for l4 = 0:1:6
119                     for l5 = 0:1:6
120                         y0=[l1*pi/6;l2*pi/6;l3*pi/6;l4*pi/6;l5*pi/6];
121                          options=optimset('GradObj','on');
122                         % calling the function
123                     y =fsolve(@(y) selfconsistent(y,gamma,kappa)...
124                      ,y0, [], [], [], [], -pi*ones(5,1), pi*ones(5,1));
125  % PART 3: Substitute the solution into the energy equation in terms of
126  %the phases
127                         z0 = y;
128                         [z,fvals]=fmincon(@(z) energyphases(z,gamma,kappa)...
129                          ,z0, [], [], [], [], -pi*ones(5,1), pi*ones(5,1));
130                             % store the results in a matrix
131                             G(iter, 1)= {z};
132                             G(iter, 2) = {fvals};
133                             iter = iter+1;
134                         end
```

```matlab
135                 end
136             end
137         end
138     end
139 % Take the solutions that give the global minimum for each value of gamma
140     [~, ind] = min([G{:,2}]);
141     H(n,:) = G(ind,:);
142 end
143 z1 = zeros(numgamma,1);
144 z2 = zeros(numgamma,1);
145 z3 = zeros(numgamma,1);
146 z4 = zeros(numgamma,1);
147 z5 = zeros(numgamma,1);
148 for j = 1:numgamma
149     z = H{j,1};
150     z1(j) = z(1);
151     z2(j) = z(2);
152     z3(j) = z(3);
153     z4(j) = z(4);
154     z5(j) = z(5);
155 end
156 % plot the relative phases against gamma
157 figure;
158 hold on
159 plot(gammavec, z1,'b');
160 plot(gammavec, z2,'g');
161 plot(gammavec, z3,'r');
162 plot(gammavec, z4,'m');
163 plot(gammavec, z5,'k');
```

References

[1] . `http://www.mathworks.se/help/optim/ug/fmincon.html`. Accessed: 2014-01-04.

[2] . `http://www.mathworks.se/help/optim/ug/fsolve.html`. Accessed: 2013-11-11.

[3] J. R. Abo-Shaeer, C. Raman, J. M. Vogels, and W. Ketterle. Observation of vertex lattices in Bose-Einstin condensates. *Science*, 292:476–479, 2001.

[4] M. Abramowitz and I. Stegun. *Handbook Of Mathematical Functions With Formulas, Graphs and Mathematical Tables*. U. S Government Printing Office, Washington, tenth edition, 1972.

[5] M. Aizenman, E. H. Lieb, R. Seiringer, J. P. Solovej, and J. Yngvason. Bose-Einstein quantum phase transition in an optical lattice model. *Physical Review A*, 70(2):023612, 2004.

[6] H. K. Anderson. Bose-Einstein condensates in optical lattices. Ph.D Thesis. *University of Aarhus*, 2008.

[7] M. H. Anderson, J. R. Esher, M. R. Mattews, C. E. Wieman, and E. A. Cornell. Observation of Bose-Einstein condensation in a dilute atomic vapour.

Science, 269:198–201, 1995.

[8] N. W. Ashcroft and N. D. Mermin. *Solid State Physics*. Brooks Cole, Belmont, CA, 1976.

[9] A. T. Balukbasi and M. Iskin. Superfluid-Mott insulator in spin-orbit coupled Bose-Hubbard model. *Physical Review A*, 89:043603, 2014.

[10] C. Becker, P. Soltan-Panahi, J. Kronjäger, S. Dörscher, K. Bongs, and K. Sengstock. Ultracold quantum gases in triangular optical lattices. *New Journal of Physics*, 12:065025, 2010.

[11] S. M. Bilenky. *Introduction To Feynman Diagrams*. Pergamon, New York, 1974.

[12] E. Bittner. *Quantum Mechanics: Lecture Notes On Quantum Chemistry*. University of Houston, Houston, 2003.

[13] I. Bloch. Ultracold quantum gases in optical lattices. *Nature Physics*, 1:23–30, 2005.

[14] N. N. Bogoliubov. *The Many Body Problem*. W. A. Benjamin, New York, 1961.

[15] S. N. Bose. Planks gesetz und lichtquanhypothese. *Zeitschrift fur Physik A Hadrons and Nuclei*, 26:178–181, 1924.

[16] C. C. Bradley, C. A. Sackett, and R. G. Hulet. Evidence of Bose-Einstein condensation in an atomic gas with attrative interaction. *Physical Review Letters*, 75:1687–1691, 1995.

[17] C. C. Bradley, C. A. Sackett, and R. G. Hulet. Bose-Einstein condensation of lithium: Observation of limited condensate number. *Physical Review Letters*, 78(6):985–989, 1997.

[18] H. Bruus and K. Flensberg. *Introduction To Many-Body Quantum Theory in Condensed Matter Physics*, volume 2. Oxford University Press, Oxford, 2005.

[19] Z. Cai, X. Zhou, and C. Wu. Magnetic phases of bosons with synthetic spin-orbit coupling in optical lattices. *Physical Review A*, 85:061605(R), 2012.

[20] L. D. Carr. *Understanding Quantum Phase Transitions*. CRC Press, New York, 2011.

[21] M.-S. Chang, C. D. Hamley, M. D. Barrett, J. A. Sauer, K. M. Fortier, W. Zhang L. You, and M. S. Chapman. Observation of spinor dynamics in optically trapped ^{87}Rb Bose-Einstein condensates. *Physical Review Letters*, 92(14):140403, 2004.

[22] G. Chen and Y. Wu. Quantum phase transition in a multicomponent Bose-Einstein condensate in optical lattices. *Physical Review A*, 67:013606, 2003.

[23] S. Chu. Nobel Lecture: The manipulation of neutral particles. *Reviews of Modern Physics*, 70:685–706, 1998.

[24] C. N. Cohen-Tannoudji. Nobel Lecture: Manipulating atoms with photons. *Reviews of Modern Physics*, 70:707–719, 1998.

[25] P. Coleman. *An Introduction To Many-Body Physics*. Rutgers University, New Jersey, 2004.

[26] L. N. Cooper. Bound electron pairs in a degenerate fermi gas. *Physical Review*, 104(4):1189–1190, 1956.

[27] E. A. Cornell and C. E. Wieman. Nobel lecture: Bose-Einstein condensation in a dilute gas, the first 70 years and some recent experiments. *Reviews Modern Physics*, 74(3):875–893, 2002.

[28] K. B. Davis, M. O. Mewes, M. R. Andrews, N. J. van Druten, D. S. Durfee, D. M. Kurn, and W. Ketterle. Bose-Einstein condensation in a gas of sodium atoms. *Physical Review Letters*, 75:3969–3974, 1995.

[29] Z. Dutton, N. S. Ginsberg, C. Slowe, and L. V. Hau. The art of taming light: Ultra-slow and stopped light. *Europhysics news*, 35:33–39, 2004.

[30] A. Einstein. *Sizber. kgl. Preuss. Akad. Wiss.*, page 261, 1924.

[31] A. Einstein. *Sizber kgl. Preuss. Akad. Wiss*, page 3, 1925.

[32] A. L. Fetter and J. D. Walecka. *Quantum Theory Of Many-Particle Systems.* Dover Publications Inc., New York, 2003.

[33] M. P. A Fisher, P. B Werchman, G. Grinstein, and D. S Fisher. Boson localization and the superfluid-insulator transition. *Physical Review B*, 40(1):546–569, 1989.

[34] J. K. Freericks, H. R. Krishnamurthy, Yasuyuki Kato, Naoki Kawashima, and Nandini Trivedi. Strong-coupling expansion for the momentum distribution of the Bose-Hubbard model with benchmarking against exact numerical results. *Physical Review A*, 79:053631, 2009.

[35] V. Galitski and I. B. Spielman. Spin-orbit coupling in quantum gases. *Nature*, 494:49–54, 2013.

[36] J. J. Gareia-Ripoll, M. A. Martin-Delgado, and J. I. Cirac. Implementation of spin Hamiltonians in optical lattices. *Physical Review Letters*, 93(25):250405, 2005.

[37] H. A. Gersch and G. C. Knollman. Quantum cell model for bosons. *Physical Review*, 129(2):959–967, 1963.

[38] I. S. Gradshteyn and I. M. Ryzhik. *Table Of Integrals, Series and Products*. Academic Press, New York, seventh edition, 200'7.

[39] M. Greiner, O. Mandel, T. Esslinger, T. W. Hanseh, and I. Bloch. Quantum phase transition from a superfluid to a Mott insulator in a gas of ultracold atoms. *Nature*, 415:39–44, 2002.

[40] M. Greiner, O. Mandel, T. Rom, A. Altmeyer, A. Widera, T. W. Hänsch, and I. Bloch. Quantum phase transiton from a superfluid to a Mott insulator in an ultracold gas of atoms. *Physica B:Condensed Matter*, 329-333:11–12, 2003.

[41] R. Grimm, M. Weidemüller, and Y. B. Ovchinnikov. Optical dipole traps for neutral atoms. *Advances in Atomic, Molecular and Optical Physics*, 42(95), 2000.

[42] M. C. Gutzwiller. Effect of correlation on the ferromagnetism of transition metals. *Physical Review*, 134(4A):A923–A941, 1964.

[43] Z. Hadzibabic, P. Kruger, M. Cheneau, B. Battelier, and J. Dalibard. Berezinskii–Kosterlitz–Thouless crossover in a trapped atomic gas. *Nature*, 441:1118–1121, 2006.

[44] F. D. M. Haldane. Model for a quantum Hall effect without Landau levels: Condensed-matter realization of the "parity anomaly". *Physical Review Letters*, 61(18):2015–2018, 1988.

[45] D. S. Hall, M. R. Mattews, J. R. Ensher, C. E. Wieman, and E. A. Cornell. Dynamic of component separation in a binary mixture of Bose-Einstein condensates. *Physical Reviews Letters*, 81(8):1539–1542, 1998.

[46] L. V. Hau, S. E. Harris, Z. Dutton, and C. H. Behroozi. Light speed reduction to 17 metres per second in an ultracold atomic gas. *Nature*, 397:594–598, 1999.

[47] P. C. Hemmer. *Kvantemekanikk*. Tapir Academisk Forlag, Trondheim, 5th edition, 2005.

[48] D. Hsieh, D. Qian, L. Wray, Y. Xia, Y. S. Hor, R. J. Cava, and M. Z. Hasan. A topological Dirac insulator in a quantum spin hall phase. *Nature*, 452:970–975, 2008.

[49] Y. Imry. On the statistical mechanics of coupled order parameters. *Journal of Physics*, C8:567, 1975.

[50] M. Iskin. Strong-coupling expansion for the two-species Bose-Hubbard model. *Physical Review A*, 82:033630, 2010.

[51] D. Jaksch, H. Briegel, J. I. Cirac, C. W. Gardiner, and P. Zoller. Entanglement of atoms via cold controlled collisions. *Physical Review Letters*, 82(9):1975–1978, 1999.

[52] D. Jaksch, C. Bruder, J. I. Cirac, C. W. Gardiner, and P. Zoller. Cold bosonic atoms in optical lattices. *Physical Review Letters*, 81(15):3108–3111, 1998.

[53] G. Jo, J. Choi, C. A. Christensen, T. A. Pasquini, Y. Lee, and W. Ketterle. Phase-sensitive recombination of two Bose-Einstein condensates on an atom chip. *Physical Review Letters*, 98:180401, 2007.

[54] G. Juzeliūnas, J. Ruseckas, M. Lindberg, L. Santos, and P. Öhberg. Quasirelativistic behavior of cold atoms in light fields. *Physical Review A*, 77(R):011802, 2008.

[55] J. Kasprzak, M. Richard, S. Kundermann, A. Baas, P. Jeambrun, J. M. J. Keeling, F. M. Marchetti, M. H. Szyman acuteska, R. André, J. L. Staehli, V. Savona, P. B. Littlewood, B. Deveaud, and Le Si Dang. Bose–Einstein condensation of exciton polaritons. *Nature*, 443:409–414, 2006.

[56] Y. Kawaguchi and M. Ueda. Spinor Bose-Einstein condensates. *Physics Reports*, 520:253–381, 2012.

[57] E. Kengne and R. Vaillancourt. Stabilized solution in attractive Bose-Einstein condensates in hyperbolic potential. *Scientific Proceedings of Riga Technical University, Boundary Field Problems and Computer Simulation*, 29(48):81–94, 2006.

[58] W. Ketterle, D. S. Durfee, and D. M. Stamper-Kurn. Making, probing and understanding Bose-Einstein condensates.

[59] T. Kinoshita, T. Wenger, and D. S. Weiss. Observation of a one-dimensional Tonks-Girardeau gas. *Science*, 305:1125–1128, 2004.

[60] C. Kittel. *Introduction to Solid State Physics*. John Wiley & Sons Inc., New Caledonia, Eighth edition, 2005.

[61] M. König, S. Wiedmann, C. Brüne, A. Roth, H. Buhmann, L. W. Molenkamp, X.-L. Qi, and S.-C. Zhang. Quantum spin Hall insulator state in HgTe quantum wells. *Science*, 318(4):766–770, 2007.

[62] J. D. Koralek, C. P. Weber, J. Orenstein, B. A. Bernevig, S.-C. Zhang, S. Mack, and D. D. Awschalom. Emergence of the persistent spin helix in semiconductor quantum wells. *Nature*, 458:610–613, 2009.

[63] L. D. Landau and E. M. Lifshitz. *Quantum Mechanics: Non-Relativistic Theory*. Pergamon Press, Oxford, third edition, 1981.

[64] J. Larson, J.-P. Martikainen, A. Collin, and E. Sjöqvist. Spin-orbit-coupled Bose-Einstein condensate in a tilted optical lattice. *Physical Review A*, 82:043620, 2010.

[65] A. E. Leanhardt, T. A. Pasquini, M. Saba, A. Schirotzek, Y. Shin, D. Kielpinsk, D. E. Prietchard, and W. Ketterle. Cooling Bose-Einstein condensates below 500 picokelvin. *Science*, 301:1513–1515, 2003.

[66] A. J. Leggert. Bose-Einstein condensation in the alkali gases: Some fundamental concepts. *Review of Modern Physics*, 73:307–356, 2001.

[67] M. Lewenstein, A. Sanpera, V. Ahufinger, B. Damskis, A. Sen, and U. Sen. Ultracold atomic gases in optical lattices: mimicking condensed matter physics and beyond. *Advances in Physics*, 56:243–379, 2007.

[68] E. H. Lieb, R. Seirenger, J. P. Solovej, and J. Yngvason. *The Mathematics of Bose gas and its condensation*. Berhauser Verlag, Berlin, 2000.

[69] Y.-L. Lin, K. Jiménez-Garćia, and I. B. Spielman. Spin-orbit coupled Bose-Einstein condensates. *Nature*, 471:83–88, 2011.

[70] J. Linder and A. Sudbø. Calculation of drag and superfluid velocity from the microscopic parameters and excitations energy of a two-component Bose-Einstein condensate in an optical lattice. *Physical Review A*, 79:063610(1–10), 2009.

[71] X. P. Liu. Excitation spectrum and phase separation in double Bose-Einstein condensates in optical lattices. *Physical Review A*, 76:053615, 2007.

[72] D.-S. Lühmann, O. Jürgensen, M. Weinberg, J. Simonet, P. Soltan-Panahi, and K. Sengstock. Quantum phases in tunable state-dependent hexagonal optical lattices. *e-print:http://arXiv:1401.5961v1*, 2014.

[73] S. Mandal, K. Saha, and K. Sengupta. Superfluid-insulator transition of two-species bosons with spin-orbit coupling. *Physical Review B*, 86:155101, 2012.

[74] M. R. Mathews, B. P. Anderson, P. C. Haljan, D. S. Hall, C. E. Wiemann, and E. A. Cornell. Vortices in Bose-Einstein condensates. *Physical Review Letters*, 83(13):2498–2501, 1999.

[75] H. J. Metcalf and P. van der Straten. *Laser Cooling and Trapping*. Springer, Berlin, 1999.

[76] T. Mishra, R. V. Pai, , and B. P. Das. Phase separation in a two-species Bose mixture. *Physical Review A*, 76:013604, 2007.

[77] G. Modugno, M. Modugno, F. Riboli, G. Roati, and M. Inguscio. Two atomic species superfluid. *Physical Review Letters*, 89(19):190404, 2002.

[78] O. Morsch, J. H. Müller, M. Chrisniati, D. Ciampini, and Arimondo. Bloch oscillations and mean-field effects of Bose-Einstein condensates in 1D optical

lattices. *Physical Review Letters*, 87(14):140402, 4 pages, 2001.

[79] O. Morsch and M. Oberthaler. Dynamics of Bose-Einstein in optical lattices. *Review of Modern Physics*, 78:179–215, 2006.

[80] J. Mun. Bose-Einstein condensates in optical lattices: The superfluid to Mott insulator phase transition. PhD Thesis. *MIT*, 2008.

[81] C. J. Myatt, E. A. Burt, R. W. Ghrist, E. A. Cornell, and E. E. Wieman. Production of two overlapping Bose-Einstein condensates by sympathetic cooling. *Physical Review Letters*, 78(4):586–589, 1997.

[82] H. T. Ng. Topological phases in spin-orbit coupled dipolar lattice bosons. *e-print:http://arXiv:1405.4068v1*, 2014.

[83] K. E. O'Hara, L. Ó. Súilleabháin, and J. P. Wolfe. Strong nonradiative recombination of exciton in Cu_2O and its impact on Bose-Einstein statistics. *Physical Review B*, 60:10565–10568, 1999.

[84] V. Palchykov, C. von Ferber, R. Folk, Yu. Holovatch, and R. Kenna. Critical phenomena on scale-free networks: Logarithmic corrections and scaling functions. *Physical Review E*, 82:011145, 2010.

[85] S. B. Papp. Experiment with two-species Bose-Einstein condensate utilizing widely tunable interparticle interactions. Ph.D Thesis. *University of Colorado*, 2007.

[86] B. Paredes, A. Widera, V. Murg, O. Mandel, S. F olling, I. Cirac, G. V. Shlyapnikov, T. W. H ansch, and I. Bloch. Tonks-Girardeau gas of ultracold atoms in an optical lattice. *Nature*, 429:277–281, 2004.

[87] B. Pasquiou, E. Maréchal, G. Bismut, P. Pedri, L. Vernac, O. Gorceix, and B. Laburthe-Tolra. Spontaneous demagnetization of a dipolar spinor Bose gas in an ultralow magnetic field. *Physical Review Letters*, 106:255303S, 2011.

[88] F. B. Pedersen, G. T. Einevoll, and P. C. Hemmer. Wannier functions for the Kronig-Perney model. *Physical Review B*, 44(11):5470–5475, 1991.

[89] C. J. Pethick and H. Smith. *Bose-Einstein Condensation in Dilute Gases*. Cambridge University Press, Cambridge, 2008.

[90] W. D. Phillips. Nobel Lecture: Laser cooling and trapping of neutral atoms. *Reviews of Modern Physics*, 70(3):721–741, 1998.

[91] L. Pitaevskii and S. Stringari. *Bose-Einstein Condensation*. Claderon Press, Oxford, 2003.

[92] H. Pu, W. Zhang, and P. Meystre. Ferromagnetism in a lattice of Bose-Einstein condensates. *Physical Review Letters*, 87(14):140405, 2001.

[93] X.-L. Qi. Topological insulators and superconductors. *Review of Modern Physics*, 83(4):1057–1110, 2011.

[94] J. Radić, T. A. Sedrakyan, I. B. Spielman, and V. Galitski. Vortices in spin-orbit coupled Bose-Einstein condensates. *Physical Review A*, 84:063604, 2011.

[95] C. J. Regal, M. Greiner, and D. S. Jin. Observation of resonance condensation atom pairs. *Physical Review Letters*, 92(4):040403, 2004.

[96] T. Rom, T. Best, O. Mandel, A. Widera, M. Greiner, T. W. Hänsch, and I. Bloch. State selective production of molecules in optical lattices. *Physical*

Review Letters, 93(7):073002, 2004.

[97] S. Sachdev. *Quantum Phase Transitions.* Second Edition. Cambridge University Press, Cambridge, 2011.

[98] K. Sengupta and N. Dupuis. Mott-insulator-to-superfluid transition in the Bose-hubbard model: A strong-coupling approach. *Physical Review A*, 71:033629, 2005.

[99] K. Sheshadri, H. R. Krishnamurthy, R. Pandit, and T. V. Ramakrishnan. Superfluid and insulating phases in an interacting-boson model: Mean-Field Theory and the RPA. *Europhysics Letters*, 22(4):257–363, 1993.

[100] P. Soltan-Panahi, D.-S. Lühmann, J. Struck, P. Windpassinger, and K. Sengstock. Quantum phase transition to unconventional multi-orbital superfluidity in optical lattices. *Nature Physics*, 8:71–75, 2012.

[101] P. Soltan-Panahi, J. Struck, P. Hauke, A. Bick, W. Plenkers, G. Meineke, C. Becker, , P. Windpassinger, M. Lewenstein, and K. Sengstock. Multi-component quantum gases in spin-dependent hexagonal lattices. *Nature Physics*, 7:434–440, 2011.

[102] D. M. Stamper-Kurn, M. R. Andrews, A. Chikkatur, S. Inonye, H. Meisner, J. Stenger, and W. Ketterle. Optical confinement of a Bose-Einstein condensate. *Phyiscal Review Letters*, 80(10):2027–2030, 1998.

[103] T.D. Stanescu, B. Anderson, and V. Galitski. Spin-orbit coupled Bose-Einstein condensates. *Physical Review A*, 78:023616, 2008.

[104] J. Stenger, S. Inouye, D. M. Stamper-Kurn, H.-J. Miesner, A. P. Chikkatur, and W. Ketterle. Spin domains in ground-state Bose–Einstein condensates.

Nature, 396:345–348, 1998.

[105] T. Stöferle, H. Moritz, C. Schori, M. Kohl, and T. Esslinger. Transition from a strongly interacting 1D superfluid to a Mott insulator. *Physical Review Letters*, 92:130403, 2004.

[106] M. Takamoto, F. Hong, R. Higashi, and H. Katori. An optical lattice clock. *Nature*, 435:321–324, 2005.

[107] J. Tang, H. Yu, J. Yan, and Z. Zhou. Exact nonstationary solutions of a two-compponents Bose-Einstein condensate. *Communication in Theoretical Physics*, 53:282–284, 2010.

[108] C. Tsallis. Diagonalization methods for the general bilinear Hamiltonian of an assembly of bosons. *Journal of Mathematical Physics*, 19:277–286, 1978.

[109] D. van Oosten, P. van der Straten, and H. T. C. Stoof. Quantum phases in an optical lattice. *Physical Review A*, 63:053601, 2001.

[110] C. Wang, C. Gao, C.-M. Jian, and Hui Zhai. Spin-orbit-coupled Bose-Einstein condensates. *Physical Review Letters*, 105:160403, 2010.

[111] G. H. Wannier. The structure of electronic excitation levels in insulating crystals. *Physical Review*, 52:191–197, 1937.

[112] S. Watanabe and T. Usui. Phase transition in coupled order parameter. *Progress of Theoretical Physics*, 73(6):1305–1319, 1985.

[113] C.-J. Wu, I. Mondragon-Shem, and X.-F. Zhou. Unconventional Bose–Einstein condensations from spin-orbit coupling. *Chinese Physics Letters*, 28(9):097102, 2011.

[114] S.-K. Yip. Bose-Einstein condensation in the presence of artificial spin-orbit interaction. *Physical Review A*, 83:043616, 2011.

[115] T. Zhang, R.-H. Yue, and W. M. Liu. Quantum phase transition of two component dipolar bosons in optical lattices. *Physical Review A*, 340:228–236, 2007.